AD-A086 079 PENNSYLVANIA STATE UNIV UNIVERSITY PARK APPLIED RESE--ETC F/G 20/4
A METHOD OF CORRECTING FOR THE EFFECTS OF THE SIDEWALL BOUNDARY--ETC(U)
MAR 80 P P JACOBS N00024-79-C-6043
UNCLASSIFIED ARL/PSU/TM-80-44 NL

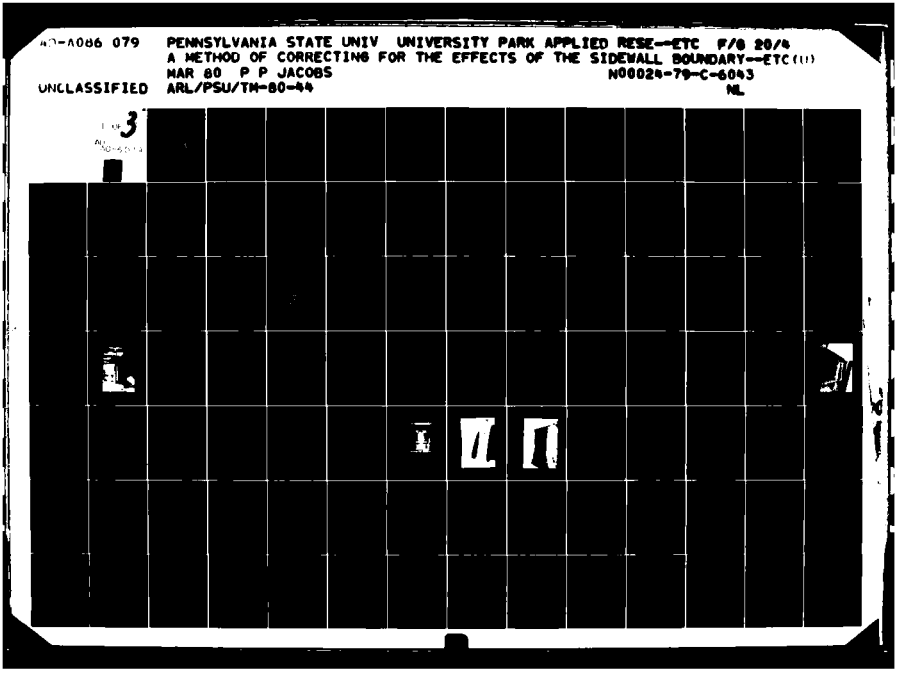

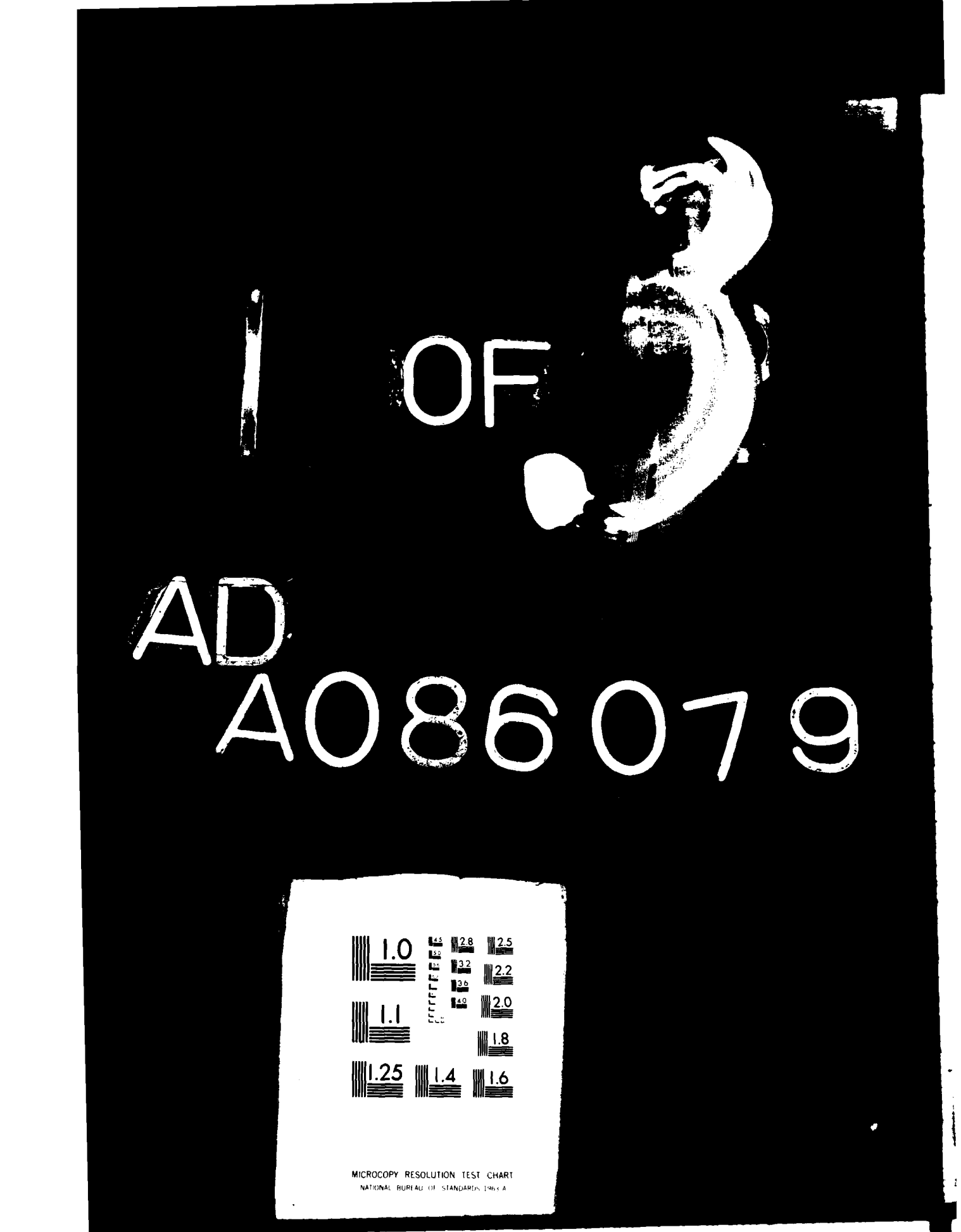
1 OF 3
AD
A086079
1.0
1.1
1.25
1.4
1.6
1.8
2.0
2.2
2.5
2.8
3.2
3.6
4.0
MICROCOPY RESOLUTION TEST CHART
NATIONAL BUREAU OF STANDARDS 1963 A

(12)

A METHOD OF CORRECTING FOR THE EFFECTS OF THE SIDEWALL BOUNDARY LAYER IN TWO-DIMENSIONAL AIRFOIL TESTING

Paul P. Jacobs, Jr.

Technical Memorandum
File No. TM 80-44
March 31, 1980
Contract No. N00024-79-C-6043

Copy No. 4

The Pennsylvania State University
APPLIED RESEARCH LABORATORY
Post Office Box 30
State College, PA 16801

NAVY DEPARTMENT

NAVAL SEA SYSTEMS COMMAND

UNCLASSIFIED

SECURITY CLASSIFICATION OF THIS PAGE (When Data Entered)

REPORT DOCUMENTATION PAGE

READ INSTRUCTIONS BEFORE COMPLETING FORM

1. REPORT NUMBER: TM 80-44
2. GOVT ACCESSION NO.: AD-A086079
3. RECIPIENT'S CATALOG NUMBER:

4. TITLE (and Subtitle): A METHOD OF CORRECTING FOR THE EFFECTS OF THE SIDEWALL BOUNDARY LAYER IN TWO-DIMENSIONAL AIRFOIL TESTING.
5. TYPE OF REPORT & PERIOD COVERED: Technical Memorandum
6. PERFORMING ORG. REPORT NUMBER:

7. AUTHOR(s): Paul P. Jacobs, Jr.
8. CONTRACT OR GRANT NUMBER(s): N00024-79-C-6043

9. PERFORMING ORGANIZATION NAME AND ADDRESS:
Applied Research Laboratory
P. O. Box 30
State College, PA 16801
10. PROGRAM ELEMENT, PROJECT, TASK AREA & WORK UNIT NUMBERS:

11. CONTROLLING OFFICE NAME AND ADDRESS:
Naval Sea Systems Command - Code 63R-31
12. REPORT DATE: March 31, 1980
13. NUMBER OF PAGES: 153

14. MONITORING AGENCY NAME & ADDRESS (if different from Controlling Office): 156
15. SECURITY CLASS. (of this report): UNCLASSIFIED
15a. DECLASSIFICATION/DOWNGRADING SCHEDULE:

16. DISTRIBUTION STATEMENT (of this Report)
Approved for Public Release. Distribution Unlimited
Per NAVSEA - April 14, 1980

17. DISTRIBUTION STATEMENT (of the abstract entered in Block 20, if different from Report)

18. SUPPLEMENTARY NOTES: ARL/PSU/TM-80-44

19. KEY WORDS (Continue on reverse side if necessary and identify by block number)
side-wall, boundary layer, two-dimensional, force, hydrofoil, thesis

20. ABSTRACT (Continue on reverse side if necessary and identify by block number)
This thesis presents the results of a hydrofoil force balance design study in which the influence of sidewall boundary layers on two-dimensional force measurements is emphasized. Past problems encountered with the present hydrofoil force balance at the Applied Research Laboratory of The Pennsylvania State University are reviewed in order to provide background information for the present study and a two-phase test program designed to identify those

DD FORM 1 JAN 73 1473 EDITION OF 1 NOV 65 IS OBSOLETE

391007

UNCLASSIFIED

SECURITY CLASSIFICATION OF THIS PAGE (When Data Entered)

factors associated with the presence of sidewall boundary layers which can influence two-dimensional force measurement in water tunnels and wind tunnels is presented.

In the first series of experiments, a doubly supported balance is used to test a NACA 0012 airfoil. Lift and drag are presented for comparison with published NACA data. In the second series of tests, a cantilever balance which is similar in principle to the original water tunnel balance is designed and tested. NACA 0012 airfoils of aspect ratios of 1.0 and 2.0 are tested in the 48-inch wind tunnel. Lift and drag data for the tests are presented. Lift data are in good agreement with NACA data, whereas drag data reflect a difference of the same order of magnitude as that reported by two previous authors.

From these measurements, various factors which influence two-dimensional force measurement and force balance design are identified, and a correction factor which accounts for spurious drag readings is derived. Lift and drag data from the present study and from the work of others with the correction factor applied are presented for both symmetrical and cambered profiles. Final corrected data are in good agreement with NACA data in all cases, indicating that accurate two-dimensional force measurements can be obtained with the new cantilever balance and correction procedure.

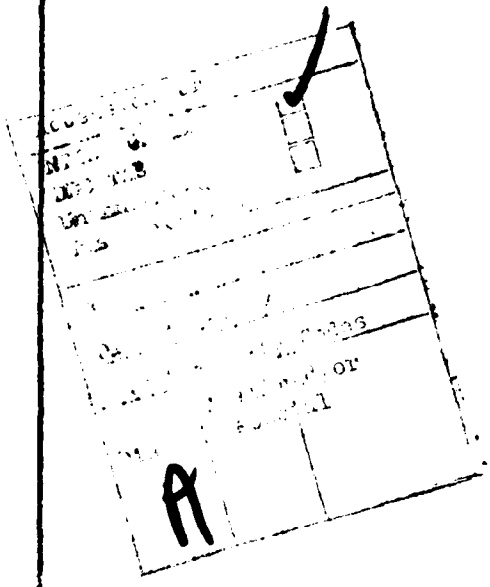

ABSTRACT

This thesis presents the results of a hydrofoil force balance design study in which the influence of sidewall boundary layers on two-dimensional force measurements is emphasized. Past problems encountered with the present hydrofoil force balance at the Applied Research Laboratory of The Pennsylvania State University are reviewed in order to provide background information for the present study and a two-phase test program designed to identify those factors associated with the presence of sidewall boundary layers which can influence two-dimensional force measurement in water tunnels and wind tunnels is presented.

In the first series of experiments, a doubly supported balance is used to test a NACA 0012 airfoil. Lift and drag data are presented for comparison with published NACA data. In the second series of tests, a cantilever balance which is similar in principle to the original water tunnel balance is designed and tested. NACA 0012 airfoils of aspect ratios of 1.0 and 2.0 are tested in the 48-inch wind tunnel. Lift and drag data for the tests are presented. Lift data are in good agreement with NACA data, whereas drag data reflect a difference of the same order of magnitude as that reported by two previous authors.

From these measurements, various factors which influence two-dimensional force measurement and force balance design are identified, and a correction factor which accounts for spurious drag readings is derived. Lift and drag data from the present study and from the work of others with the correction factor applied are presented for both

symmetrical and cambered profiles. Final corrected data are in good agreement with NACA data in all cases, indicating that accurate two-dimensional force measurements can be obtained with the new cantilever balance and correction procedure.

TABLE OF CONTENTS

LIST OF FIGURES

LIST OF TABLES

NOMENCLATURE

Symbols from the text are listed herein. Variable names for the two computer programs are listed separately in Appendix C.

Symbol	Definition
A_i, o_j	elements of simultaneous equations matrix representing trignometric functions of α in Equations (C2) and (C3)
AR	aspect ratio (span/chord)
b	airfoil semi-span
B_i	elements of simultaneous equations matrix representing forces A and B in pounds as determined by Equation (C1)
c	airfoil chord
C_d	section drag coefficient with boundary corrections applied
C_{dn}	section drag coefficient uncorrected
C_D	total airfoil drag coefficient
C_{D_i}	increment of additional drag coefficient due to slot in airfoil
C_ℓ	section lift coefficient, corrected
C_{ℓ_α}	slope of C_ℓ-versus-α curve
$C_{\ell_{\alpha_o}}$	slope of C_ℓ-versus-α curve in portion where slope is constant
$C_{\ell_{max}}$	maximum section lift coefficient

Symbol	Definition
C_{ℓ_u}	section lift coefficient uncorrected
C_L	total airfoil lift coefficient
$C_{L_{max}}$	maximum total airfoil lift coefficient
$C_{m_{1/4}}$	section coefficient of moment about 1/4-chord point, corrected
$C_{m_{1/4_u}}$	section coefficient of moment about 1/4-chord point, uncorrected
D	generalized drag force
$\vec{D}$	total drag force vector
d	diameter of force transmitting shaft
da	incremental area of wake perpendicular to airstream
$\vec{D}a$	vector component of drag force along axis of ribbon A
D_B	drag force due to horizontal buoyancy
$\vec{D}_B$	vector component of drag force along axis of ribbon B
$dC_\ell/d\alpha$	slope of C_ℓ-versus-α curve
$(dC_\ell/d\alpha)_o$	slope of C_ℓ-versus-α curve in portion where curve is constant
D_e^*	energy in secondary flows created by strut-wall intersections
$dP/d\ell$	static pressure change per unit length of test section channel
d(x/c)	incremental element of chord length

Symbol	Definition
dy/dx	airfoil shape parameter
$F_{A,B}$; $Force_{A,B}$	force in pounds as measured by ribbon A or ribbon B
h	tunnel height
K	a constant
$K_{A,B}$	calibration constant for ribbon A or B which converts volts to pounds of force
$\vec{L}$	total lift force vector
$\vec{L}_A$	vector component of lift force along axis of ribbon A
$\vec{L}_B$	vector component of lift force along axis of ribbon B
n	variable used to simplify Equation (6), $n = 4\left(1 + (1/2)(t/c)\right)/\left(15\pi(\delta/c)\right)$
P	airfoil basic pressure distribution
q	$(1/2)\rho V^2$
q_o	$(1/2)\rho V_o^2$
Re	Reynolds number, corrected for boundary conditions
Re_u	Reynolds number, uncorrected
s, span	airfoil span
t	airfoil thickness
U_o	free-stream velocity
V	airspeed downstream of airfoil; reference velocity corrected

Symbol	Definition
V_o	airspeed upstream of airfoil
V_u	reference velocity uncorrected
$Volts_{A,B}$	voltage measurement of ribbon A or B
X_i	elements of simultaneous equations matrix representing unknown forces, lift and drag
y	airfoil spanwise coordinate; airfoil area coordinate in Appendix B
α	airfoil angle of attack, corrected for boundary conditions
α_u	airfoil angle of attack, uncorrected for boundary conditions
δ/c	sidewall boundary layer thickness parameter
ε	total blockage correction
ε_{sb}	correction for solid blockage
ε_{wb}	correction for wake blockage
θ	angle of resultant force on force transmitting shaft due to gap flows
Λ	pressure distribution correction parameter, defined in Appendix A
ρ	mass density
σ	tunnel geometry parameter; $\alpha = (\frac{\pi^2}{48})(\frac{c}{h})^2$
τ	gap width

ACKNOWLEDGMENTS

The author wishes to express his appreciation to several members of the staff of the Garfield Thomas Water Tunnel. Particular thanks are extended to his thesis advisor, Dr. Blaine R. Parkin, whose in-depth knowledge of the subject was an invaluable resource. The cheerful, positive attitude displayed by Dr. Parkin throughout the course of the investigation was a source of inspiration.

Grateful acknowledgment is expressed to Mr. George B. Gurney for the measurement expertise which he provided. Mr. Gurney's thorough manner and patience contributed greatly to the author's overall education.

A note of thanks is also extended to Mr. Allen L. Treaster, who provided sound technical guidance during the investigation and in the preparation of the manuscript.

This work was sponsored by the Naval Sea Systems Command (Code 63R-31).

CHAPTER I

INTRODUCTION

Recently at the Applied Research Laboratory of The Pennsylvania State University (ARL/PSU), a cantilever-type balance was designed to measure the lift, drag, and pitching moment characteristics of a hydrofoil in cavitating flow. As a preliminary verification of the test setup, several standard NACA (National Advisory Committee for Aeronautics) airfoils were tested. Data from these tests were compared to those previously published by NACA and by those measured by Kermeen (1) at the California Institute of Technology. The ARL/PSU test results differed substantially from both sets of previously published data. Kermeen did not specifically address the problem of water tunnel balance design because he used a balance of established accuracy. However, there are also slight differences between the results Kermeen reported and those reported by NACA. Because of these considerations, a program was initiated to study the problem of hydrofoil balance design with a particular emphasis on the action of the tunnel walls and viscous effects on the measured forces.

The ultimate goal of the program was to develop the capability of accurately measuring force coefficients characteristic of new hydrofoil profiles in fully wetted and cavitating flows. To achieve this objective, five intermediate objectives were established.

The first of these objectives was to determine why the 12-in. water tunnel balance failed to measure the forces accurately.

The second objective was to build and test a balance which was similar in principle to the ARL/PSU water tunnel balance for use in the 48-in.-diameter wind tunnel. By use of the 48-in. wind tunnel, larger airfoil geometries could be employed in an effort to duplicate water tunnel Reynolds numbers (Re). Waterproofing problems and the large forces involved in water flows are also eliminated in wind tunnel testing.

The third objective was to determine what factors (and their magnitude) affect flow past a hydrofoil in a two-dimensional channel. The understanding of factors affecting the flow can possibly give an insight as to why, hydrodynamically speaking, the original ARL/PSU balance failed. Such knowledge can also provide a sound information base for designing or modifying hydrofoil balances.

The fourth objective was to determine a theoretical and/or empirical correction procedure to use with the existing balance, one accounting for all important physical interactions in the channel and converting the balance measurements into accurate two-dimensional forces. Depending on the adequacy of the correction procedure, a decision would be made whether to continue to use the existing balance in conjunction with a correction procedure or to redesign the balance based on new knowledge.

The fifth objective was to formulate a standard procedure for measuring and reducing data with the ultimate tunnel-balance configuration at ARL/PSU. This procedure would be documented to provide a reference for future two-dimensional hydrofoil testing.

CHAPTER II

BACKGROUND

Although air and water are both fluids, there are fundamental differences between air and water tunnel testing. Consideration of these differences led to the conclusion that a cantilever balance system as described in Chapter III is the best choice for water tunnel testing.

A traditional method of measuring force coefficients in wind tunnels has been by use of pressure taps. In a two-dimensional channel, lift being created by an airfoil exerts a force on the ceiling and floor of the tunnel. By placing pressure taps on these walls and integrating the pressures, the lift can be determined. Drag forces can also be determined by placing pressure taps along the surface of the airfoil and integrating the readings in the drag direction. Another method of measuring drag with pressure sensitive instruments is to measure the momentum deficit created by the airfoil in a two-dimensional channel. This measurement is accomplished by traversing a pressure probe through the airfoil wake and integrating the readings.

Testing airfoil shapes in water (hydrofoils) introduces additional problems. Among these problems are handling larger gross forces and waterproofing requirements. The major area of concern, however, involves cavitation. When hydrofoils are tested in water tunnels, they may operate in three different flow regimes. The first regime is noncavitating or fully wetted flow. This range of flow is that which falls within the scope of the present study, and it differs little from

low-speed wind tunnel testing. The second regime is the partial cavitation range or that regime where the cavitation bubble begins and ends on the surface of the body. The third regime is fully cavitating flow or cavity flow. The present research concentrates on the first flow regime.

A balance system and correction procedure for water tunnel testing must be capable of accurately measuring forces in all three flow regimes. Compared to wall effects in fully wetted flows, the wall effects on fully cavitating profile forces are not as pronounced provided that the cavitation number is based on measured cavity pressure. Elaborate cavity flow calculations can be used to correct the force data in this last case. Although sidewall boundary layer effects are still observed in the fully cavitating flow regime, past experience indicates that they have a negligible effect on the measured forces in this case. The effects of tunnel walls in the partially cavitating regime are beyond the scope of this study.

Placing pressure taps on a hydrofoil's surface or on the tunnel walls will cause premature cavitation and cavitating taps have been shown to give spurious pressure readings. This is obviously unacceptable, especially when tests are being conducted in the partial cavitation regime. For these reasons, water tunnel testing is best performed by directly measuring the forces with a balance.

With a mechanical balance, aerodynamic forces can be measured directly without pressure taps marring the model surface. Mechanical balances are, however, not totally free of problems. Balances measure all forces applied to a model. If forces occur on a model which are not those associated with two-dimensional flow (due to such causes as

secondary flows where the model intersects a tunnel wall), the balance will also measure them. A correction factor is then required to reduce this total force to a two-dimensional force. Despite the required corrections, mechanical balances appear to be the best method for measuring forces on cavitating hydrofoils. Previous work by various authors substantiates this point of view.

2.1 Baseline Data

As a prelude to the present study, it would be beneficial to examine published wind tunnel data to establish a credible reference frame for the data of this study. A wealth of airfoil test data were measured by NACA at the Langley and Ames research centers in the 1930's and 1940's. Loftin and Smith (2) conducted numerous tests on a variety of two-dimensional airfoil shapes at Langley Aeronautical Laboratory in 1949. They used airfoils of 3-ft chord which completely spanned a rectangular test section of 3-ft width and 7.3-ft height. Lift measurements were made by taking the difference between integrated pressure reactions on the floor and ceiling of the tunnel. Lift was also measured by use of a three-component force balance. Small gaps were allowed between the walls and airfoil tips to permit freedom of movement of the model. Although these end gaps are a source of error, the two sets of lift measurements agreed within the experimental error of the test. Drag measurements were made with a wake survey apparatus. The model end gaps were sealed with felt packing which reduced errors due to induced drag. Pitching moment was measured by a torsional balance.

Jacobs and Sherman (3) tested numerous airfoil profiles as a function of Reynolds number (Re). They tested at Re values as low as 170,000. These tests were within the range of Re achievable in the 48-in. wind tunnel at ARL/PSU. The airfoils tested in Reference (3) were finite aspect ratio models which did not completely span the wind tunnel. In effect, three-dimensional data were measured and corrected to two-dimensional data. The authors reported that the magnitude of experimental errors increased as Re was lowered. They further stated that drag and pitching moment results became relatively inaccurate below Re = 800,000 due to limitations imposed by the sensitivity of the measuring equipment. Inaccuracy of these quantities became so pronounced that airfoil characteristics dependent on drag and pitching moment results (optimum lift coefficient, aerodynamic center of pressure, etc.) were considered unreliable and in most cases were not presented below Re = 800,000. The data presented in Reference (3) should be verified as an integral step in this study.

2.2 Previous Water Tunnel Results

Kermeen (1) conducted a series of experiments to determine whether accurate force measurements could be obtained with a recently modified hydrofoil force balance (4) at the California Institute of Technology (CIT). He used a cantilever hydrofoil balance arrangement (Figure 1) and tested NACA 4412 and Walchner profile 7 hydrofoils.

The airfoil was originally mounted on a stub spindle as depicted on the left of Figure 2. This arrangement necessitated small clearance gaps on each end of the airfoil. Kermeen stated that this arrangement caused problems. There were radial interferences due to deflection of

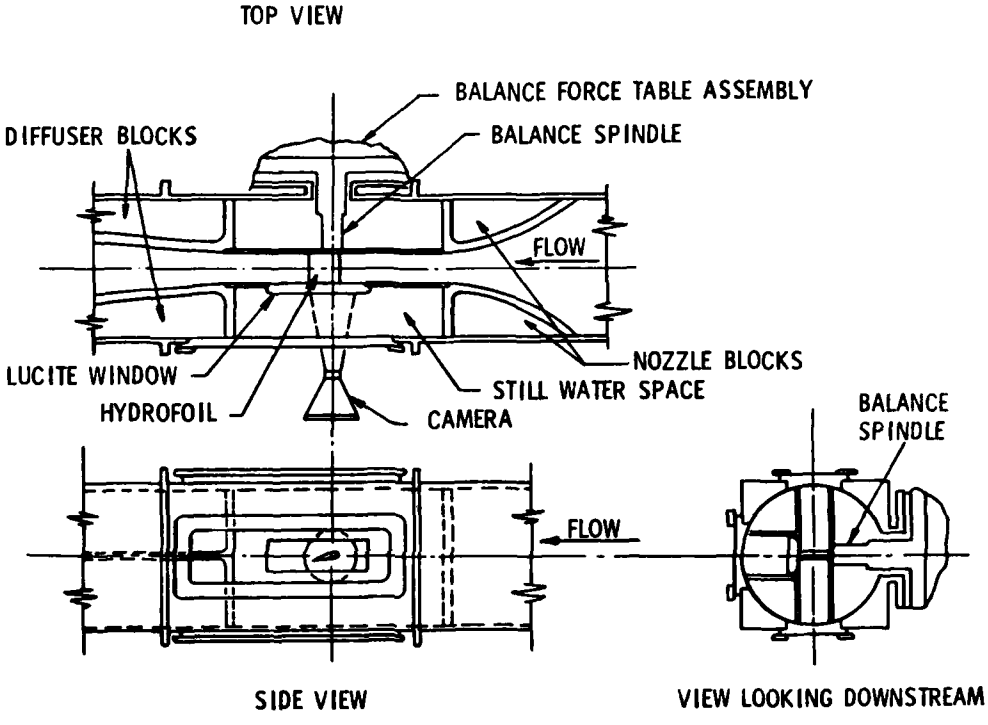

Figure 1. Sketch showing setup of Kermeen's balance-hydrofoil system. Reproduced from Reference (1).

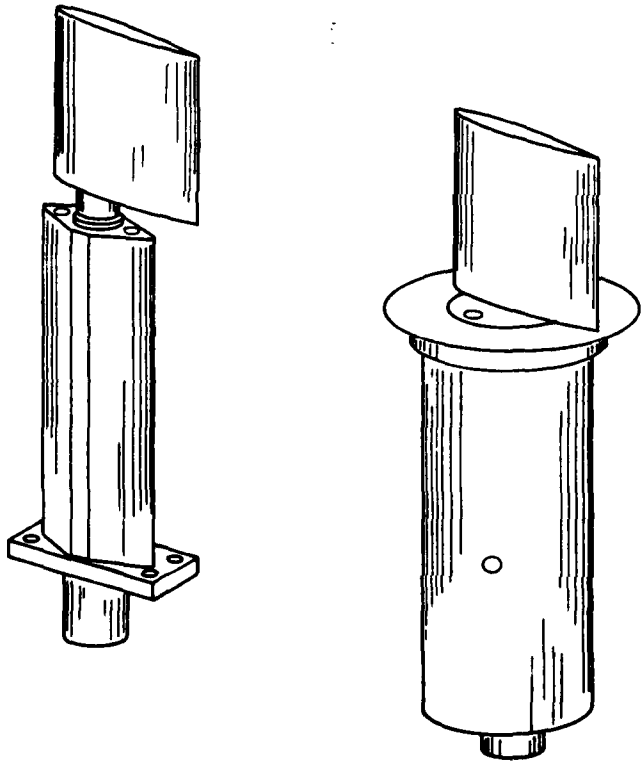

Figure 2. NACA 4412 hydrofoil models used by Kermeen. The original stub spindle is shown on the left. The newer spindle-disk assemply is shown on the right.

the two-dimensional channel walls. There was also a problem of water jetting through the stub spindle clearance gap from the high-pressure dead-water region. For these reasons, Kermeen switched to the enlarged spindle disk arrangement pictured on the right of Figure 2. The 5-in.-diameter disk was attached to a hydrofoil of 3-in. chord, thereby eliminating the end gap on one side of the hydrofoil.

This new arrangement eliminated corrections that may have been necessary due to the end gap on the balance side of the model. Kermeen gives a good description of five of the traditional sources of error in wind and water tunnel testing:

1. Solid blockage. This considers the effect of the model physically blocking the flow and subsequently changing the axial velocity past the hydrofoil.
2. Wake blockage. This is a similar effect and accounts for the reduction of velocity inside the hydrofoil wake.
3. Lift effect. This accounts for the compression of the streamlines around the hydrofoil due to the tunnel walls. The effect is treated as a change in hydrofoil camber and incidence angle.
4. Horizontal buoyancy. This correction compensates for the additional drag created on the model due to the existing static-pressure gradient in a two-dimensional channel.
5. Boundary layer interference. This accounts for the departure from two-dimensional flow near the walls due to the interaction of the wall boundary layer.

Kermeen also considered the effect of skin friction on the disk. He mounted the foil on the opposite side of the channel and, with a

small clearance between the disk and foil (approximately 0.002 in.), measured the forces sensed by the disk alone for various angles of attack. These tare forces were then subtracted from the appropriate test data.

In addition to the above consideration, Kermeen further examined the effect of flow through the gap between the hydrofoil end and the tunnel wall. With a gap as small as 0.002 in., the author reported that flow through this gap was clearly visible. He varied the gaps from 0.001 in. to 0.032 in. and for an angle of attack of 4^{o} found that the drag coefficient increased by 25%. The lift was reduced by 8% for these same conditions. The moment coefficient appeared to be unaffected by gap size.

In his final data reduction, Kermeen chose to include corrections for all of the tunnel interference effects except boundary layer interference. He felt that the boundary layer's effect on lift was negligible and he made no statement about its effect on drag. He also included corrections for the tare forces on the disk. He did not specifically state whether or not he included corrections for the gap effect. Kermeen's lift and moment data for the NACA 4412 profile agreed very closely to the NACA data (3). The drag data agreed well in the lower drag range but for attack angles greater than 5^{o} Kermeen's results showed higher drag values. The thrust of Kermeen's study was to demonstrate as clearly as possible that the balance could accurately measure hydrodynamic forces. This enabled him to compare his new data on cavitating and noncavitating Walchner hydrofoils with Walchner's results, which were not very accurate. He did not attempt to determine

what factors beyond the classical corrections affected balance performance.

Earlier studies of a similar nature were conducted by Daily (5) at the California Institute of Technology (CIT). He ran a series of tests on a NACA 4412 hydrofoil using a three-component force balance (from which the balance of Kermeen's report was derived) in the high-speed water tunnel.

Daily's setup is depicted in Figure 3. He used a cantilever arrangement with a small supporting spindle. The size of the supporting spindle resulted in clearance gaps on each end of the model. Because of the magnitude of the forces at the higher angles of attack, Daily used a full-span and a split-span hydrofoil. Splitting the span in half, as indicated in Figure 3, enabled the balance to sense only half of the gross forces on the hydrofoil. The full-span model was used for testing at the lower angles of attack and the semi-span version was used for testing in the higher lift range.

Daily implied that his data required few corrections. He reported that boundary layer effects in the region where the hydrofoil meets the tunnel wall should be neglected. Since the foil was mounted only one tunnel diameter from the final contraction of the flow, the boundary layer is relatively thin when it interacts with the foil. He further reported that incipient cavitation photographs suggested a uniform spanwise flow. Daily also claimed that the clearance gap between the tunnel walls and the model test span was small enough to make its effect negligible. He further stated that wall interference or "blocking" was negligible at low angles of attack and increased with increasing angles. The magnitude of the blocking effect was not evaluated for his tests.

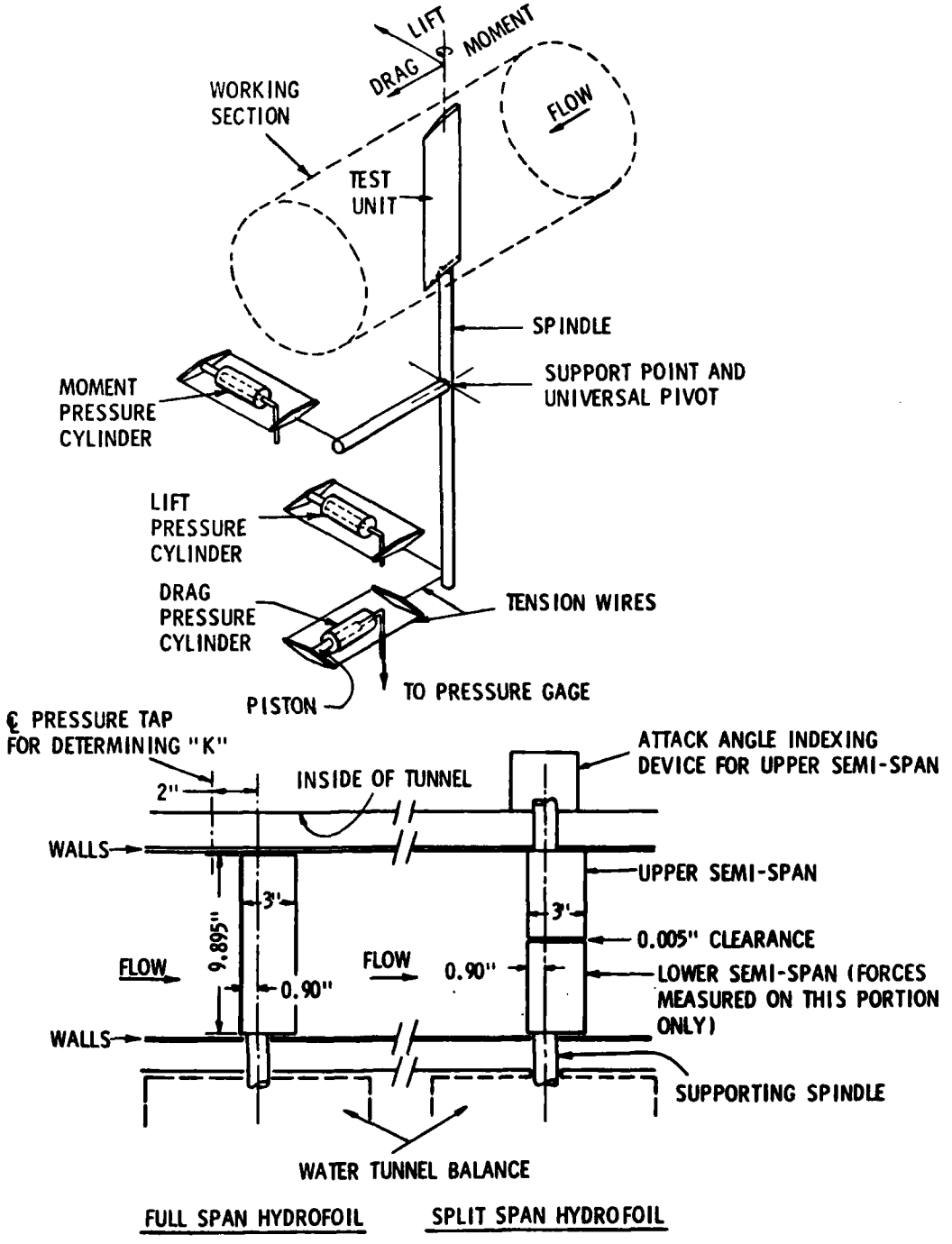

Figure 3. Sketches illustrating Daily's balance-hydrofoil system. The top sketch shows a schematic diagram of the balance. The bottom sketch shows details of the model installations in the tunnel working section.

Daily compared his test results to the NACA wind tunnel tests of Reference (3). He generally found good agreement at low angles of attack but his measurements differed by as much as 10% at the higher angles of attack. He further concluded that the low lift range was the operating range of many hydrofoil applications and that with his test setup good comparative results could be obtained.

2.3 Recent ARL Water Tunnel Tests

In the previously mentioned test program at ARL/PSU, the work of Kermeen and Daily was used as a guide for designing the hydrofoil and balance hardware. The ARL/PSU balance and a typical hydrofoil are shown in Figure 4. This three-component balance measured lift, drag, and pitching moment by use of strain gages attached to tension members which are aligned axially and normally to the hydrofoil (Figure 4). The spindle attachment on the foil was a compromise between Kermeen's larger-than-chord disk and Daily's equal-to-hydrofoil-thickness spindle. The aspect ratio (AR) of the ARL/PSU hydrofoils was 0.9 as compared to Daily's AR = 3.33 and Kermeen's AR = 0.97.

In the original ARL/PSU program, a NACA 4412 hydrofoil was tested (Figures 5A and 5B). The pitching moment results agreed extremely well with published NACA wind tunnel data (3). The slope of the lift curve and $C_{L_{max}}$ were approximately 20% lower than published data. The drag curve was within 25% of published data at the zero-lift condition. However, at all other values of lift, the corresponding drag values were higher than published data by as much as a factor of ten. These conclusions were obtained from uncorrected data taken just prior to the termination of the force phase of the test program.

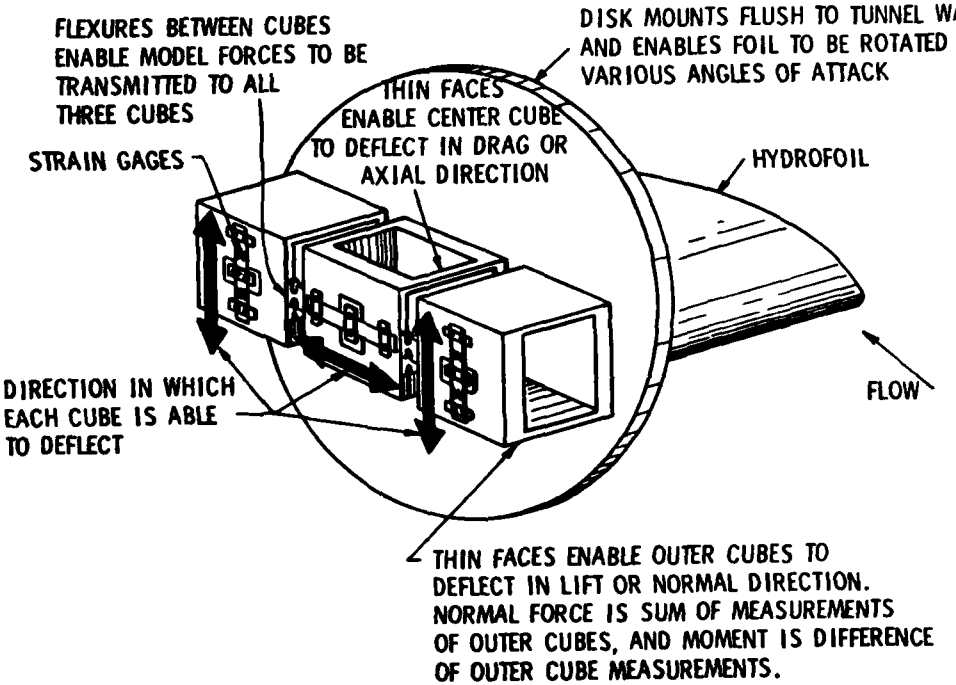

Figure 4. Simplified sketch of original ARL/PSU water tunnel balance and hydrofoil system.

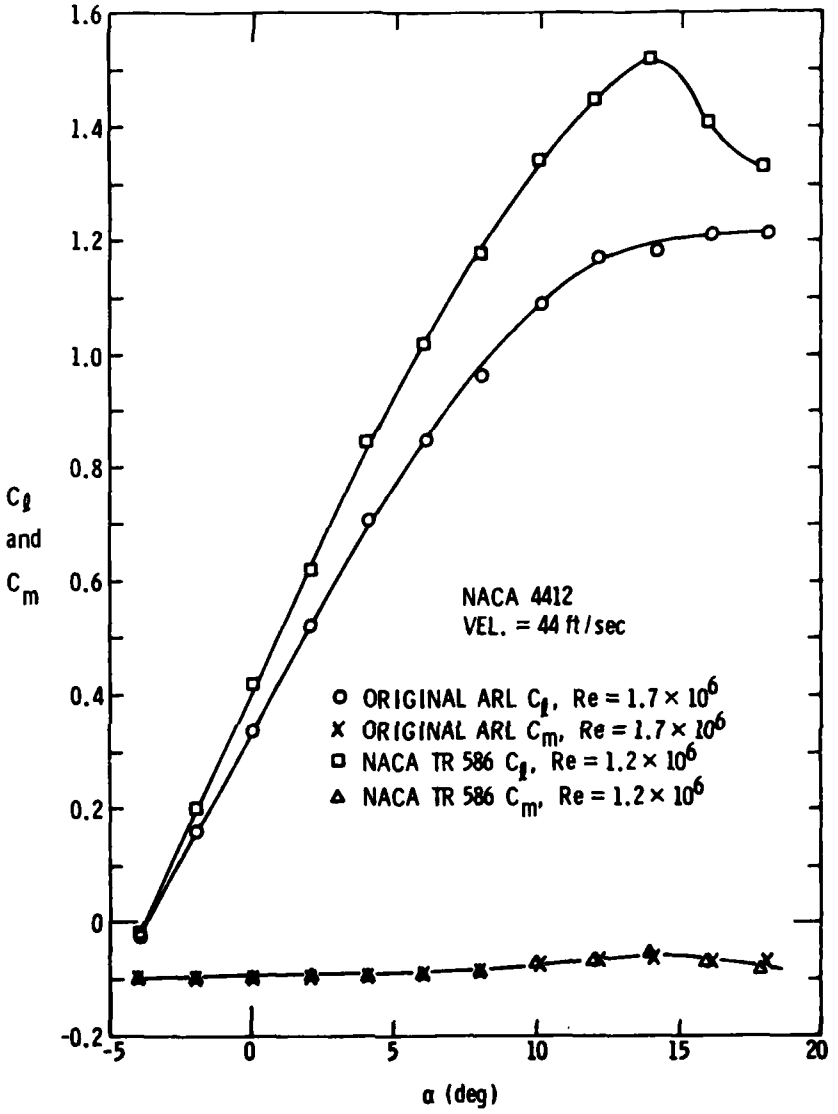

Figure 5A. C_ℓ-versus-α and C_m-versus-α results for original ARL/PSU water tunnel tests.

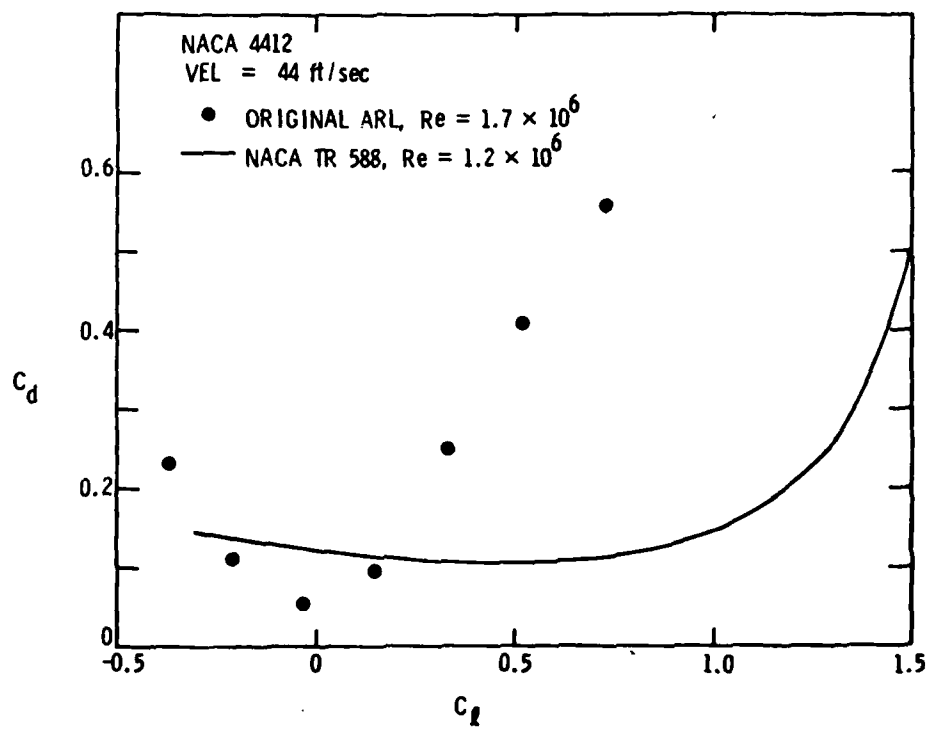

Figure 5B. C_ℓ versus C_d for original ARL/PSU water tunnel balance compared to NACA data for same conditions.

Several attempts were made to correct the problems with the balance. When the balance was mounted in the horizontal configuration, it was noted that the hydrofoil deflected severely under loads due to weaknesses in the flexures between the force cubes. In order to eliminate this problem, the balance was rotated 90^{o} so that the cubes were in a vertical configuration. This rotation eliminated the model deflection problem but required the drag or axial force to be measured as the sum of two cube readings instead of one. At high angles of attack, the axial force was small compared to the normal force. This vertical arrangement meant that a small force was being divided in half and that drag was being measured as the sum (or difference, depending on the signs of the calibration constants) of two small values. The realignment of the balance was one of several attempts, all of which failed to solve the problem.

2.4 Further Pertinent Data

More recently, an extensive investigation of profile forces was conducted by Otsuka and Sugiyama (6). They conducted numerous tests on an airfoil spanning a rectangular channel with a variable clearance between the airfoil tip and the channel wall. They measured section lift and drag forces at various spanwise locations while varying the airfoil angle of attack, boundary layer thickness, and tip clearance. They placed numerous pressure taps on the airfoil surface and integrated pressure readings to determine the forces. An interesting feature of their data (on a plot of C_d-versus-span location) was that accurate section C_d values could apparently be obtained for a given airfoil when the measuring probe was far enough away from the tunnel wall. This

is the fact which earlier NACA investigators had used in order to obtain reliable airfoil section data.

2.5 Discussion of Data Base

Consideration of the work of these previous authors yielded several salient points which were useful in designing a program to accomplish the goals of this report.

First, in order to establish correction factors for a given balance design, there must exist some absolute data base for comparison purposes. For a given airfoil, the lift, drag, and pitching moment characteristics must be known before the magnitude of the balance corrections can be determined. The NACA data for the Reynolds numbers being considered here (generally $Re \leq 1{,}000{,}000$) appeared to be insufficient. Therefore, it was necessary to generate a valid data base for comparison purposes.

The second point concerned the approach used by NACA in obtaining their data. Lift, drag, and pitching moment were, in most cases, measured independently and by the most accurate technique for each force. Lift and pitching moment could be measured accurately by force balances, while drag could be more accurately obtained by momentum surveys via pressure surveys. The idea of measuring quantities separately (using the most accurate technique for each) and combining data seems to be an excellent solution to the problem of establishing a reference data base. Data shown in Figure 6, taken from Kermeen, supported this idea. Lift and pitching moment coefficients for a NACA 4412 airfoil are presented. Consideration must be given to the spread of Reynolds numbers. However, all factors considered, the data

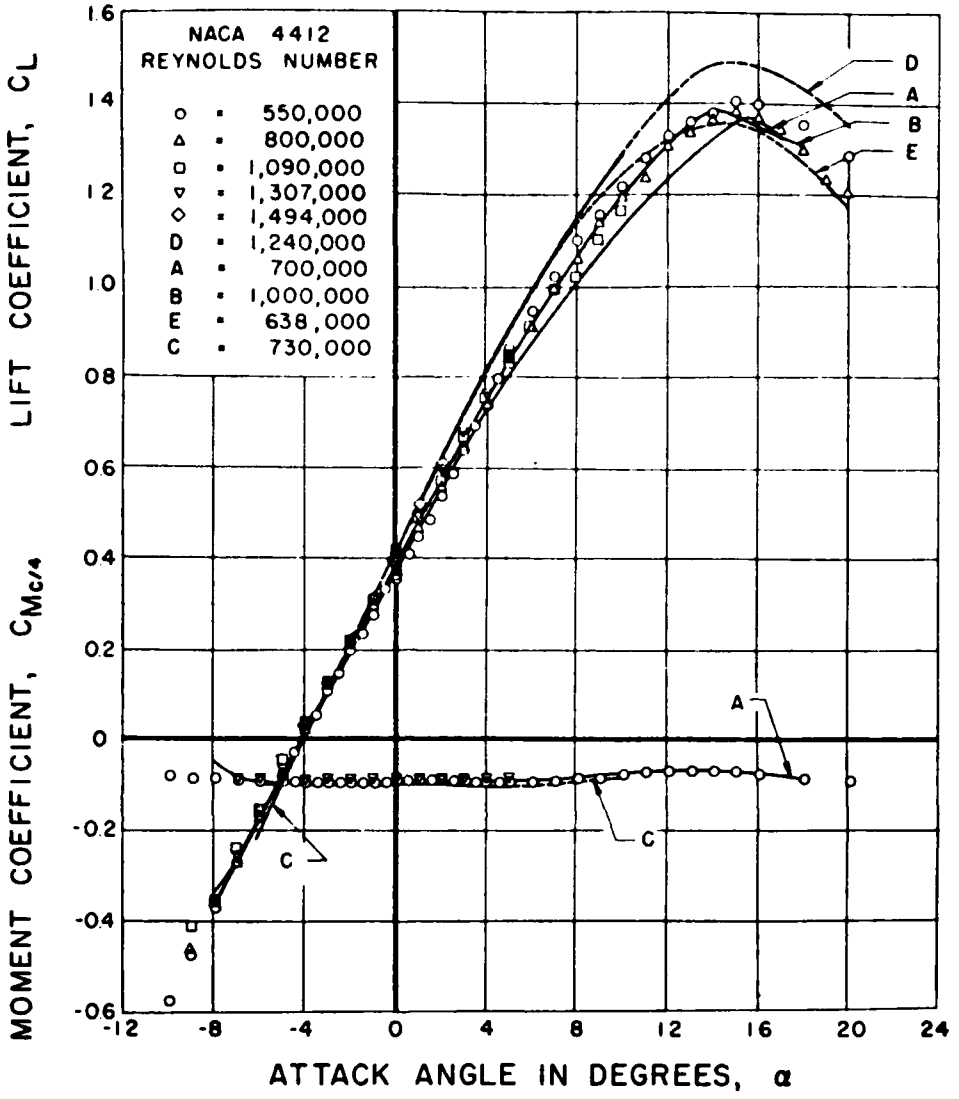

Lift coefficient and moment coefficient about the quarter chord point as functions of angle of attack for the NACA 4412 hydrofoil for noncavitating flow. The data points in this figure are the results of the present tests. The curves are from the following sources:

A and B. Langley Two-Dimensional, Low Turbulence Wind Tunnel, 1949.

C. J. W. Daily, Hydrodynamics Laboratory, C.I.T., 1944.

D and E. NACA Variable Density Wind Tunnel, 1937.

Figure 6. Lift and moment data reported by Kermeen. Reproduced from Reference (1).

are in excellent agreement. Since the different experimental results agree well with each other and Reference (2) states that lift measured by both pressure surveys and a force balance shows no significant difference, the logical conclusion is that the lift values for a set of reference data can be obtained by measuring with a force balance. Roughly the same argument also holds for measuring pitching moment coefficients.

The drag measurements required special consideration. The polars of Figure 7 show that there is poor agreement in measured drag coefficients between the several experiments. Because of the small forces involved and the sensitivity of drag to various factors (gap flows, induced effects, tare forces, etc.), accurate drag measurement seemed to be the most difficult problem to contend with in designing a force balance. The solution to this problem seemed to lie in traversing a pressure probe through the wake of a given airfoil at a spanwise position such that end wall and tip gap effects are negligible. Integration of the pressure readings would then give an accurate section drag coefficient. Otsuka and Sugiyama's work seemed to indicate that this was possible.

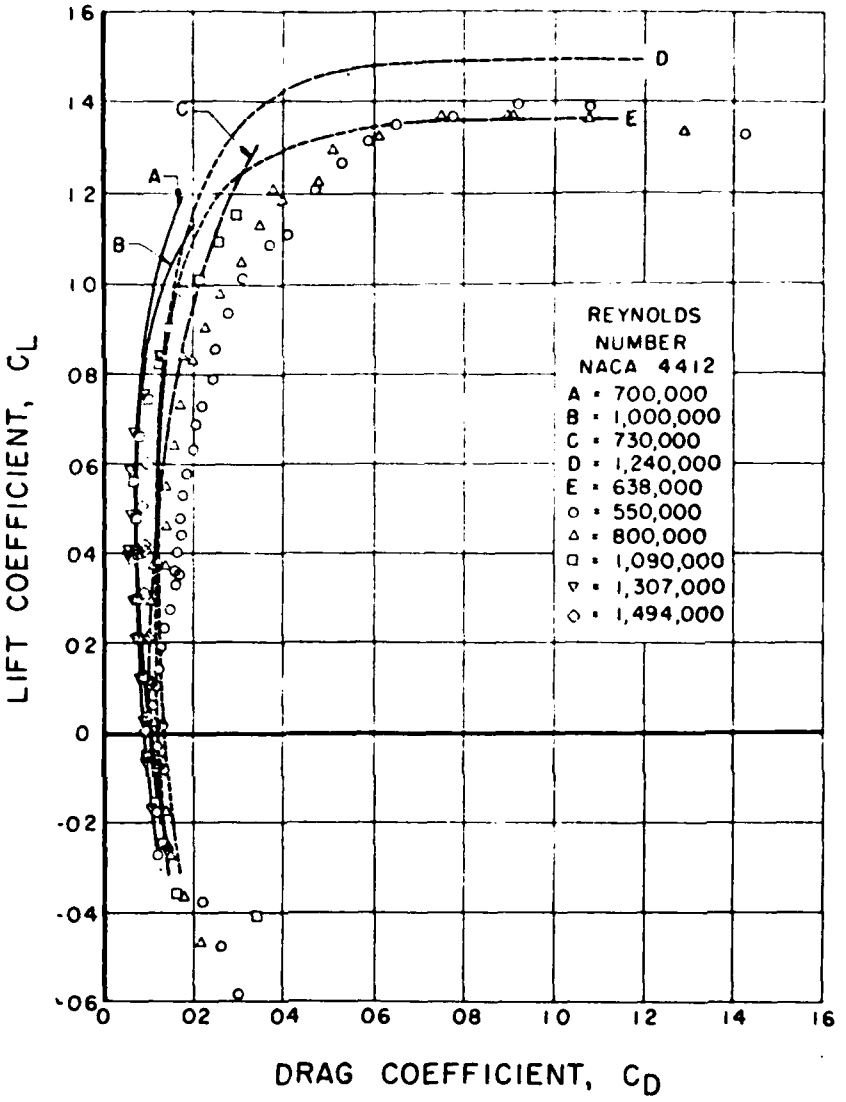

Polar diagram for the NACA 4412 hydrofoil in noncavitating flow. The data points are from the present tests. The curves are from the following sources:

A and B. Langley Two-Dimensional, Low Turbulence Wind Tunnel, 1949

C. J. W. Daily, Hydrodynamics Laboratory, C.I.T., 1944.

D and E. NACA Variable Density Wind Tunnel, 1937.

Figure 7. Lift-versus-drag results reported by Kermeen. Reproduced from Reference (1).

CHAPTER III

METHODS AND PROCEDURES

3.1 Test Program

A test program was formulated after analyzing all the available background material. The first step would be to develop competence with strain gage measurements and basic wind tunnel techniques. It was felt that since the measurement of pitching moment coefficient has never proven to be particularly difficult only lift and drag measurements would be considered. This would also simplify the hardware manufacturing problem. An existing, doubly supported balance* would be used during this preliminary phase. This balance (Figure 8) would enable forces to be measured on a well-documented airfoil shape in the absence of an incoming boundary layer.

The next step would be to build a cantilever balance for use in the 48-in. wind tunnel. This balance would duplicate as closely as possible the geometry and principle of operation of the existing 12-in. water tunnel balance. This balance would be used to measure lift coefficients for the selected airfoil profile at various angles of attack. For these same angles of attack, a pressure traverse would be used to measure drag

*A doubly supported balance refers to a configuration where the model is supported from both sides of the tunnel and each support has its own force measuring device. By contrast, a cantilever balance herein refers to a configuration where the model is supported from only one side of the tunnel with a single force measuring device attached to the support. The term cantilever balance is also used to refer to the force balance described in Section 3.4.

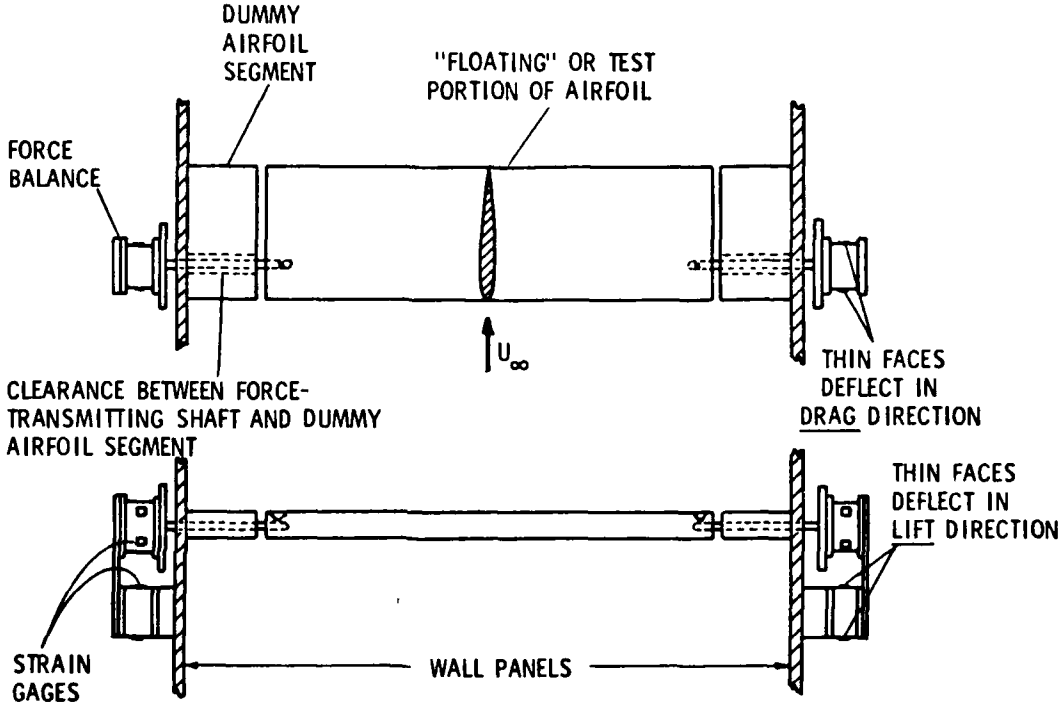

Figure 8. Doubly supported balance. Balance elements are on either side of tunnel. Measurements are summed to produce total forces on model.

coefficients. The resulting C_d and C_ℓ values would be combined to produce a C_ℓ-versus-C_d curve. This curve would be verified by the NACA data to provide a data base for determining correction factors in the final force balance phase of the investigation.

The next step would be a variation of parameters to determine their effect on measurements. Airfoils of different aspect ratio, disks of various sizes, and boundary layers of varying thickness would be studied. These data would be analyzed and final conclusions drawn regarding what factors significantly influence this type of testing.

3.2 Doubly Supported Balance Phase

The doubly supported balance as depicted in Figure 8 was designed to measure forces on an airfoil in the absence of an incoming boundary layer. The dummy portions of the airfoil extend into the flow beyond the thickness of the sidewall boundary layers. The three-dimensional flows occurring at the airfoil-tunnel wall intersection act upon the dummy portion of the foil ends, and these spurious reactions are not transmitted to the balance.

The force cubes were mounted on two parallel wooden (birch veneer particle board) 4 ft x 8 ft panels. The wind tunnel test section had an octagonal shape and installation of the parallel panels converted the test section to a rectangular channel. The airfoil setup is shown on Figure 9. Here the system is mounted on a box-type frame used to calibrate the balance outside of the wind tunnel. The parallel walls shown on Figure 9 simulate the panels which were placed in the wind tunnel. The force cubes were mounted on the outside of the panels (see Figure 8).

Figure 9. Doubly supported balance setup in calibration box.

There are four force cubes in the system - two on each side of the tunnel. Each cube is designed to deflect in only one of the three cardinal directions and to be rigid in the other two directions. The cubes are mounted on each side of the channel so that one cube is free to deflect in the horizontal or drag direction and the other cube is free to deflect in the vertical or lift direction. Strain gages are attached to the deflecting faces of the cubes. The strain gages produce a voltage which is proportional to the force applied to the cube. Reference (7) provides details on the operation of strain gages.

The cubes are mounted in a fixed position on the tunnel walls such that the deflecting axis of one pair is perpendicular to the tunnel flow. The shaft which transmits forces from the airfoil to the force cubes is fixed to the airfoil with four setscrews. The angle of attack can be changed by loosening the setscrews, rotating the airfoil about the shaft to the desired angle, and then tightening the setscrews.

The cubes were calibrated by first mounting them on a box as on Figure 9. Known weights were suspended from the force transmitting shaft and the corresponding output was recorded. A calibration constant in lb/volt was then determined for each cube. After the lift constants were determined, the box was rotated 90^{o} so that the drag constants could be determined. Additionally, interactive constants were determined by loading various grams of "lift" on the shaft and reading the corresponding volts of "drag." This was done for each pair of cubes. An interactive constant for volts of lift per gram of drag was not determined because the high ratio of lift to drag for airfoils (and the design of the force gages) makes the drag effect on lift negligible.

This fact was verified by loading the cubes with representative values of lift and drag simultaneously.

Prior to mounting the balance in the wind tunnel, a pressure probe was traversed vertically in the channel formed by the two wooden panels to verify flow uniformity. These results are shown in Figure 10. Traverses were also made perpendicular to the sidewall of the tunnel and the tunnel ceiling to determine boundary layer thickness. These results are shown in Figures 11A and 11B. These runs were all made at Re = 330,000. This Re was chosen since it was the highest achievable Re for which data were published in Reference (3). The plots show that there was a uniform flow in the channel and that the sidewall boundary layer thickness was less than the span of the dummy airfoils.

Lift and drag data were measured using the doubly supported balance and a NACA 0012 airfoil. The airfoil was made of mahogany and had a chord of 6 in. and span of 14.725 in. Final corrected data are shown in Figures 12 and 13. The corrections applied were for solid blockage, wake blockage, lift effect, and horizontal buoyancy. An additional correction was applied to account for the air being drawn through the slot between the dummy section and the tested airfoil. In this small gap, the bar which transmits forces to the balance is exposed. As the airfoil becomes more heavily loaded at higher angles of attack, the larger pressure difference between the suction and pressure surfaces of the airfoil causes a higher dynamic pressure to be sensed by the bar. A correction term for this additional drag was determined and applied to the data. This correction procedure is discussed in Section 3.3.

To determine the accuracy of the balance readings, drag was measured by traversing a total pressure probe through the airfoil wake and

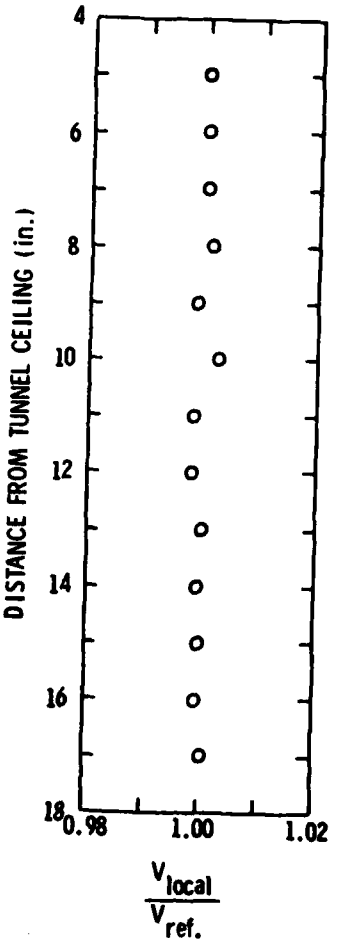

Figure 10. Velocity profile measured in the empty channel.

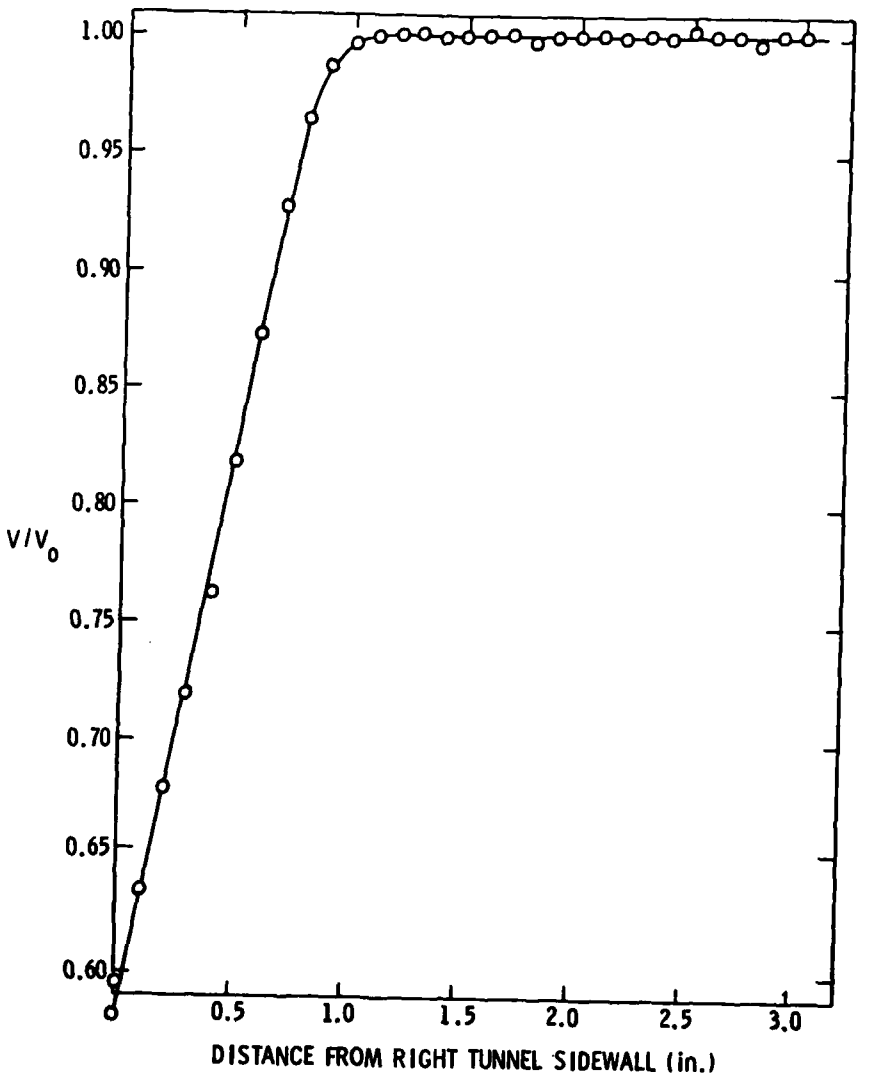

Figure 11A. Velocity profile measured near tunnel wall.

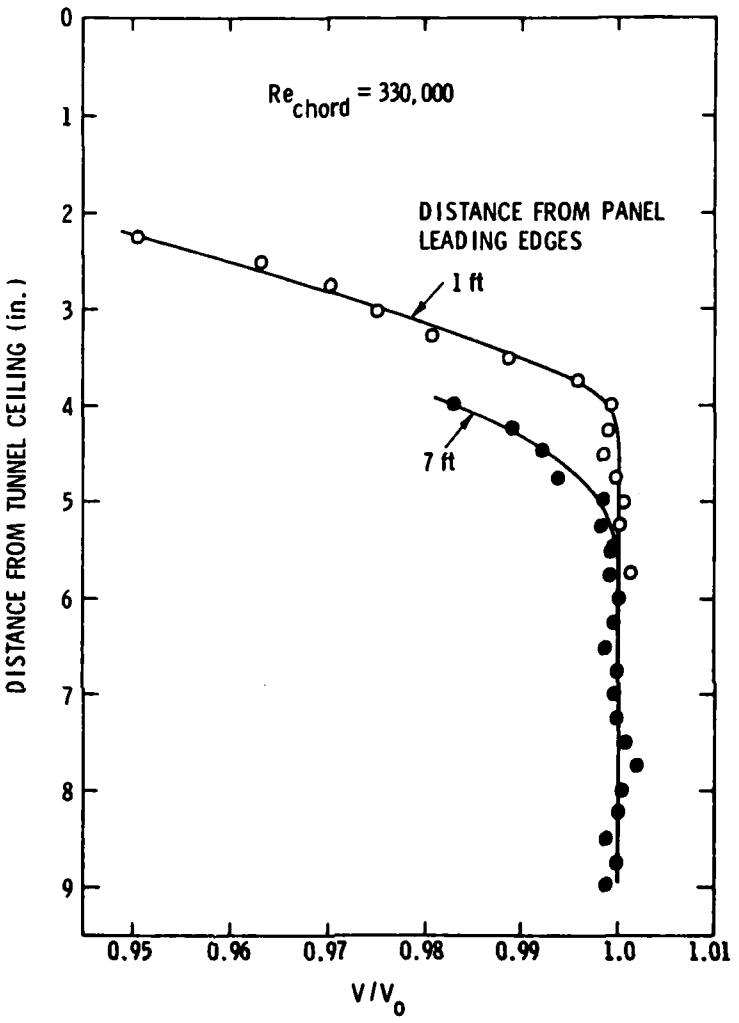

Figure 11B. Velocity profiles measured near tunnel ceiling. The traversable probe was mounted in the front and rear of the channel as shown to indicate boundary layer growth.

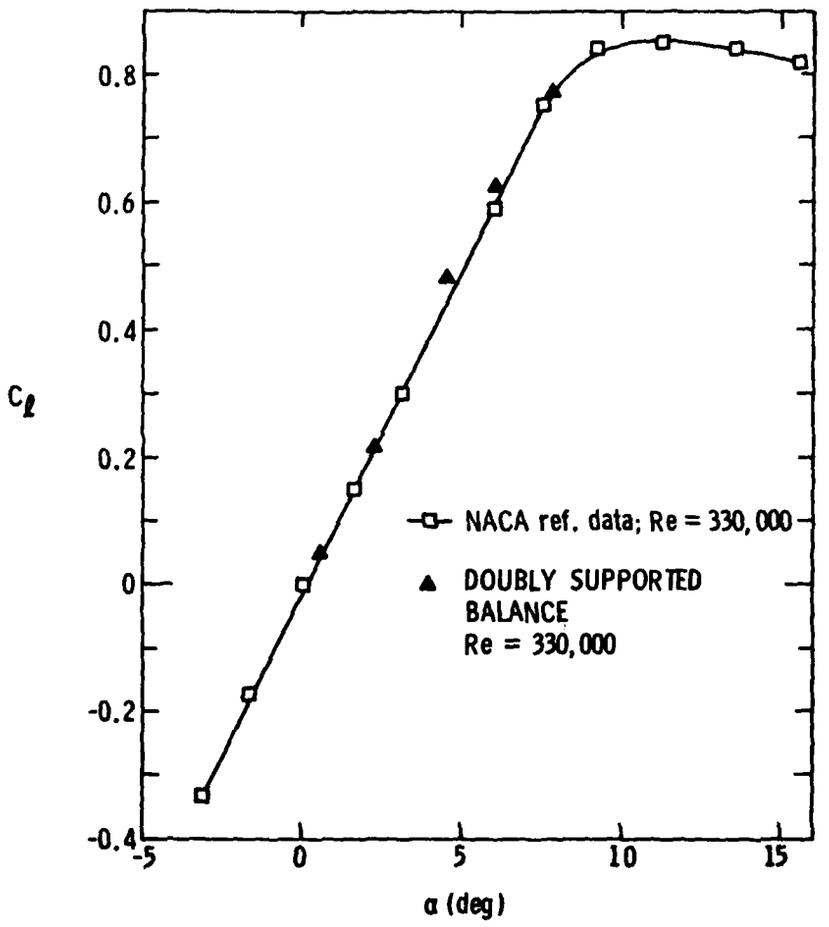

Figure 12. C_ℓ-versus-α results for doubly supported balance.

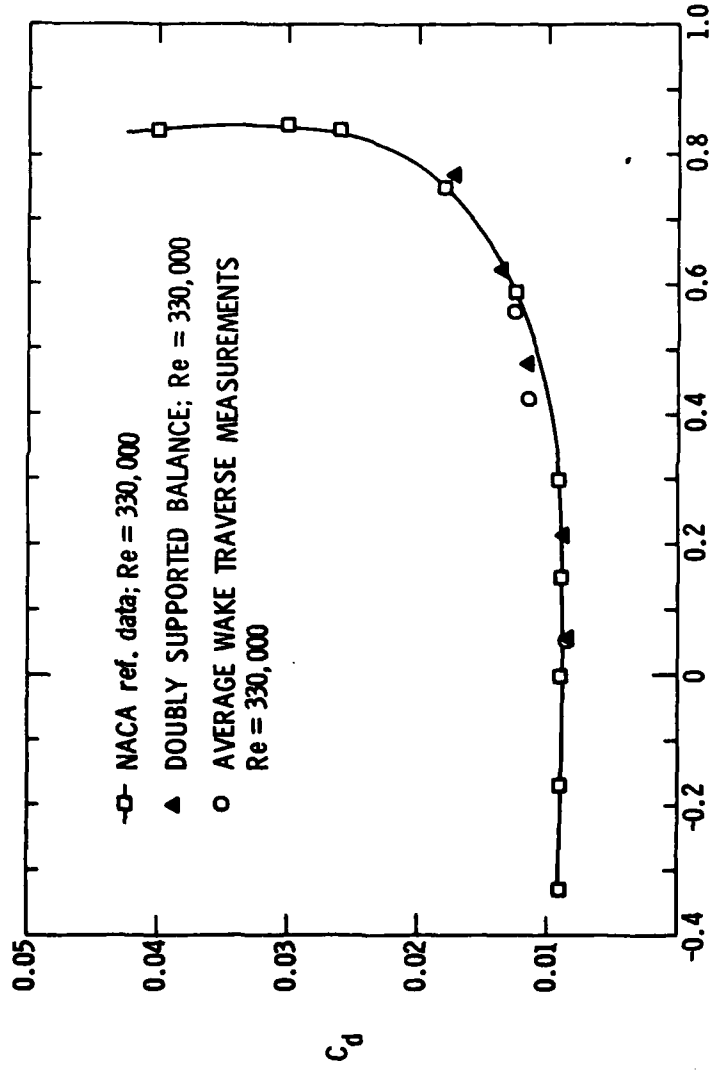

Figure 13. C_ℓ-versus-C_d results for doubly supported balance. Also shown are results of drag determined by momentum deficit technique.

integrating the results as discussed in Appendix B. A traversible total pressure probe was mounted in the tunnel one chord length behind the airfoil. A reference pitot-static tube was likewise mounted to a tunnel sidewall at the same downstream location. This enabled a ratio of local to free-stream dynamic pressures to be obtained. This spatial variation of pressure ratios is a function of the momentum deficit created by the model and, thus, a measure of the section drag coefficient at the particular spanwise location of the probe traverse. A typical wake profile is shown in Figure 14. Wake traverses were made for angles of attack of approximately 0^{o}, 4^{o}, and 6^{o}. The spanwise location of the surveys was also varied. Shown in Figure 15 are the results of the various surveys.

For direct force measurements with the doubly supported balance, the use of the previously mentioned interactive constants proved to be erroneous. The original mounting technique involved mounting the force cubes on each panel using a carpenter's level to assure proper vertical alignment. Known weights were then placed on the force transmitting shaft (simulating a "negative" lift) and drag voltages were noted. This spurious drag voltage would then be subtracted out of measured drag voltages during each test as a step in the data reduction process. The interactive constant would have to be recalculated each time the balance was remounted or adjusted on the tunnel wall. The results of this type of operation were unsatisfactory. Lift measurements were erratic and drag measurements were too large by one order of magnitude. It was ultimately decided to eliminate the interactive term by a different mounting technique. The cubes were adjusted (with the voltmeter operating) until an application of pure negative lift (by suspending known weights from the force transmitting shaft) resulted in a zero (or

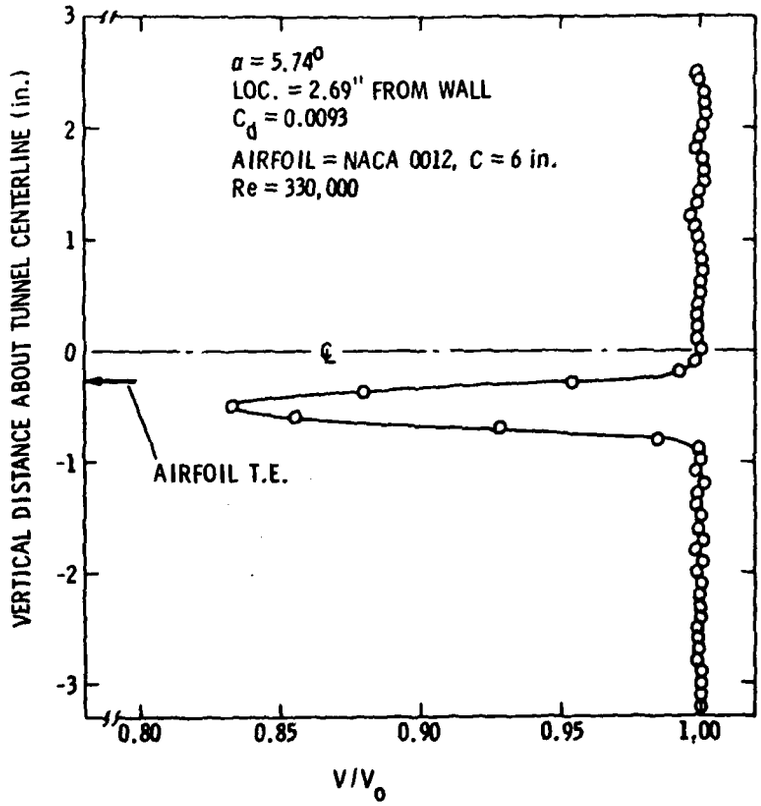

Figure 14. Typical wake profile.

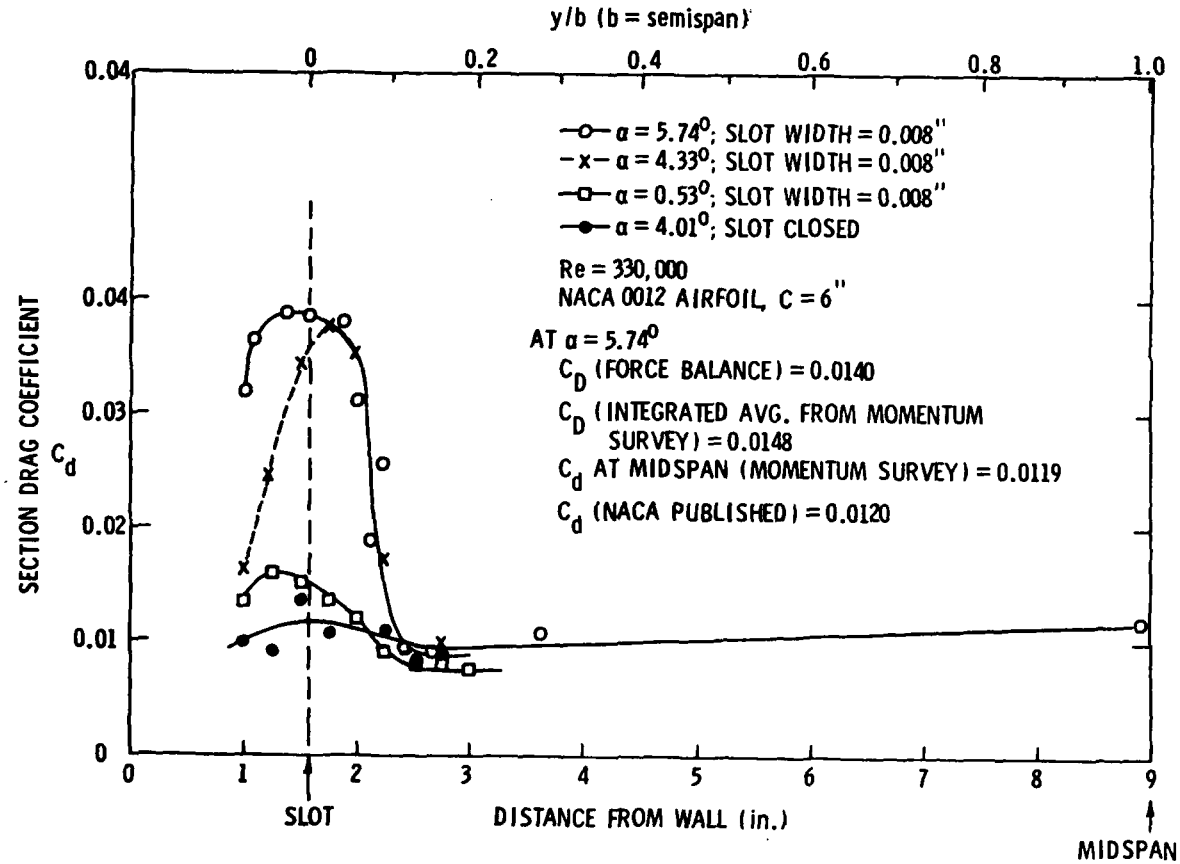

Figure 15. C_d-versus-span location; data by momentum survey technique (during doubly supported balance phase).

negligibly small) reading on the drag channel of the voltmeter. This technique resulted in a dramatic improvement in the accuracy of the readings.

Another technique that required attention was the method of measuring angle of attack. It became obvious that the angle of attack had to be measured as precisely as the various force coefficients. The ultimate technique for measuring the angle is depicted in Figure 16. A field artillery gunner's quadrant was used in conjunction with an airfoil template. The template was constructed so that it contacted the airfoil at the leading edge and at two other points on the airfoil's upper surface. The upper surface of the template was machined so that when the device was placed on the airfoil the machined surface was parallel to the chordline. The gunner's quadrant measures angles from the horizontal (using a bubble level) in mils (6,400 mils equals 360^{o}). This technique enables the angle of attack to be measured accurately to $\pm 0.056^{o}$.

3.3 Experimental Results from the Doubly Supported Balance

Shown in Figure 15 are several interesting results. For a given angle of attack, the section drag coefficient, C_d, as measured by the wake traverse increased in the vicinity of the slot between the model and the dummy airfoil sections. The magnitude of the increased C_d also appears to be related to the amount of lift being created by the model. The increased drag near the tip of the airfoil (slot region) is quite similar to the behavior reported by Otsuka and Sugiyama in Reference (6). The data of Figure 15 show that for values of y/b greater than 0.15 the effect of the tip gaps on C_d is negligible. As

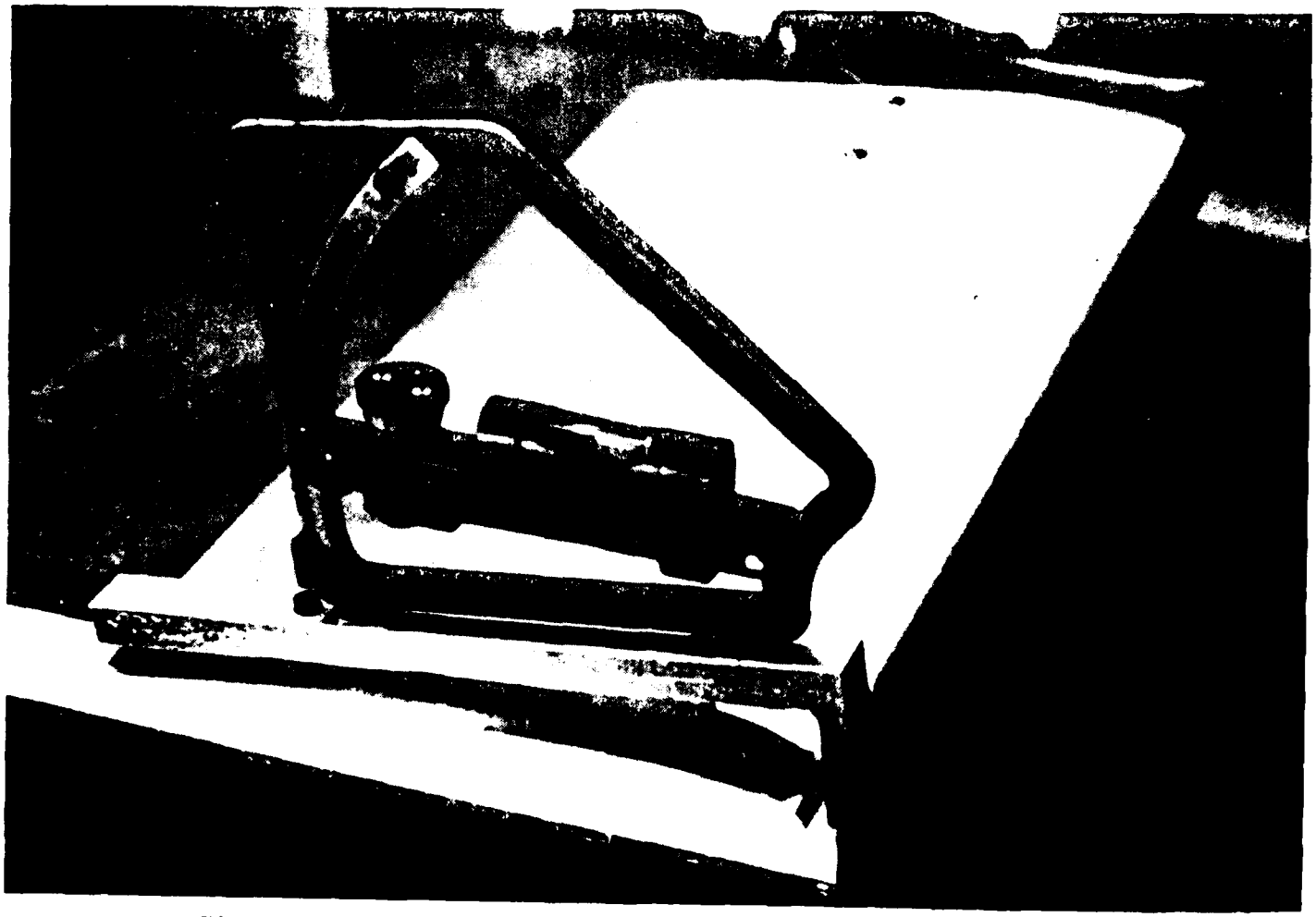

Figure 16. Angle-of-attack measuring technique showing artillery gunner's quadrant used with airfoil template.

the plot shows, for $\alpha = 5.74^{o}$ the section C_d measured at the mid-span position ($C_d = 0.0119$) is in excellent agreement with the NACA data ($C_d = 0.0120$). The area under the curve for $\alpha = 5.74^{o}$ was measured with a planimeter and normalized by the airfoil span. This gave a computed $C_d = 0.0148$, which is in good agreement with the balance measured $C_d = 0.0140$. This seems to indicate that the balance is measuring a total drag coefficient, C_D, for the airfoil which includes the effect of three-dimensional flow at the wing tips. The wing is considered to be that portion of the two-dimensional airfoil model excluding the two dummy airfoil segments.

Another interesting result is the shape of the wake behind the airfoil. Figure 17 shows how the wake profile takes on a double spiked shape approximately 0.5 in. inboard of the airfoil tip. This shape is most likely due to shed vorticity and further indicates an absence of two-dimensional flow conditions in this vicinity.

Lakshminarayana (8) conducted studies on the induced drag associated with a chordwise slot at the center span position of a single airfoil. He suggests the additional drag coefficient to be given by

$$C_{D_i} = 0.7\left(\frac{C_L^2}{AR}\right)\frac{\tau}{c} \quad , \tag{1}$$

where C_L = lift coefficient, AR = aspect ratio, τ = width of slot, c = airfoil chord, and C_{D_i} = increment of additional drag coefficient due to slot in airfoil.

A further correction was derived to account for the flow through the slot physically impinging on the force transmitting shaft. Assuming that flow through the slot is directed at a 45^{o} angle to the free stream

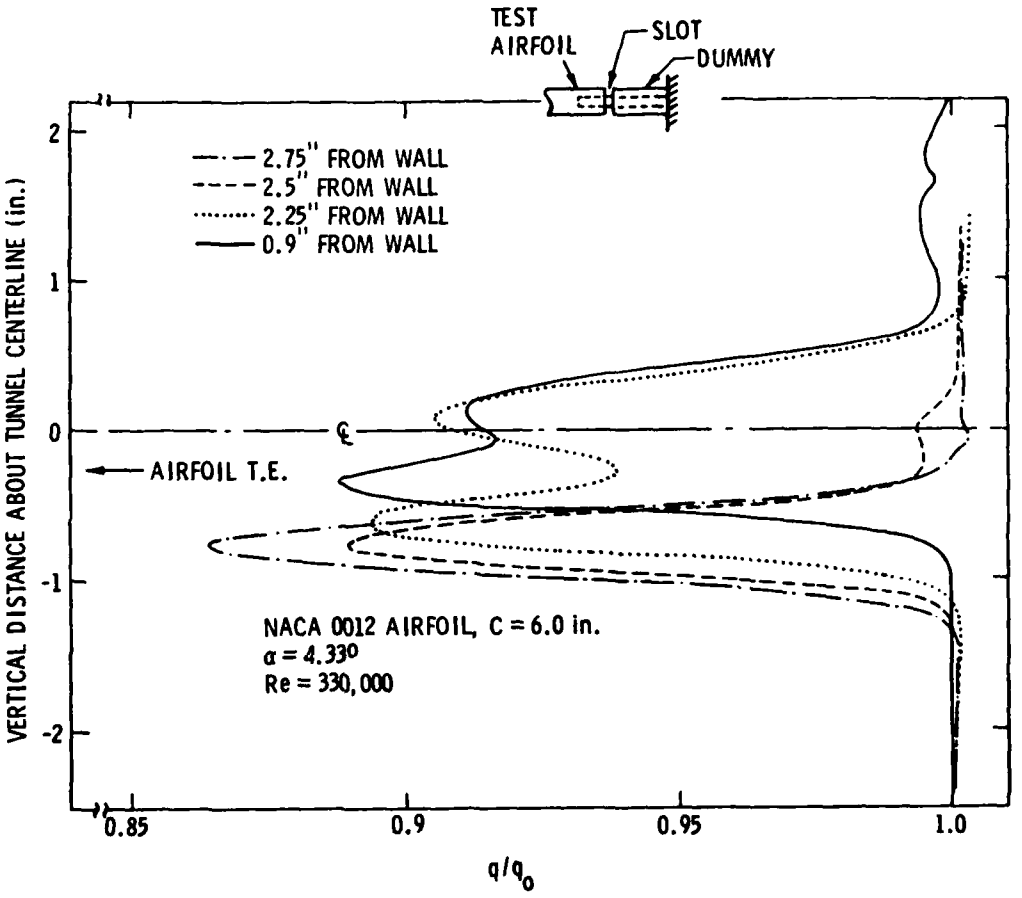

Figure 17. Wake profiles in vicinity of slot for doubly supported balance showing development of double-spiked profile. Also shown are approximate spanwise locations of traverses.

(flow visualization studies conducted by Lakshminarayana [8] indicate that this is a reasonable assumption), an additional component of drag due to dynamic pressure on the bar would be sensed by the balance.

$$\Delta C_D = \cos\theta(\text{nondimensional dynamic pressure on bar}) \quad , \qquad (2)$$

where θ is the angle of the resultant force (Figure 18). Setting C_d for a cylinder (bar) equal to 1.0, the drag component of force exerted on the bar becomes

$$\Delta(\text{Drag})_{bar} = \cos\theta(\tfrac{1}{2}\rho V^2)(\text{circumference of bar})(\text{gap width}) \qquad (3)$$

or

$$\Delta(\text{Drag})_{bar} = 2\cos\theta(\tfrac{1}{2}\rho V^2)(\pi d)\tau \quad , \qquad (4)$$

where d = diameter of shaft and τ = width of gap. The factor 2 is included because there are two slots, one on each end of the model. The work of Gearhart [9] suggests that flow through a narrow, sharp edged slot such as this should be modified to reflect an effective flow velocity rather than a theoretical velocity. Equation (4) then becomes

$$\Delta(\text{Drag})_{bar} = \cos\theta\rho(0.8V)^2\pi d\tau \quad , \qquad (5)$$

where V = the velocity flowing through the gap. There are several factors affecting the magnitude of this velocity: the pressure difference between the upper and lower openings of the slot due to the airfoil's suction and pressure sides, the incoming free-stream velocity, and viscous effects that occur with flow through a narrow slot. After

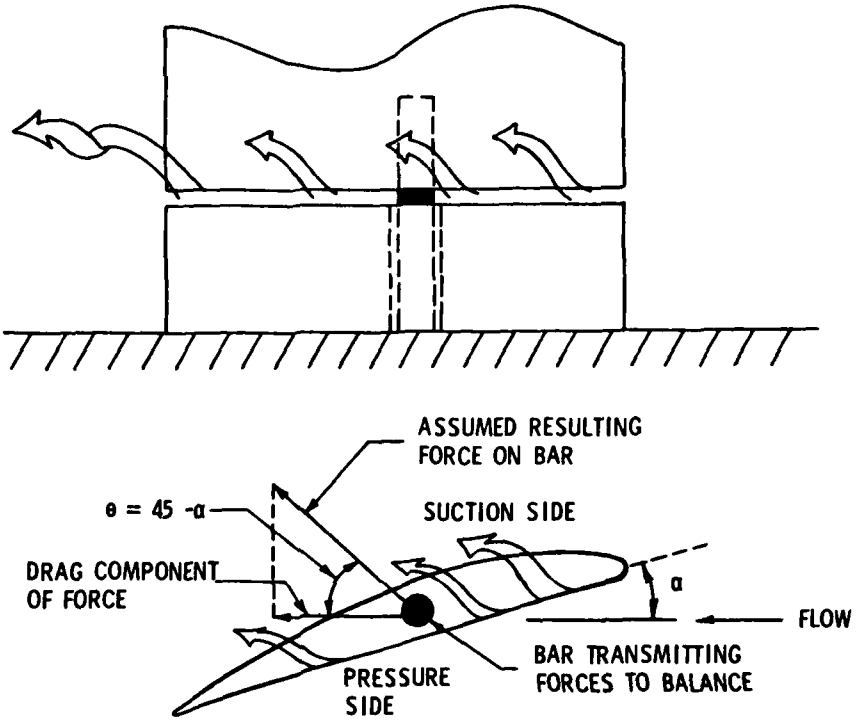

Figure 18. Illustration of possible spurious forces on shaft by flow through slot.

consideration of these effects, the magnitude of the velocity in the gap was assumed to be equal to the free-stream velocity. This value was a constant for all airfoil angles of attack and therefore the magnitude of the force vector acting on the bar was likewise. As shown in Figure 18, when α increases, the angle θ that the force vector makes with the free-stream decreases and the drag component of the force vector increases. In this manner, a drag component is created which varies with α and free-stream velocity.

Equations (1) and (5) were used to calculate a total added drag due to the chordwise slot and the bar. This added drag was subtracted from the balance readings for drag and corrected coefficients are shown on Figure 13. Also shown on the figure are three C_d values as measured by the wake traverse method. The traverses were done at the mid-span location of the airfoil for three different α's. The data of Figure 13 indicate that wake traverses for this size airfoil can give accurate C_d measurements. Further, this particular balance can be used to make accurate two-dimensional force measurements by applying suitable correction factors.

A final result of this phase of the program was the realization of the importance of model construction. The airfoil was examined and was found to have a varying thickness along the span. The thickness tapered 0.020 in. from tip to tip. Figure 15 reflects this fact in that the section drag coefficient gently decreases from mid-span to the point near the tip where slot effects begin to take over. There was also found to be a 1^{o} twist in the model from tip to tip. Since all angle of attack measurements were made from the "high" side of the model, 0.5^{o} was subtracted from each measured α to give an average total airfoil α.

3.4 Cantilever Balance Phase

The next phase of the program concentrated on duplicating the conditions encountered in the water tunnel. A two-component cantilever balance was designed and built which was similar in principle to the water tunnel balance. The balance and airfoils are shown in Figures 19, 20, and 21. The balance used the principle of a tension member as devised by Gurney (10). The tension member is a beryllium-copper strip of approximately 0.006 in. thickness. The functioning of the tension strip is illustrated in Figure 22. The outer two clamps fix the ribbon to one cube. The ribbon was clamped while under a tensile force greater than one-half the largest force that it would have to sense (in this case, 30 lb). The center clamp is fixed to the other force cube and is free to deflect in the direction of the long axis of the ribbon. As the cube which is fixed to the center clamp deflects under an applied force, one-half of the tension member experiences a greater tension and the other half experiences less tension because of the preload. The strain gages sense this and give a corresponding voltage which is calibrated for force. A second ribbon is clamped to a second cube at a 90^{o} angle to the first ribbon. The two force cubes effectively have one face in common. This design enables two forces to be measured which are acting normal to each other (i.e., lift and drag). The advantage of this system is that the cubes require very little clearance space to accommodate the small deflections. Tension members can also withstand much greater forces than the strain gage cube setup (of the doubly supported balance system) before deflection of balance parts becomes a problem. The resulting high sensitivity balance can then be designed very compactly.

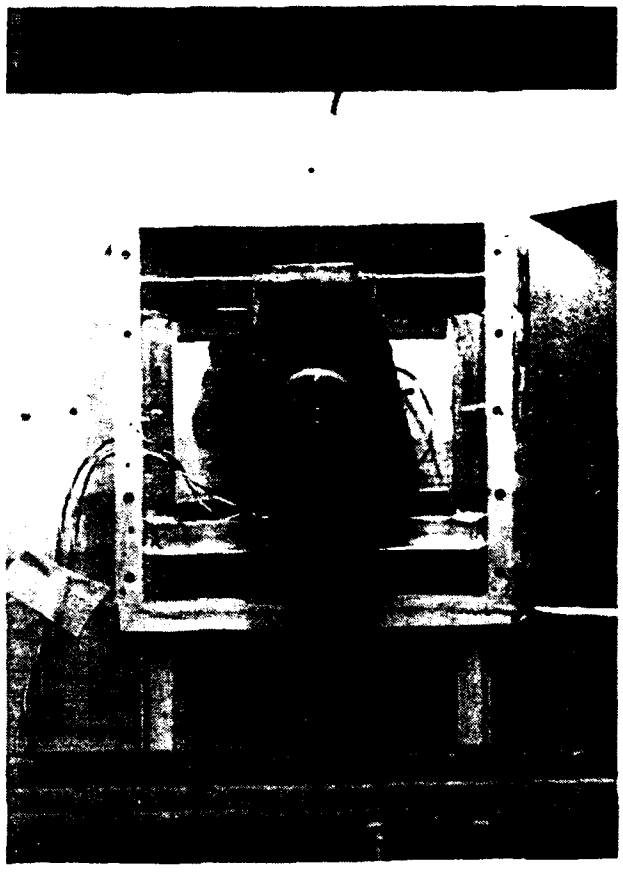

Figure 19. Cantilever balance installed on tunnel wall. Also shown are angle-of-attack indicator dial and wooden square frame which supports a cover. The cover shields the balance from air flowing between the two-dimensional channel wall and the octagonal wind tunnel wall.

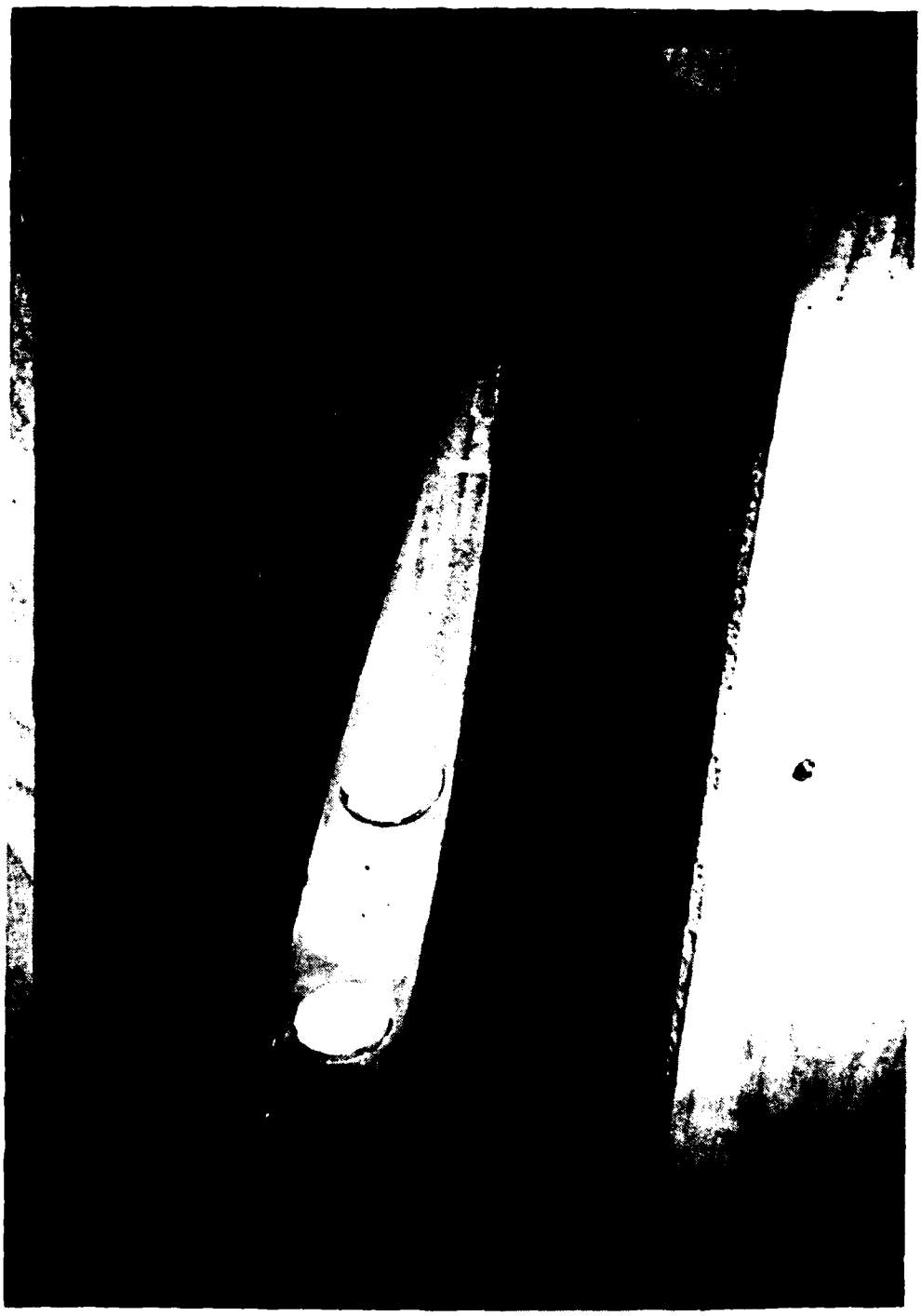

Figure 20. Airfoil with 18-in. chord and no disk mounted in wind tunnel.

Figure 21. Airfoil with 9-in. chord and 11-in.-diameter disk.

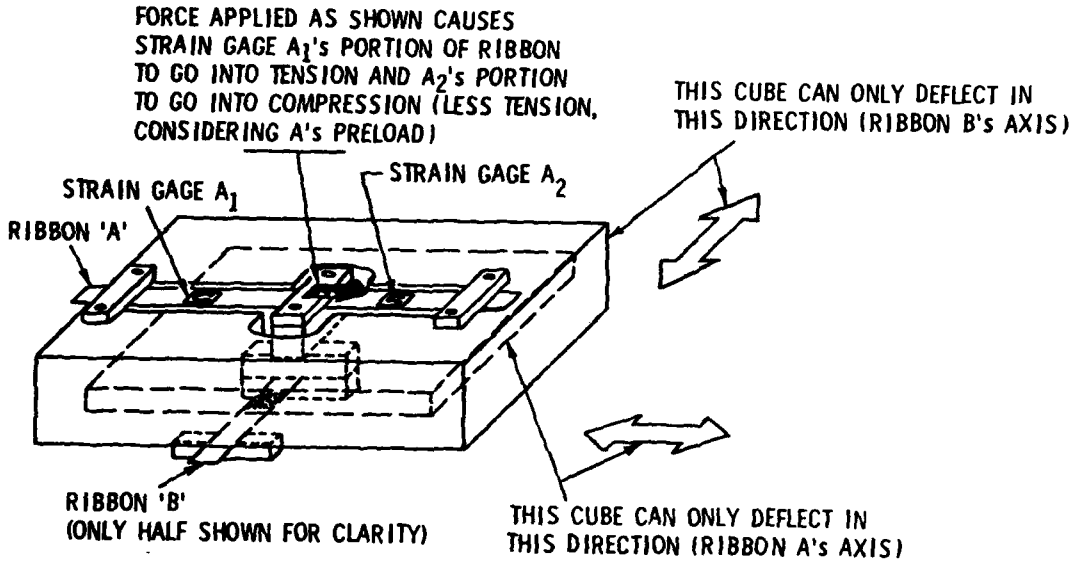

Figure 22. Simplified illustration of the manner in which the cantilever balance functions.

The balance and airfoil system is shown in simplified form in Figure 23. Originally, the balance was mounted so that the ribbons formed a 45^{o} angle with the free stream. This configuration was tried in an attempt to have each ribbon measure approximately the same gross force. In the doubly supported phase, the drag cubes measured forces of a lower order of magnitude than the lift cubes. It was theorized that this difference in the order of magnitude of the two forces could have been a source of the problem with the water tunnel balance. Ultimately, for reasons detailed in Section 3.5, the balance was aligned so that one ribbon measured normal forces and the other ribbon measured axial forces as depicted in Figure 23. The balance rotated with the model as angle of attack was changed.

Two airfoil models of different AR were then fashioned for use with the cantilever balance. A NACA 0012 airfoil was machined of aluminum. This model has a chord of 9 in. and a span of 18.375 in. for an aspect ratio of 2.04. The model weighed approximately 11 lb 14 oz. A second model was made of a two-part expandable urethane foam. A master airfoil was machined from aluminum (span = 18.375 in., chord = 18 in., weight = 40 lb). A high-strength mold was then made from this master. The two-part foam was mixed and poured into the mold. The foam expanded within the mold and gave a lightweight duplicate airfoil. Some shrinkage resulted from this manufacturing technique (approximately 0.001 in. per in.), but the finished product was considered quite satisfactory. The final model weight was approximately 10 lb 12 oz.

The calibration procedure for the cantilever balance was similar to that of the doubly supported balance. Each ribbon was calibrated with known weights after the balance was mounted in the tunnel. The

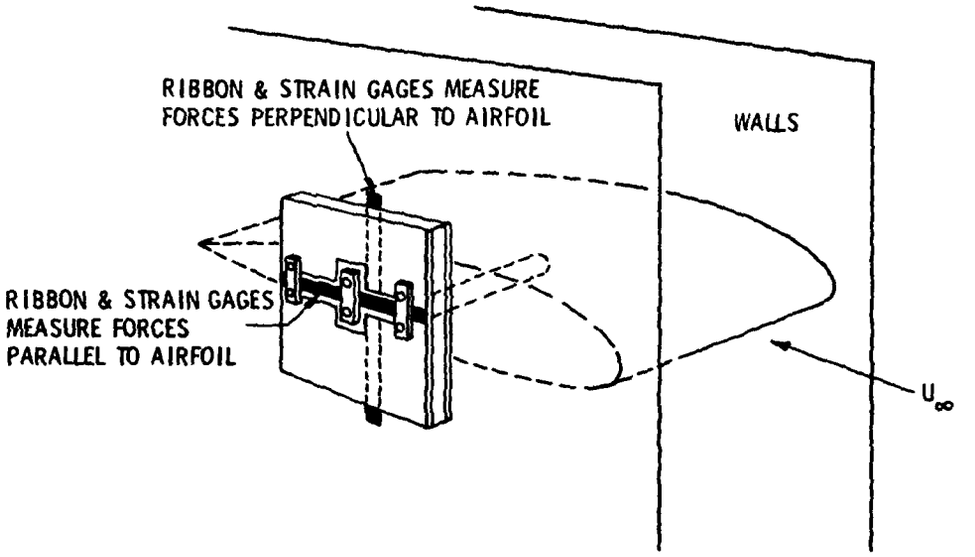

Figure 23. Simplified sketch of cantilevered balance. Balance mounts on tunnel wall. A shaft protrudes through the wall and is fixed to the tested airfoil. The balance rotates with the airfoil.

calibrations were performed after the interactive constants were electronically zeroed out in a fashion similar to that of the previous phase. Reduction of the raw data for this balance configuration is explained in Appendix C.

The first survey made in this test phase was a measure of the tunnel's static pressure gradient to determine the horizontal buoyancy correction. Static pressure taps were placed in one of the 4 ft x 8 ft panel walls at four axial locations. The taps were located 1, 3, 5, and 7 ft from the panel's leading edge and 1 ft from the panel floor. The results are shown in Figure 24. The airfoil was not mounted in the tunnel for these tests. Pressures are plotted versus channel position for four velocities as indicated. The pressures were nondimensionalized by dynamic pressure to give an average value of $(dP/d\ell)/q = 0.01236\ ft^{-1}$, where $dP/d\ell$ = static pressure change per unit length in channel $(lb/ft^2)/ft$ and $q = (1/2)\rho V_o^2$.

The balance was mounted 28 in. from the leading edge of the wooden panels. This position was chosen to ensure a thin incoming boundary layer. It was felt that the boundary layer could be thickened later for comparison testing. However, adding 2 in. of #100 sandpaper to the leading edges of the panels failed to make a significant change in the boundary layer thickness. After further consideration, it was felt that the balance should have been mounted farther downstream on the channel wall. This would have given leading edge disturbances more time and distance to grow into a thicker boundary layer. Results of the boundary layer surveys are shown on Figure 25.

The next step in the program was to mount the airfoil with the chord of 9 in. An 11-in.-diameter disk was also mounted on one end of

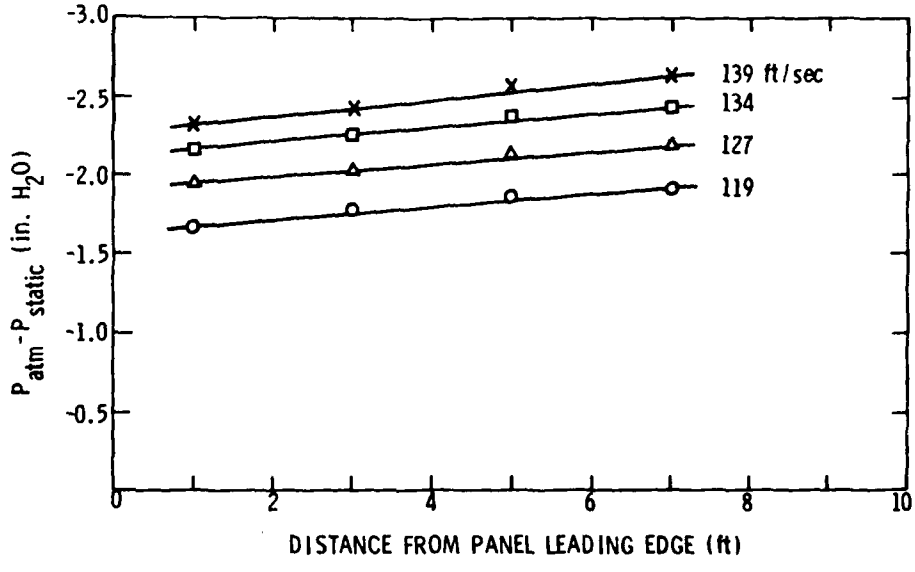

Figure 24. Static pressure gradient in open channel.

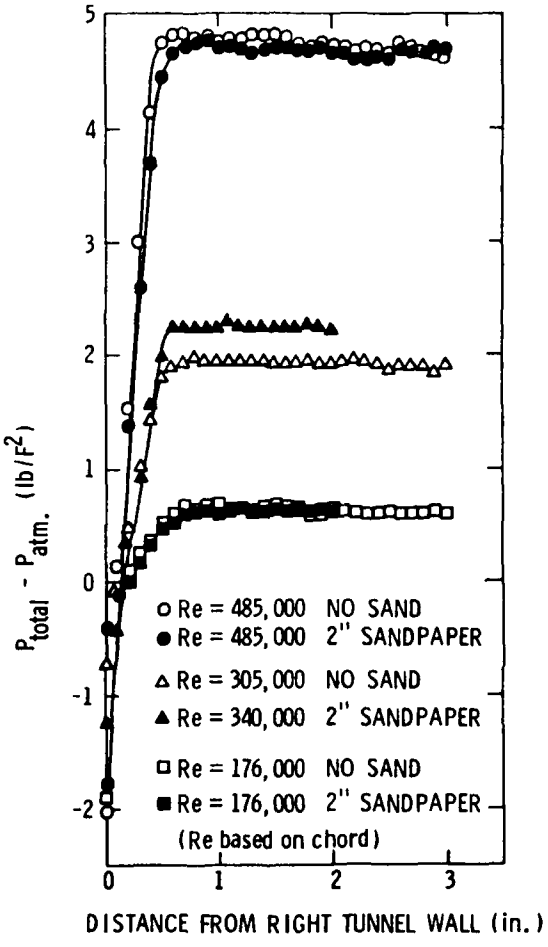

Figure 25. Boundary layer surveys with and without 2 in. of #10 sandpaper.

the airfoil simulating the spindle disk configuration of Kermeen. With the airfoil in place, wake measurements were made with the traversable probe as in the two-component balance phase. Several of the wake profiles are shown in Figures 26 and 27. The profiles show the double spike in the vicinity of the airfoil-wall intersection similar to that seen with the doubly supported balance. Figure 28 contains a plot of section drag coefficients, C_d, versus span location. The plots also indicate that beyond a certain spanwise location ($y/b > 0.22$ in this case) the effect of the tunnel walls on the probe C_d measurements is negligible.

The 9-in. airfoil-11-in. disk combination was then tested at various angles of attack. Next the disk by itself was mounted to the balance. The airfoil was mounted from the opposite side of the tunnel with a gap between the airfoil tip and disk of 0.004 in. In this manner, tare forces on the disk were determined. The tare forces were then subtracted from the total measured forces. The total forces, tare forces, and corrected data are shown in Figures 29, 30, and 31. The corrected data include the traditional corrections previously mentioned in connection with Kermeen's work.

The lift measurements obtained with the balance were combined with drag data measured with the traversable probe (for given angles of attack) and plotted in comparison with the NACA data, Figure 31. There is excellent agreement between the two sets of data. These two sets of data established a reference base for the determination of correction factors.

At this point, there existed an error in the balance-measured C_d which varied from zero to approximately 30% of the NACA reference data

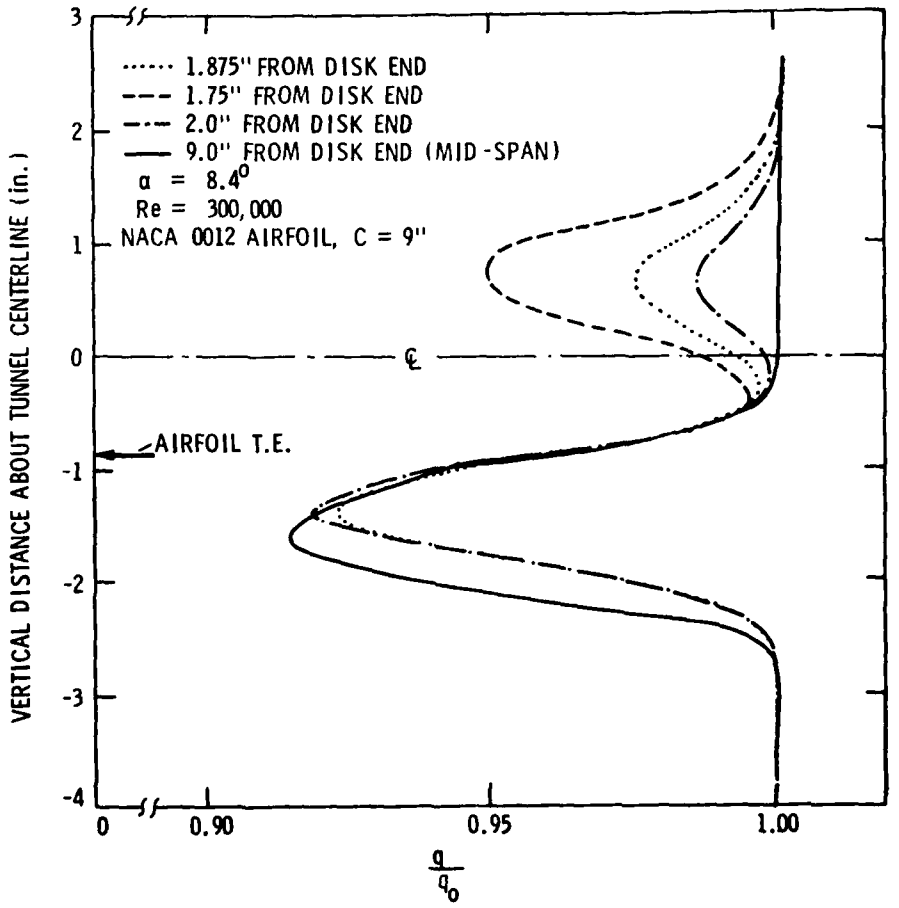

Figure 26. Wake profiles in the vicinity of the airfoil-disk intersection showing growth of a second wake behind airfoil upper surface.

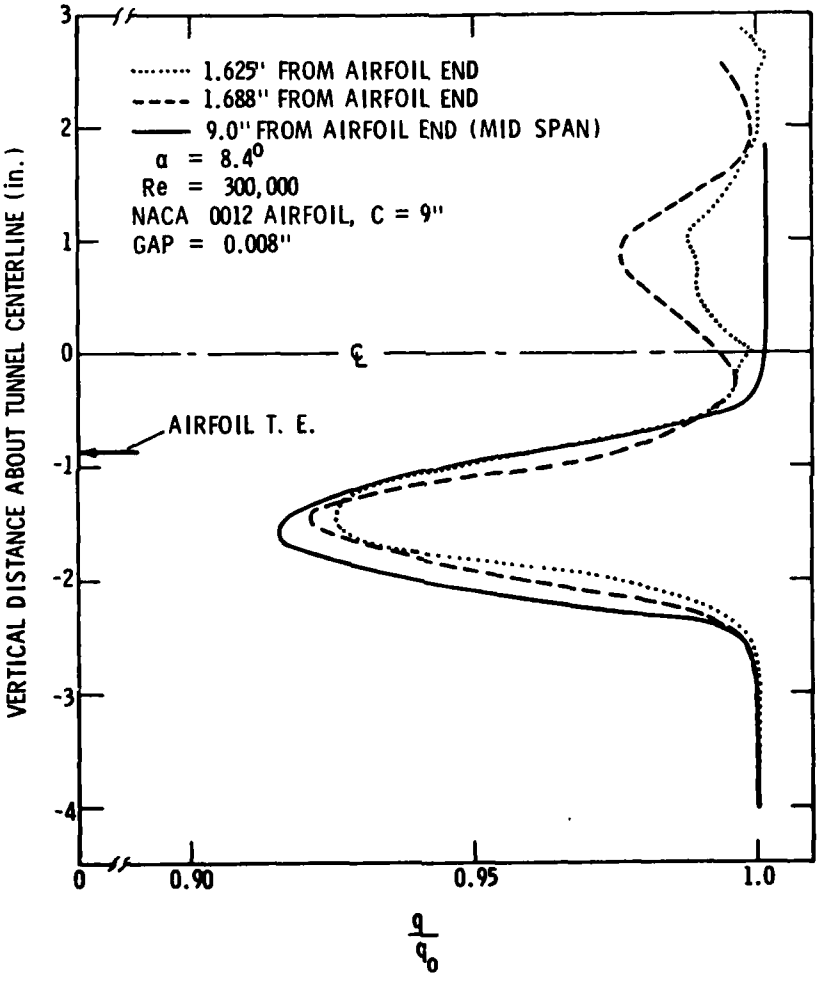

Figure 27. Wake profiles in vicinity of airfoil free (gap between airfoil and wall) end, showing growth of a second wake behind airfoil upper surface.

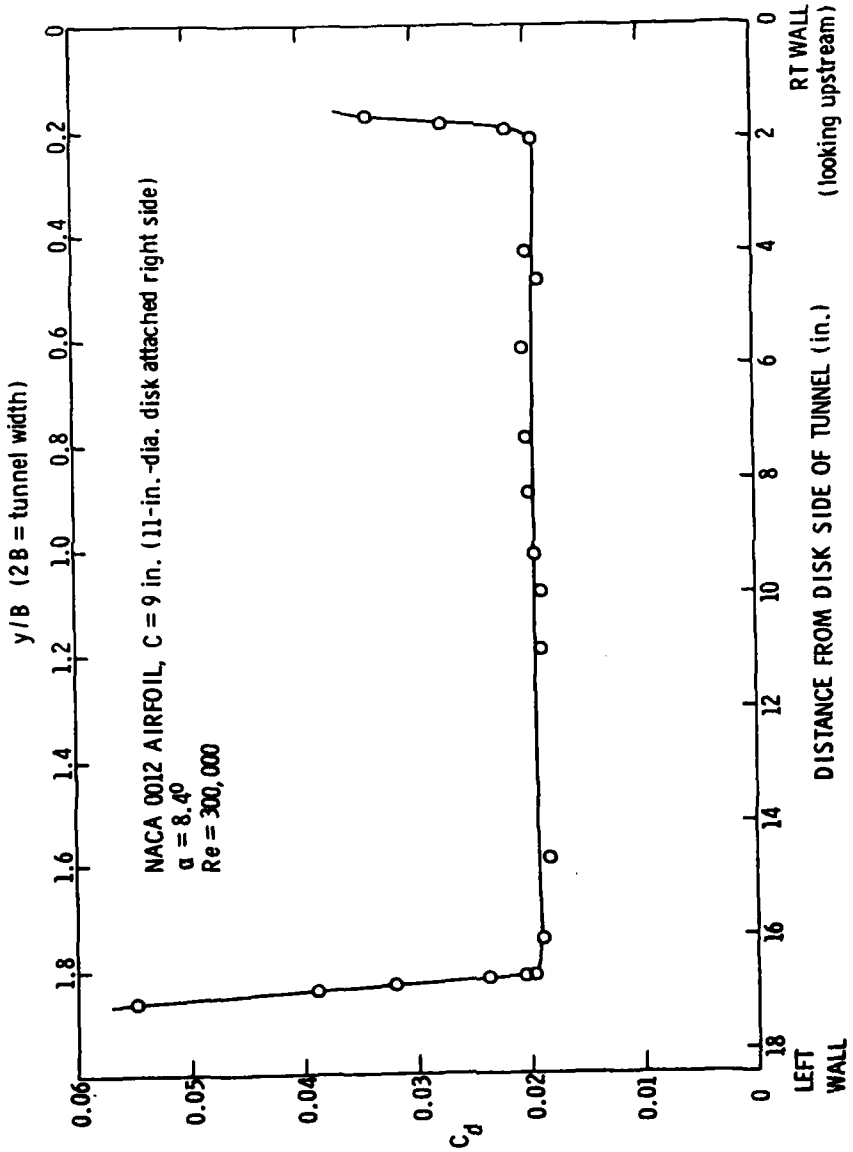

Figure 28. Section drag coefficients versus span location, momentum deficit technique.

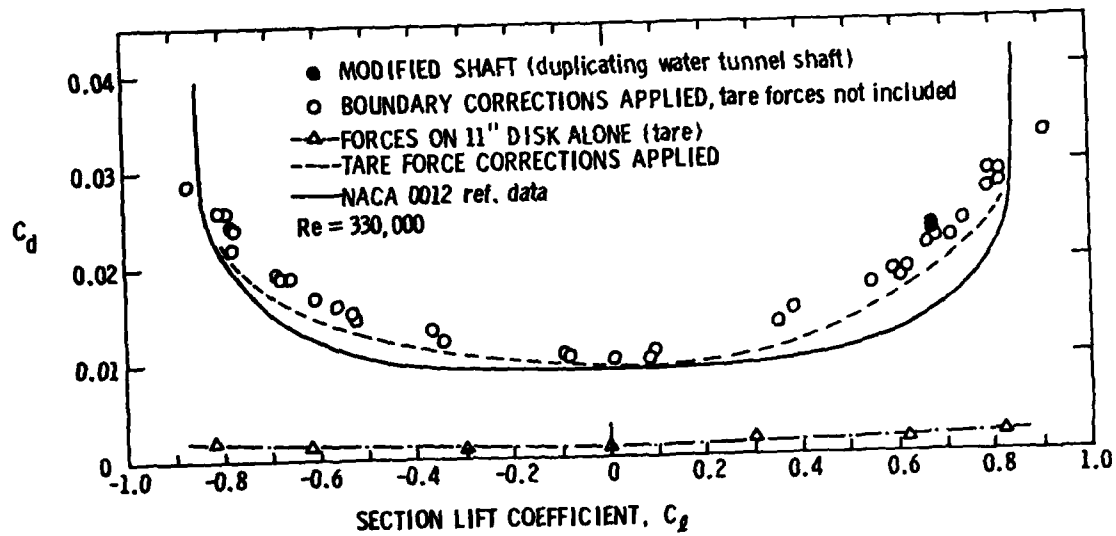

Figure 29. C_ℓ versus C_d for NACA 0012 airfoil with 9-in. chord and 11-in.-diameter disk attached. Tare forces on disk alone are also shown.

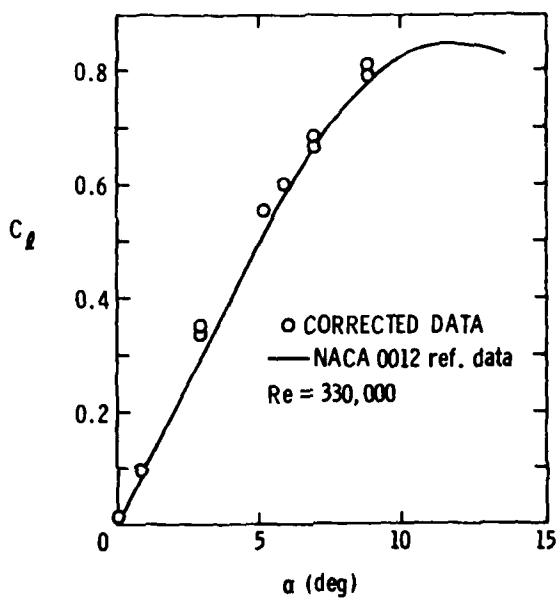

Figure 30. C_ℓ versus α for NACA 0012 airfoil, 9-in. chord with 11-in. disk attached. All corrections applied.

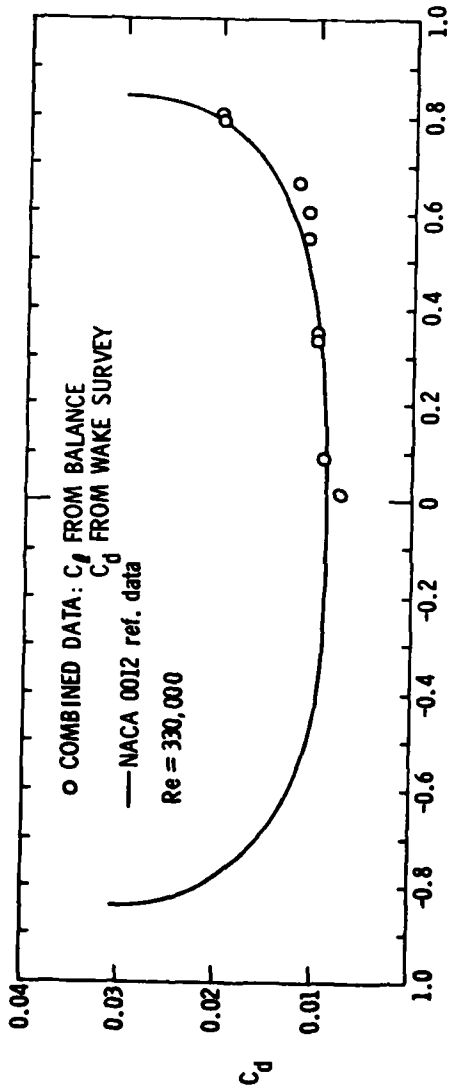

Figure 31. Comparison of NACA data with C_ℓ and C_d data taken by different techniques.

at the higher C_ℓ values (Figure 29). The error trend was similar in nature to that reported by Daily and Kermeen. The first attempt to deduce the cause of this error involved studying the effect of the gap between the airfoil tip and the channel wall.

A fiber optics instrument (Fotonic Sensor) was used to measure precisely the size of the airfoil tip gap. A probe capable of directing or detecting a small beam of light was imbedded in the tunnel wall. The light would be reflected off the aluminum airfoil tip and give an accurate measure of the distance between the probe (flush with tunnel wall) and airfoil tip. Using this technique, the gap was varied from 0.001 in. to 0.010 in. while maintaining an angle of attack of 5.9°. For this range of end gap, it was found that there are no significant effects on C_d measurement and that C_L values decreased by less than 1%. These data reinforce previous investigations (11) that, if the tip gap can be held sufficiently small, viscous forces predominate and the effect of the gap on airfoil forces becomes negligible.

In an attempt to determine the importance of the disk size, the 9-in. chord model was tested without an attached disk. The results are shown in Figures 32A and 32B. Data taken with a disk attached to the 9-in. airfoil and tare forces subtracted are also shown for comparison. C_ℓ tare forces due to the disk were negligible and are not included in Figure 32A. The traditional buoyancy and blockage corrections have been applied. As Figure 32B shows, the disk does not appear to be essential. This is important information from a manufacturing standpoint.

At one point, the C_ℓ-versus-α curve showed a peculiar behavior. Near $C_{\ell_{max}}$, the C_ℓ values showed evidence of a sharp stall which was not in agreement with the NACA data (the open squares in Figure 33). The

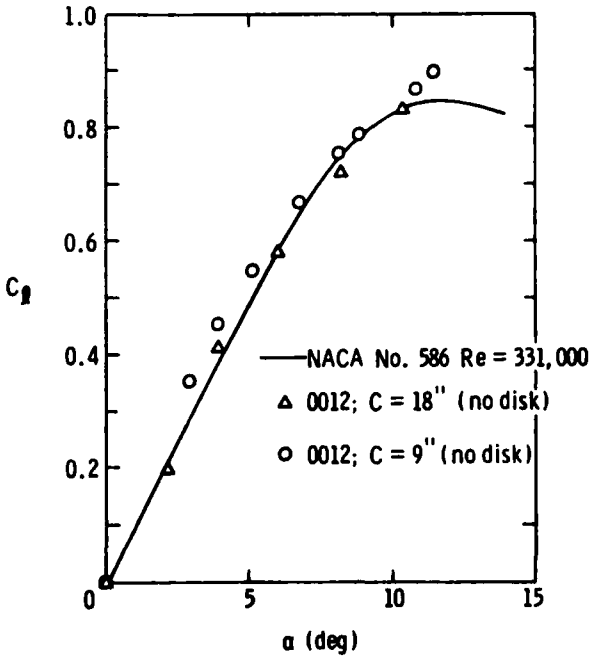

Figure 32A. C_ℓ versus α (corrected) for 18-in.- and 9-in.-chord airfoils without disks.

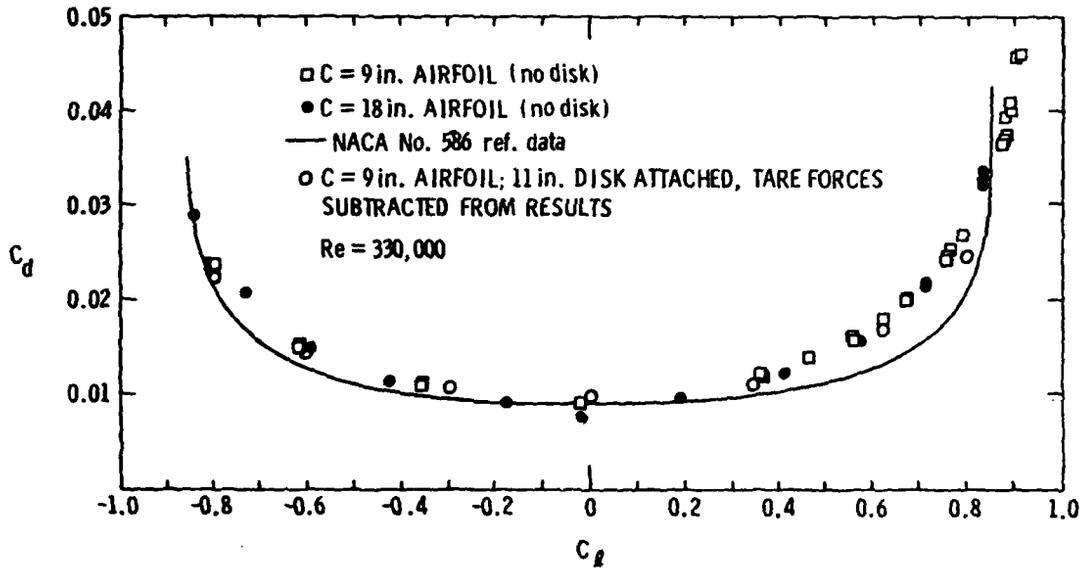

Figure 32B. C_ℓ versus C_d (traditional corrections only applied) for 9-in. and 18-in.-chord airfoils without disks. Also shown are data for 9-in.-chord airfoil with disk attached and disk tare forces subtracted from measured results.

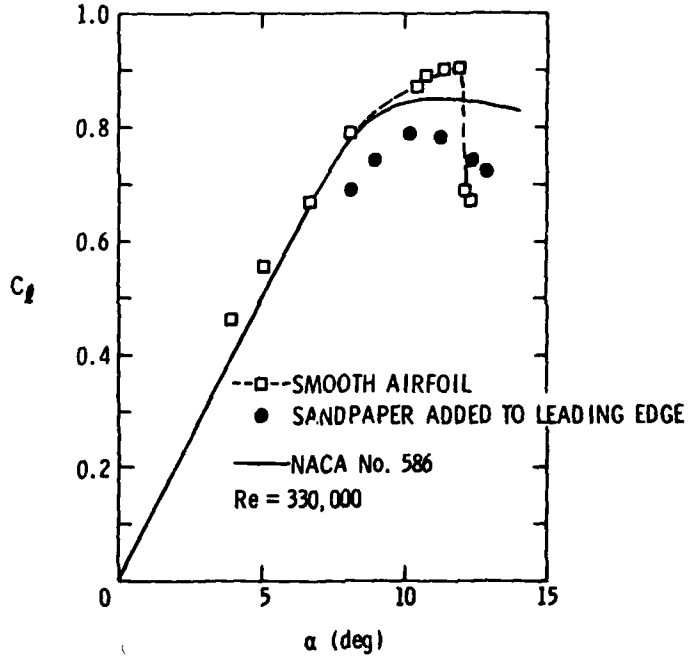

Figure 33. C_ℓ versus α for 9-in.-chord aluminum airfoil with and without sandpaper on leading edge. The graph indicates that laminar separation causes sharp stall characteristics.

smooth finish on the aluminum model suggested that possibly laminar seperation was occurring. To investigate this, a 1/4-in. strip of #100 sandpaper was glued to the leading edge of the airfoil to trip the boundary layer. The C_ℓ-versus-α curve was then "smoothed out" to the appropriate shape as shown by the solid circles in Figure 33. The C_ℓ values were lower due to the sandpaper, but the behavior of the curve in the stall region proved that laminar separation had occurred.

In a further attempt to discover the source of additional drag readings, the flow on the spindle side of the airfoil was considered. It was felt that there was a possibility that at high C_ℓ's the flow could be drawn through the gaps between the model tips and the tunnel walls. On the balance side, this flow could be directly impinging on the force transmitting bar and causing the balance to read slightly higher values. This is the same condition considered in the doubly supported balance phase. To find out if this force was significant, a stub spindle arrangement was fashioned as depicted in Figure 34.

The test setup was designed to measure only spurious drag readings. The test was further designed to determine whether this type of additional drag was of a sufficiently large magnitude to explain the behavior of the original water tunnel balance. The airfoil was mounted from the opposite wall of the tunnel as in the previous tare tests. A stub spindle which protruded 0.020 in. into the airstream was attached to the balance (Figure 34). A continuity tester with leads attached to the airfoil and balance was used to keep the gap between the stub and the airfoil as small as possible. Under these conditions, air flows in the vicinity of the model-wall intersection are closely duplicated and the balance measured only the forces exerted on the shaft. The drag forces

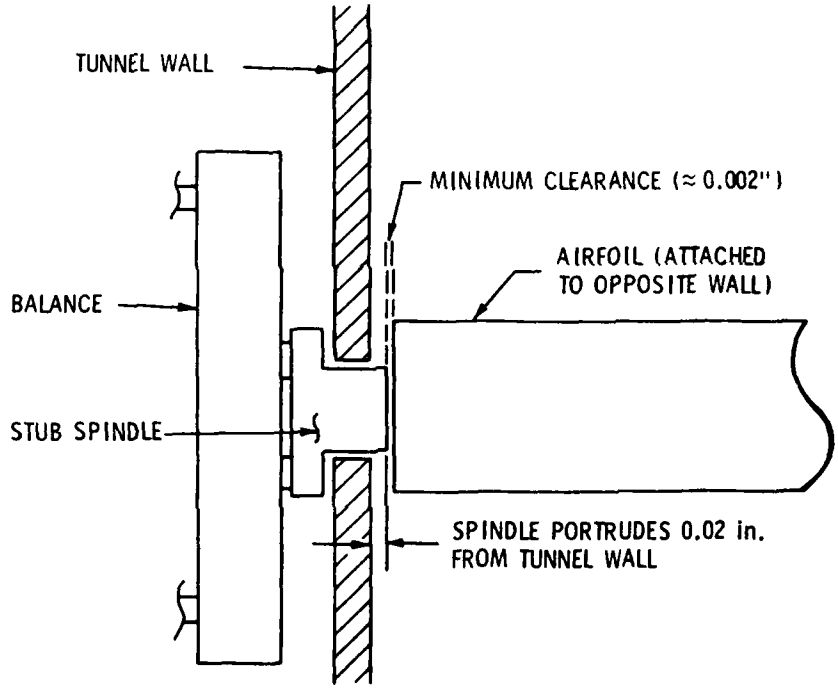

Figure 34. Stub spindle setup to determine forces acting on force transmitting shaft by flows through end gap.

were nondimensionalized by the airfoil planform area so that the resulting C_D increment could be subtracted from the model C_D. The results are shown in Table 1.

As shown in Table 1, small amounts of drag were measured by the balance. The value of this drag increment increased with angle of attack. Based on this information, it was then felt that the shaft-airfoil junction should be made to duplicate more closely that used in the water tunnel. The hydrofoil-shaft arrangement used in the water tunnel is shown in Figure 35. At the point of attachment, there was a 0.090-in. gap between the plane of the smooth face of the shaft and the hydrofoil tip. This meant that the force transmitting shaft was effectively a long rectangular shaped beam. It was theorized that this broad beam lying in the end gap flow could result in large measured drag increments. The wind tunnel model was modified as shown in Figure 36. A wooden spacer made the shaft diameter larger, and the area between the larger shaft and airfoil was waxed-in to duplicate the 0.090-in. standoff of the water tunnel model. This configuration (Figure 36) was tested at $\alpha = 7^{o}$. The amount of spurious drag sensed obviously did not cause the drag measurement to vary by an order of magnitude. Therefore, the flow impinging on th force transmitting shaft was ruled out as a major source of error.

The final portion of the experimental phase was the testing of the large airfoil (chord = 18 in.). This test was conducted without a disk on the balance end of the model. The results are shown in Figures 32A and 32B.

TABLE 1

Drag Increment Measured by Cantilever Balance on Stub Spindle of Figure 34.

Re = 18,330 (based on spindle dia = 0.5 in.)

α (deg)	C_d (based on c = 9 in.)
0.0	0.00001
7.1	0.0002
7.77	0.00055
8.9	0.0008
10.8	0.0013

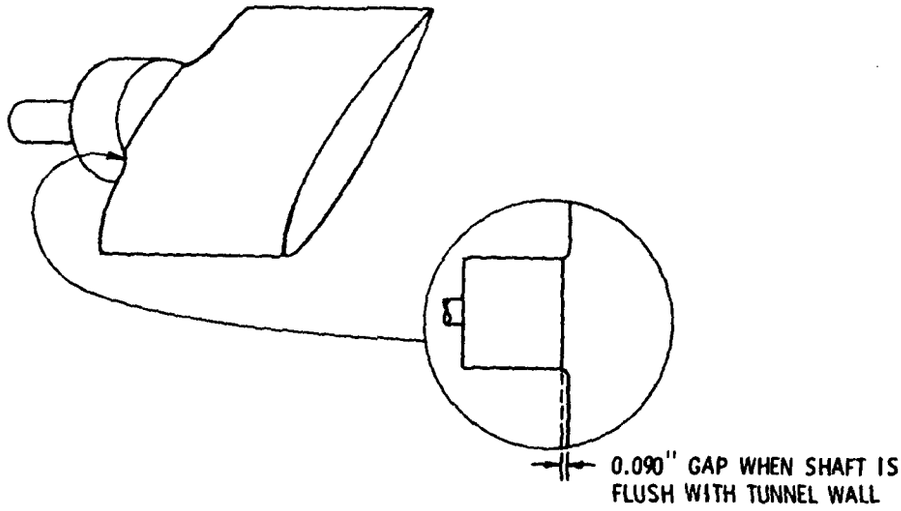

Figure 35. Water tunnel shaft and hydrofoil as used in experiments. Inset illustrates gap that existed on balance side of hydrofoil.

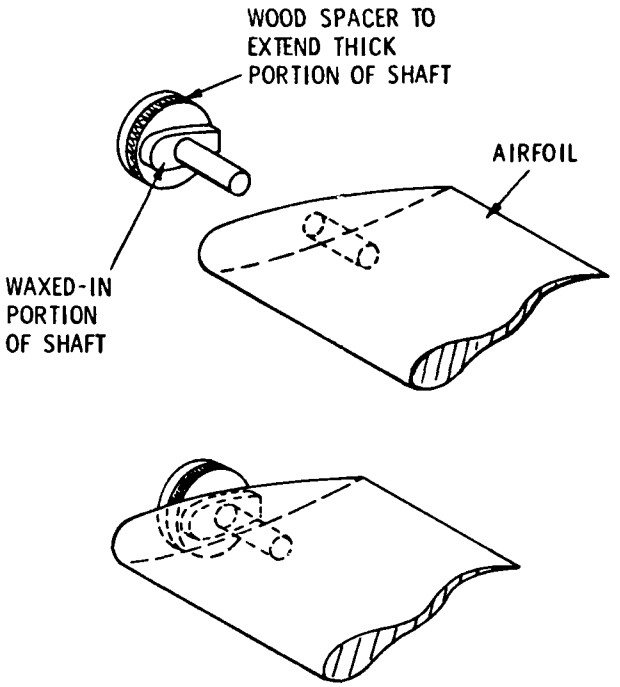

Figure 36. Modification applied to wind tunnel airfoil to duplicate configuration of water tunnel hydrofoil and shaft of Figure 35.

3.5 Experimental Results for Cantilever Balance Phase

Results from this phase of the experiments indicate that the mounting of this type of balance is critical. At the higher angles of attack, the ratio of lift force to drag force becomes very high. The drag force appears to be too small to measure as the difference or sum of two small numbers. When the balance was mounted with the ribbon at a 45^{o} angle with respect to the free stream, the axial force was shared between both tension members. When the balance was remounted so that one tension member measured all of the axial force and the other tension member measured all of the normal force, the results were dramatically better.

Another significant result stems from the Fotonic Sensor tests. The data indicate that within a certain range the size of the gap between the airfoil tip and tunnel wall has a negligible effect on C_{ℓ} and C_{d} measurements.

The idea of using a disk on the balance end of the model yielded interesting results. Experimental data on tests with and without the disk indicate that the inclusion of the disk is not necessary. This is from an aerodynamic standpoint, however. Use of a disk to facilitate making angle-of-attack changes, aiding in alignment, etc., may be desirable from a hardware design standpoint.

Another interesting result concerns the effect of aspect ratio. The airfoil of 9-in. chord had an aspect ratio of 2. The 18-in. airfoil had an aspect ratio of 1.0. From the experimental data (Figures 32A and 32B), the effect of aspect ratio variation appears to be small (at least for these two AR's).

CHAPTER IV

ANALYSIS AND DISCUSSION

As the experimental results demonstrated, measuring C_ℓ and C_d seperately (by the most accurate technique for each) and combining the results produced a satisfactory reference curve. Data generated in this manner were in good agreement with the NACA data. In order to make the balance system an accurate, two-dimensional force measuring device, a correction must be derived to account for the difference between the reference C_ℓ-versus-C_d curve and the balance-produced curve.

The difficulty in making mechanical balances perform accurately is the drag measurement. For a given airfoil operating at normal angles of attack, drag forces tend to be much smaller than the corresponding lift forces. In both the water tunnel and the wind tunnel, when the balance was set up to measure drag or axial forces by combining the output of two measuring elements, the drag results were in error by an order of magnitude. Reorienting the wind tunnel balance so that one measuring element measured normal forces and the other element measured axial forces, with no interactive terms, brought the drag data into the regime achieved by previous authors. A simple reorientation of the balance did not achieve the same results for the water tunnel balance. However, the water tunnel balance had problems with visible deflections of the model when the balance was in the most favorable (from a drag measurement standpoint) orientation.

Assuming the proper balance orientation had been selected, there was still an increment of drag to be accounted for. An increment of drag varying from zero at $C_\ell = 0$ to approximately 35% (or greater) of the published NACA value at higher C_ℓ values was reported by Kermeen and Daily in their tests of a NACA 4412 airfoil. The same general behavior of C_d was found in the results of the present report for a NACA 0012 airfoil. Since this behavior is found in mechanical balance experiments only and mechanical balances measure the forces created by non-two-dimensional flows on the model, it was assumed that the additional C_d increment documented in the three reports was due to non-two-dimensional flow effects on the model.

It has long been known that, when a strut intersects a flat surface in the presence of a nonuniform flow, secondary flows are created. In the case of an airfoil completely spanning a channel, the boundary layer on the tunnel sidewall causes a so-called horseshoe vortex to be formed which engulfs the airfoil-wall intersection. See Figure 37. This horseshoe vortex is a region of "contaminated" flow in that two-dimensional flow conditions do not exist there. In order to correct the balance measurements to two-dimensional forces on the hydrofoil, this contaminated region must be accounted for.

There are several methods of dealing with secondary flows of this nature. Suction or blowing devices can be installed which will physically remove the sidewall boundary layers. Removing the boundary layers eliminates secondary flows and enables the balance to measure forces that exist on a model immersed in purely two-dimensional flow. Another approach is to permit the model to experience the secondary flows and apply a theoretical or empirical correction to the data. Since suction

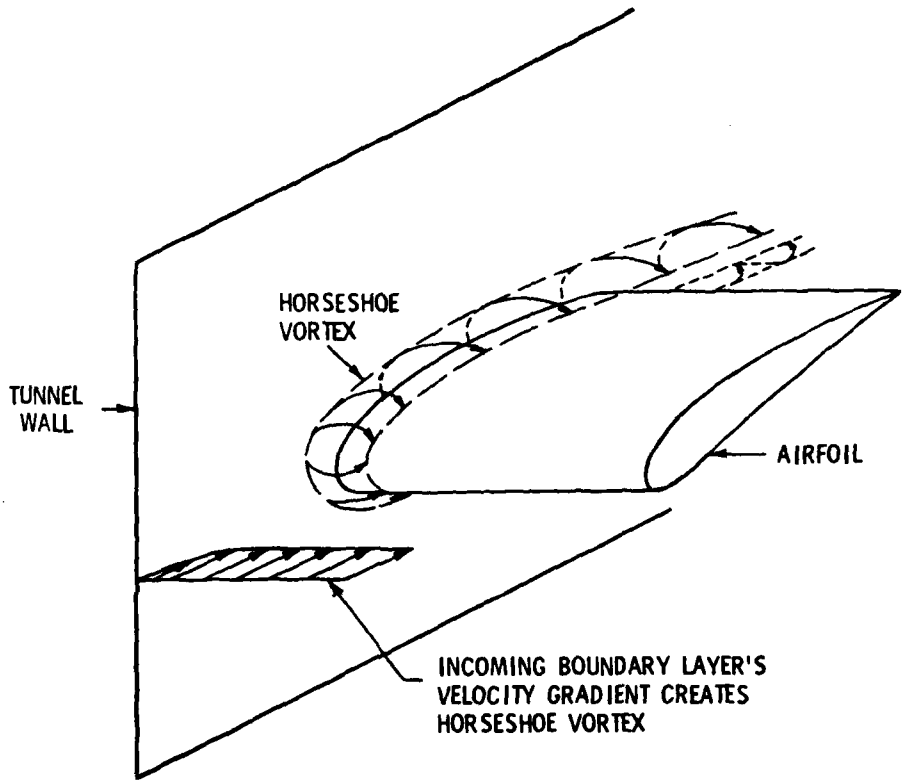

Figure 37. Horseshoe vortex created by intersection of velocity gradient and curved airfoil surface protruding from tunnel wall.

or blowing can lead to excessive cavitation in water tunnels, the use of a correction factor is preferred. To facilitate deriving a correction factor, some insight into the physical mechanism causing the additional drag associated with secondary flow must first be obtained.

An interesting study of this problem was recently completed by Barber (12). He considered the additional drag created by a strut protruding from a wall for various incoming boundary layer thicknesses. He found that the size of the horseshoe vortex varied directly with the thickness of the incoming boundary layer. He also found that the portion of the airfoil where flow separation occurred varied inversely with the size of the horseshoe vortex. He concluded that with a large horseshoe vortex viscosity caused high momentum fluid to be entrained in the corner where the airfoil trailing edge and wall intersected as shown in Figure 38. This influx of high momentum fluid enables the flow better to withstand the adverse pressure gradient existing in the corner and retards flow separation. As the figure shows, a thin vortex is not able to entrain as much of the high momentum fluid and a larger separated zone exists. Barber made numerous flow visualization experiments to verify the existence of this flow condition.

Assuming that the separated region near the trailing edge of the airfoil-wall intersection is responsible for the increment of additional drag measured, one can link a correction factor to the thickness of the incoming boundary layer. Support for this idea comes from the work of Hawthorne (13).

Hawthorne derived the following expression for the energy in secondary flows, D_e^*, created by strut-wall intersections:

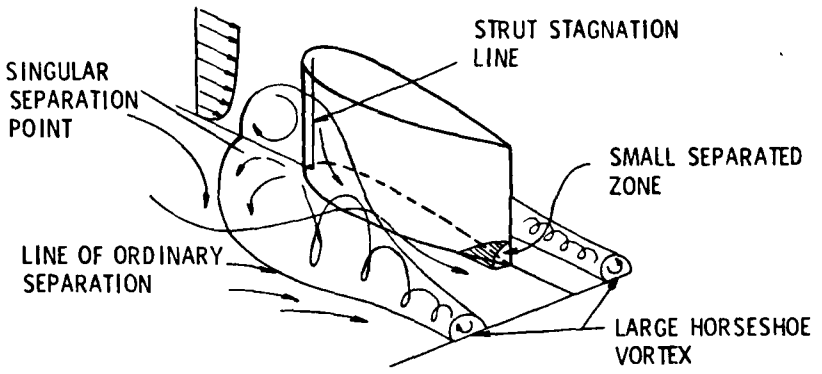

PROPOSED MODEL OF THICK BOUNDARY-LAYER-STRUT INTERACTION

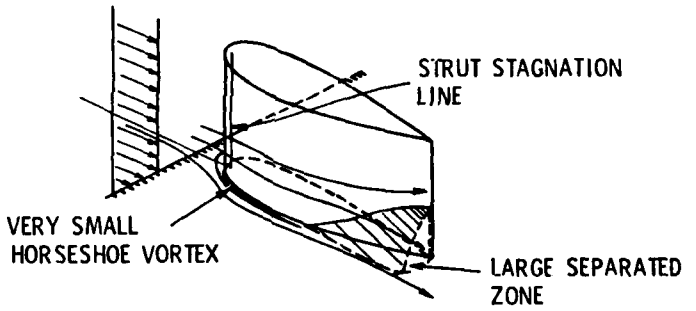

PROPOSED MODEL OF THIN BOUNDARY-LAYER-STRUT INTERACTION

Figure 38. Barber's model for the flow conditions occurring in the vicinity of an airfoil-tunnel wall intersection. Reproduced from Reference (12).

$$D_e^* = \frac{144\left(U_o^2 c^2 (t/c)^4 f(n)\right)}{25\left(1 + (1/2)(t/c)^2\right)} \quad , \tag{6}$$

where

$$f(n) = \frac{n^2}{1 + n^2} \frac{2}{\pi} \left(\frac{\pi}{4n}\left(\frac{n^2 - 1}{n^2 + 1}\right)^2 + \frac{1 - n^2}{(1 + n^2)^2} \log_e n \frac{1}{1 + n^2}\right) - \frac{1}{4n} \tag{7}$$

and ρ = density, U_o = free-stream velocity, c = chord, t = airfoil thickness, and $n = 4\left(1 + (1/2)(t/c)\right)/\left(15\pi(\delta/c)\right)$. Hawthorne shows how f(n) varies with boundary layer thickness (δ/c) as reproduced in Figure 39. The plot presents data from a bicusped strut profile in an exponential boundary layer with strut thickness values of 0.05 and 0.25. The figure shows that f(n) increases with δ/c to a maximum value at $\delta/c = 0.1$. Equation (6) states that the energy in these secondary flows is proportional to airfoil thickness to the fourth power and reaches a maximum when δ/c is approximately 0.1. Hawthorne's analysis was based on a bicusped airfoil shape and an exponential boundary layer. Although the theory does not hold for all airfoil shapes or boundary layer profiles, it is probably not unfair to assume that generally the energy in secondary flows for this type of airfoil-tunnel wall intersection is

$$D_e^* = K(t/c)^4 \left(\frac{\delta/c}{0.1}\right) \quad , \tag{8}$$

where K = constant. Assuming further that the ability of the horseshoe vortex to entrain high-momentum flow in the strut intersection and retard separation is directly related to the energy in the vortex means that the drag correction, ΔC_d, becomes

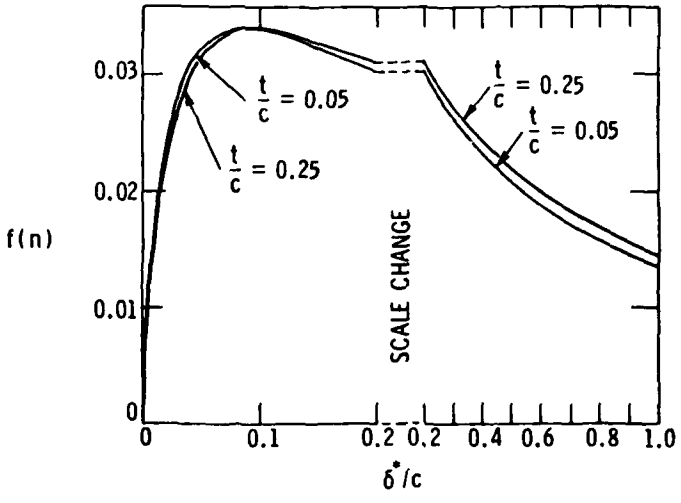

Figure 39. Hawthorne's plot of the variation of f(n) (Equation (6)) with δ^*/c for t/c = 0.05 and 0.25. Reproduced from Reference (13).

$$\Delta C_d = K \frac{f(C_\ell, C_d, \alpha, AR)}{\left((\delta/C)/0.1\right)(t/c)^4} \quad . \tag{9}$$

The C_ℓ, α, and AR effects must be derived from an analysis of the present experimental data.

Shown in Figures 40-42 are C_ℓ-versus-C_d data as reported by Daily, Kermeen, and the present study. Also shown is the deviation between the experimental data and the published NACA data. This deviation is the required correction to make experimental data match the NACA published data. The three sets of data have several similarities. The deviation of drag is zero at $C_\ell = 0$ for all three investigations. The ΔC_d curves for all three experiments increase to the point where $dC_\ell/d\alpha$ is no longer constant and then ΔC_d decreases. If $(dC_\ell/d\alpha)_o$ represents the slope of the lift curve in the constant slope portion of the curve, then the ΔC_d curve seems to behave as

$$\Delta C_d = K\left(\frac{dC_\ell/d\alpha}{(dC_\ell/d\alpha)_o}\right)^{1/2} \tag{10}$$

for all three experiments.

Assuming Equation (10) represents the contribution of α to the drag correction, one sees that ΔC_d now becomes

$$\Delta C_d = K \frac{f(C_\ell, C_d, AR)(C_{\ell_\alpha}/C_{\ell_{\alpha_o}})^{1/2}}{\left((\delta/c)/0.1\right)(t/c)^4} \quad , \tag{11}$$

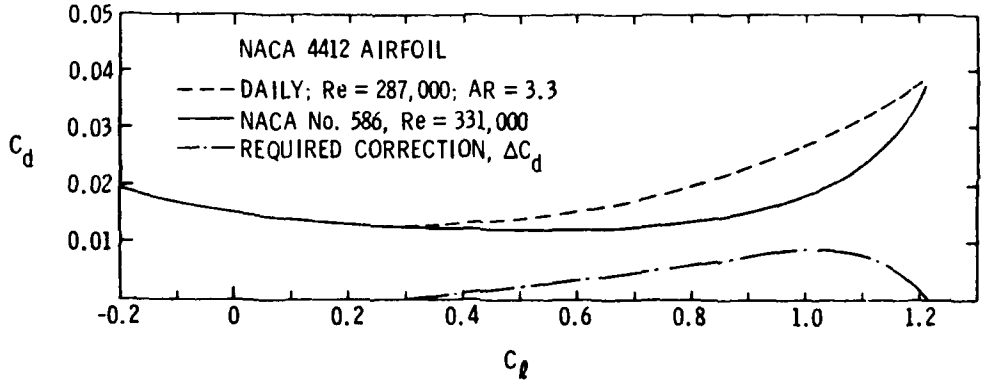

Figure 40. Daily's results (C_ℓ versus C_d) compared with NACA published data for a NACA 4412 airfoil. Also shown is the value of ΔC_d required to correct Daily's curve to the NACA curve.

AD-A086 079 PENNSYLVANIA STATE UNIV UNIVERSITY PARK APPLIED RESE--ETC F/G 20/4
A METHOD OF CORRECTING FOR THE EFFECTS OF THE SIDEWALL BOUNDARY--ETC(U)
MAR 80 P P JACOBS N00024-79-C-6043
UNCLASSIFIED ARL/PSU/TM-80-44 NL

CONT.

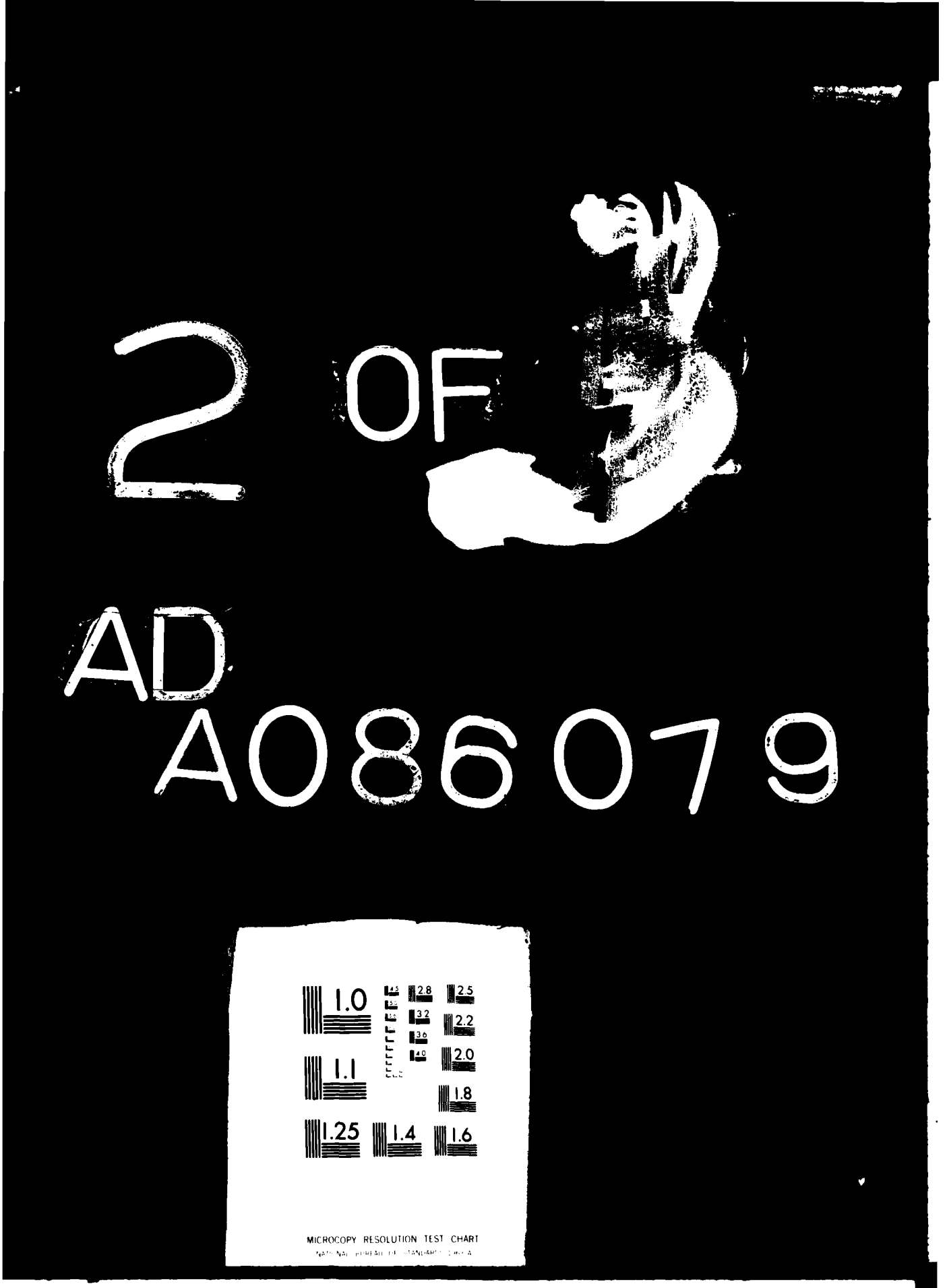

13. Hawthorne, W. J., "The Secondary Flow About Struts and Airfoils,"

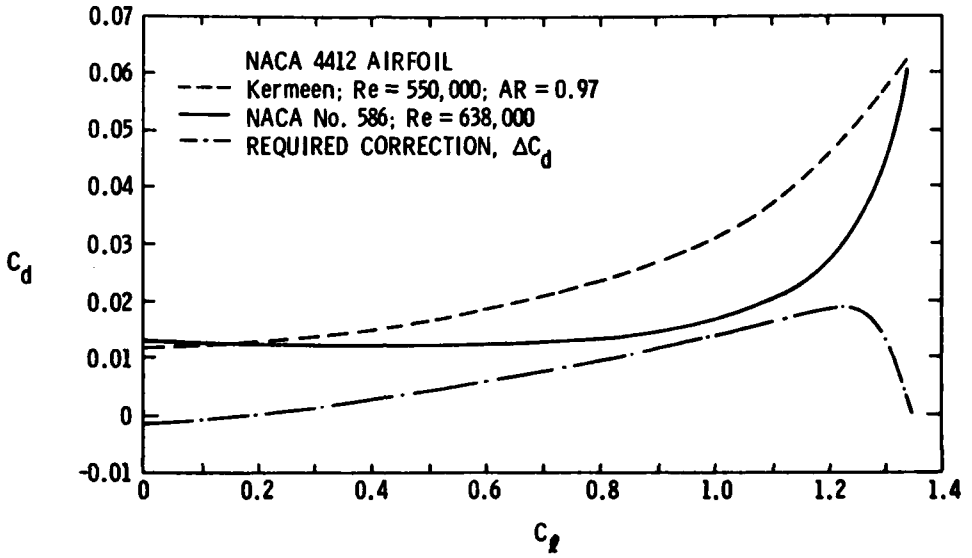

Figure 41. Kermeen's results (C_ℓ versus C_d) compared with NACA published data for a NACA 4412 airfoil. Also shown is the value of ΔC_d required to correct Kermeen's curve to the NACA curve.

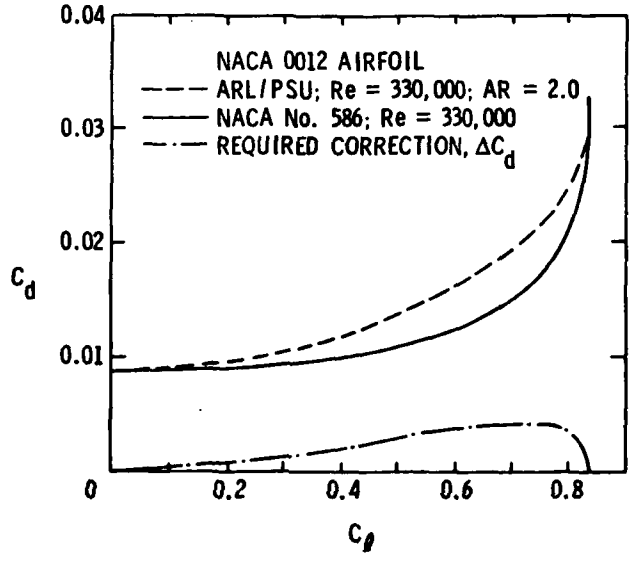

Figure 42. ARL/PSU results (C_ℓ versus C_d) compared with NACA published data for a NACA 0012 airfoil. Also shown is the value of ΔC_d required to correct the ARL/PSU curve to the NACA curve.

where $C_{\ell_\alpha} = dC_\ell/d\alpha$ and $C_{\ell_{\alpha_o}} = (dC_\ell/d\alpha)_o$. As the experimental data show, the drag correction must be zero at $C_\ell = 0$. Thus, the C_ℓ contribution should be directly proportional to the ΔC_d term. The assumed C_d correction can be the term which "individualizes" the correction to specific airfoils if it is set equal to C_{d_o} (minimum drag coefficient) of the tested airfoil. The correction now takes the form

$$\Delta C_d = K \frac{C_{d_o} C_\ell (C_{\ell_\alpha}/C_{\ell_{\alpha_o}})^{1/2}}{((\delta/c)/0.1)(t/c)^4} f(AR) \quad . \tag{12}$$

At this point, Equation (12) can be applied to the data of Figures 40-42. On a trial-and-error basis, setting $K = 0.00015$ and $f(AR) = 1/\sqrt{AR}$, one finds for the final correction that

$$\Delta C_d = \frac{0.00015\left(C_{d_o} C_\ell (C_{\ell_\alpha}/C_{\ell_{\alpha_o}})^{1/2}\right)}{((\delta/c)/0.1)(t/c)^4\sqrt{AR}(1/2)} \quad . \tag{13}$$

Shown in Figures 43-45 are the results of the three experiments with Equation (13) applied to the data. The correction works extremely well for the ARL/PSU data. There is also exceptionally good agreement when it is applied to Kermeen's data. With Kermeen's data, there is a slight deviation at the higher C_ℓ values. It must be noted that in the range $C_\ell = 1.1$ Kermeen's curve exceeds the published NACA data by approximately 90%. Another consideration is the advances made in instrumentation between Kermeen's tests and the present study. Also noteworthy is the fact that the Reynolds numbers of the two curves

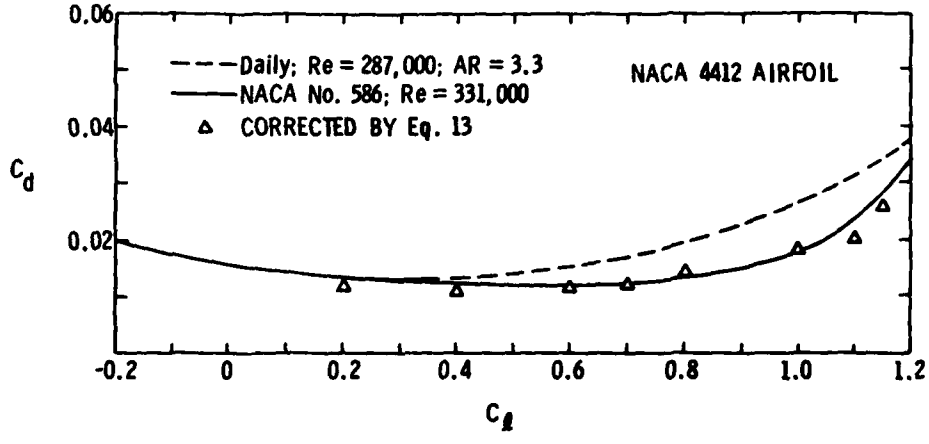

Figure 43. Daily's data corrected by Equation (13).

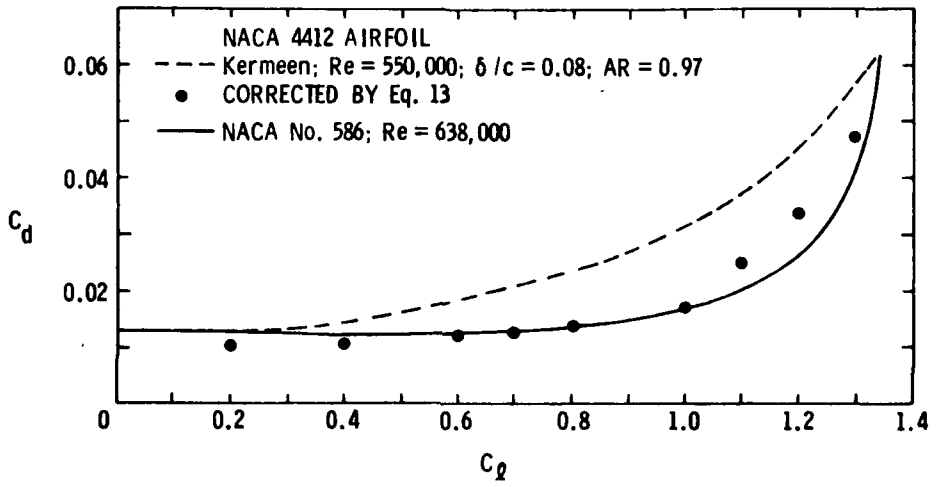

Figure 44. Kermeen's data corrected by Equation (13).

$$\Delta C_d = \frac{0.000015\, C_{do}\, C_\ell \left(\frac{C_{\ell\infty}}{C_{\ell\infty_o}}\right)^{1/2}}{\frac{\delta}{c}\left(\frac{t}{c}\right)^4 AR^{1/2}}$$

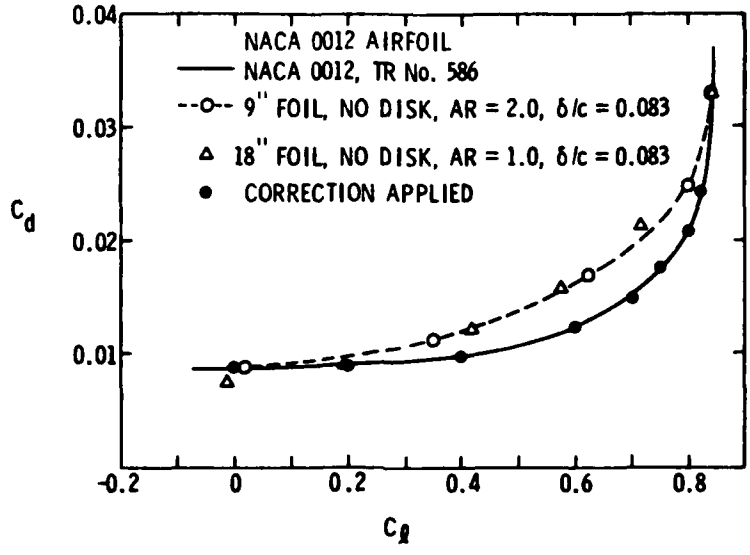

Figure 45. ARL/PSU results corrected by Equation (13).

differ by 88,000. Higher Reynolds numbers tend to make the C_ℓ versus C_d curve "flatten out." Daily's data show excellent agreement even in the high C_ℓ regime. It is interesting to note that the maximum error in Daily's uncorrected data is less than 50% of the NACA data or almost half of the error reported by Kermeen.

A feature of Equation (13) which is of critical importance is the fact that all the terms of the equation are easily determined with the existing balance system. It has been demonstrated that C_ℓ, C_{ℓ_α}, and $C_{\ell_{\alpha_o}}$ are all obtainable with the present balance using only the traditional boundary corrections. The only drag dependent term in Equation (13) is C_{d_o}. C_{d_o} is the one value on the C_ℓ-versus-C_d curve that the balance can measure and requires no correction. Had the correction been a function of the airfoil's actual or corrected drag coefficient, such as the C_{ℓ_α} term, it would be of no practical value since for a new airfoil design the corrected C_d values are unknowns.

CHAPTER V

SUMMARY, CONCLUSIONS, AND RECOMMENDATIONS

5.1 Summary and Conclusions

With the derivation of Equation (13), all five of the previously stated objectives have been met. The first stated objective was to determine what caused the original water tunnel balance to fail to measure correctly the C_d values. When measurements were begun, both balances (water and wind tunnel) were oriented in such a manner that they measured drag by summing or differencing two small force measurements. In both cases, the resulting C_d values were too large by an order of magnitude. When the wind tunnel balance was reoriented such that one measuring element sensed the total axial force on the model and the other element sensed the total normal force, the resulting C_d values were within the regime of measurements reported by previous authors. Similar reorientation of the water tunnel balance did not produce the same results. However, when the water tunnel balance was reoriented, the flexures between the measuring elements allowed the hydrofoil to deflect substantially under load, rendering the reading suspect. As Figures 5A and 5B show, both C_ℓ and C_d data had a large error. This proof is not absolute, but in light of the failure of all subsequent attempts to duplicate various error causing conditions in the wind tunnel the above reason emerges as the most probable explanation.

The second objective was to build and test a wind tunnel balance which was similar in principle to the water tunnel balance. This was

accomplished and the measured results were as good as, if not better than, the data of Kermeen (1) and Daily (5).

The third objective was to determine what factors affect flow past a hydrofoil in a two-dimensional channel or, just as important, what factors have a negligible effect.

The experimental results show that several factors are either negligible or correctable. The effect of a small gap between the airfoil tip and channel wall is negligible provided it is kept within a certain range. Gap sizes up to 0.020 in. for the 18-in.-chord model show no significant effect. Practically, if the gap can be kept as small as possible from a manufacturing tolerance standpoint (gap/chord ratio $\leq$ 0.002 in this study), it is unlikely that any significant error will be introduced by the existence of an end gap. Another factor deemed noncritical is flow in the vicinity of the force transmitting shaft. Use of a disk on the shaft end of the airfoil to protect the shaft from spurious forces does not appear to be necessary. The variation of aspect ratios used in the current test program was limited (AR = 1.0, 2.0, and 3.3). The effect of varying AR between 1.0 and 2.0 is negligible or at least difficult to discern. However, when AR = 3.3 is considered, as in Daily's data, there is an effect and the drag correction factor needs modification to reflect this. Experimentally, $f(AR) = 1/\sqrt{AR}$ serves as a suitable approximation of the aspect ratio effects.

Several factors are nonnegligible. Manufacturing techniques are critical. Surface finish on the model, spanwise twist, and model-thickness tolerances produce significant effects on measured quantities and require particular attention before satisfactory results

are obtained. The boundary layer causes a horseshoe vortex to form on each airfoil wall intersection. This vortex represents a departure from two-dimensional conditions and must be considered (and corrected) before the balance can give an accurate force representation.

The fourth objective concerned the way to implement a reliable force balance system. The recommended way is to modify the existing water tunnel balance and to use it in conjunction with Equation (13). Any balance which measures the total force on a model completely spanning a tunnel with an incoming boundary layer also measures an additional increment of drag due to the three-dimensional effect of the vortices at the sidewall-hydrofoil intersection. The use of Equation (13) appears to correct sufficiently for this drag increment. The modifications recommended are to strengthen the weak flexures, to employ only two force cubes as sensors with the cubes being oriented so that each cube measures only the total axial or total normal force, and to use a separate torsion element to measure the moment. The balance should also be mounted so that there are no interactive constants between the force cubes.

The fifth objective was to formulate a data reduction process to act as a reference procedure for future testing of this nature at ARL. The data reduction process is outlined in Appendix C. Listed in Appendix D are tabulated data from the current study. An error analysis is presented in Appendix E.

5.2 Recommendations for Future Study

Future study in the area of accurate two-dimensional force measurement should include further testing with the present wind tunnel

balance. Several different airfoils should be tested to establish a large data base for establishing the correction factor (Equation (13)). Models of various thicknesses, various aspect ratios, and various degrees of camber should be experimentally investigated.

Particular attention should be focused on the thickness variation in follow-on testing. The $(t/c)^4$ term of Equation (13) requires experimental verification because the three studies discussed herein used only airfoils of 12% thickness. Data from airfoils of differing thicknesses were not available. Since Equation (13) is empirical, it includes the effects of drag on the exposed portion of the force transmitting shaft (as discussed in Section 3.4). It is recommended that tare drag forces of this nature be further investigated to determine the extent of their contribution to Equation (13). In the author's opinion, sufficient data were not obtained in this study to address adequately this consideration.

Another recommendation is to remove the horseshoe vortex physically by a suction or blowing mechanism. Data taken in this manner should at least approach the two-dimensional if it should not be purely two-dimensional and not require use of Equation (13). A comparison test with and without the secondary vortices would be useful.

It is also recommended that the pitching moment coefficient be measured by some procedure other than by differencing the measurements of two force cubes. The addition of an extra force cube seems to exact a penalty in drag measurement. Improving the flexure setup previously mentioned, however, could possibly overcome this difficulty. Perhaps pitching moment measurements could be made with a torque tube arrangement or even with a different balance during a separate set of

experimental runs. After these recommended tests are performed in the wind tunnel, Equation (13) would be verified (or modified). The entire system should be used in a parallel water tunnel test program.

REFERENCES

1. Kermeen, R. W., "Water Tunnel Tests of NACA 4412 and Walchner Profile 7 Hydrofoils in Noncavitating and Cavitating Flows," California Institute of Technology, Report Number 47-5, February 1956.

2. Loftin, L. K., and Smith, H. A., "Aerodynamic Characteristics of 15 NACA Airfoil Sections at Seven Reynolds Numbers from 0.7×10^6 to 9.0×10^6," NACA Technical Note 1945, October 1949.

3. Jacobs, E. N., and Sherman, A., "Airfoil Section Characteristics as Affected by Variations of the Reynolds Number," NACA Technical Report 586, 1937.

4. Hotz, G. M., and McGraw, J. T., "The High Speed Water Tunnel Three-Component Force Balance," California Institute of Technology, Hydrodynamics Laboratory Report Number 47-2, January 1955.

5. Daily, J. W., "Cavitation Characteristics and Infinite Aspect Ratio Characteristics of a Hydrofoil Section," Transactions of the ASME, Vol. 71, pp. 269-284, April 1949.

6. Otsuka, S., and Sugiyama, Y., "On the Performance of a Wing Having Tip Clearance, Part 1," Memoirs of the Faculty of Engineering, Nagoya University, Vol. 21, No. 1, 1969, pp. 172-188.

7. Perry, C. C., and Lissner, H. R., Strain Gage Primer, McGraw-Hill, New York, 1955.

8. Lakshminarayana, B., and Horlock, J. H., "Tip-Clearance Flow and Losses for an Isolated Compressor Blade," Her Majesty's Stationary Office, London, Reports and Memoranda No. 3316, 1963, pp. 1-24.

9. Gearhart, W. S., "Tip Clearance Flow in Turbomachines," M. S. Thesis, The Pennsylvania State University, June 1964.

10. Gurney, G. B., "An Analysis of Force Measurement," M. S. Thesis, The Pennsylvania State University, September 1962.

11. Parkin, B. R., and Kermeen, R. W., "Water Tunnel Techniques for Force Measurements on Cavitating Hydrofoils," Journal of Ship Research, Vol. 1, No. 1, April 1957, p. 36.

12. Barber, T. J., "An Investigation of Strut-Wall Intersection Losses," Journal of Aircraft, Vol. 15, No. 10, October 1978, pp. 676-681.

13. Hawthorne, W. J., "The Secondary Flow About Struts and Airfoils," Journal of the Aeronautical Sciences, Vol. 21, September 1954.

14. Pope, A., and Harper, J. J., Low Speed Wind Tunnel Testing, John Wiley and Sons, Inc., New York, 1966.

15. Allen, H. J., and Vincenti, W. G., "Wall Interference in a Two Dimensional Flow Wind Tunnel with Consideration of the Effect of Compressibility," NACA Technical Report 782, 1944.

16. Hoerner, S. F., Fluid Dynamic Drag, Vol. 11, 1965.

17. Ross, D., and McGinley, J. H., "Flow in Closed-Jet Working Sections," The Pennsylvania State University, Ordnance Research Laboratory, Serial No. NOrd 7958-283, February 5, 1954.

18. Pankhurst, R. C., and Holder, D. W., Wind Tunnel Technique, Pitman and Sons, London, 1952.

19. Sugiyama, "Aerodynamic Characteristics of a Rectangular Wing with a Tip Clearance in a Channel," Journal of Applied Mechanics, Vol. 44, December 1977.

20. Ando, S., "Limitation of Lifting Line Theory for Wing Having Very Small Chordwise Gap," Transactions of the Japanese Society for Aeronautical and Space Sciences, Vol. 9, No. 14, 1966.

21. Freund, J., and Williams, F., Modern Business Statistics, Prentice-Hall, Inc., Englewood Cliffs, New Jersey, 1969.

22. Gerald, C., Applied Numerical Analysis, Addison-Wesley Publishing Co., Reading, Massachusetts, 1970.

APPENDIX A

THE TRADITIONAL WIND TUNNEL BOUNDARY CORRECTIONS

In testing of this nature, the presence of the tunnel walls causes flow conditions in the tunnel to be different from those in free air. Conditions are altered because of several factors and the usual method of correction is to divide the interference into several separate components and simply add them. Four types of interference are considered here as traditional corrections: solid blockage, wake blockage, lift effect, and horizontal buoyancy. The correction terms are discussed by Pope (14).

Solid blockage refers to the fact that the presence of the model in the test section reduces the area through which the fluid must flow. Because of the Bernoulli principle, the velocity of the air around the model is increased to some value greater than that which the model would experience in free-stream conditions. Pope refers to the work done by Allen and Vincenti (15) which expresses the solid blockage term, ϵ_{sb}, as

$$\epsilon_{sb} = \Lambda\sigma \quad , \tag{A1}$$

where

$$\sigma = \left(\frac{\pi^2}{48}\right)\left(\frac{c}{h}\right)^2 \quad ;$$

$$\Lambda = \frac{16}{\pi}\int_0^1 \frac{y}{c}\left((1 - P)\left(1 + \frac{dy}{dx}\right)\right)^{1/2} d\,\frac{x}{c} \quad ;$$

x,y = airfoil coordinates; c = airfoil chord; P = no-camber (basic) pressure distribution; and h = tunnel height. Values of Λ for several

airfoil families are plotted as a function of thickness in Figure 6:8 of Reference (13). The use of ε_{sb} will be discussed later.

Wake blockage is also a continuity-related condition. In the wake behind a model, the velocity is lower than in the surrounding stream. In order to satisfy conditions of continuity in a closed test section, velocity outside the wake must be higher than the velocity far upstream. In a free fluid, these velocities would be equal. The velocity is therefore accelerating past the model and the velocity at locations downstream of the airfoil is higher than in free-stream conditions. Pope gives the expression for wake blockage, ε_{w_b}, as

$$\varepsilon_{w_b} \approx \tau C_{d_u} \quad , \tag{A2}$$

where $\tau = (c/h)/4$ and C_{d_u} = uncorrected section drag coefficient. The wake blockage and solid blockage terms represent a correction to axial velocity past the airfoil and are generally combined as

$$\varepsilon = \varepsilon_{s_b} + \varepsilon_{w_b} \quad . \tag{A3}$$

This permits a velocity correction of the form

$$V = V_u(1 + \varepsilon) \quad , \tag{A4}$$

where the subscript u represents an uncorrected term (velocity in this case). The Reynolds number then becomes

$$R_e = R_{e_u}(1 + \varepsilon) \quad . \tag{A5}$$

Lift effect corrections account for the fact that the tunnel walls constrain the curved streamlines. The effects of constraining the streamlines can be approximated by regarding them as a change in airfoil camber and angle of attack. Pope expresses the lift effect as a correction to α, C_ℓ, C_d, and $C_{m_{1/4}}$:

$$\alpha = \alpha_u + \frac{(57.3)\alpha}{2\pi}(C_{\ell_u} + 4C_{m_{1/4_u}}) \quad , \tag{A6}$$

$$C_\ell = C_{\ell_u}(1 - \sigma - 2\varepsilon) \quad , \tag{A7}$$

$$C_{m_{1/4}} = C_{m_{1/4_u}}(1 - 2\varepsilon) + \frac{\sigma C_\ell}{4} \quad , \tag{A8}$$

and

$$C_d = C_{d_u}(1 - 3\varepsilon_{sb} - 2\varepsilon_{wb}) \quad , \tag{A9}$$

where $C_{m_{1/4}}$ = pitching moment coefficient about the 1/4-chord point.

Horizontal buoyancy refers to the additional drag created by the existence of a static pressure gradient in the tunnel test section. As the boundary layer builds up on the tunnel walls, the axial velocity increases to preserve continuity of the flow. Along with this increase in axial velocity is associated a decrease in static pressure. The downstream pressure is lower than the upstream pressure on the model; therefore, a spurious drag is created on the airfoil which must be subtracted from the measured drag. Pope gives Allen and Vincenti's expression for this buoyancy drag, D_b, as

$$D_b = - \frac{6h^2}{\pi} \Lambda\sigma \frac{dp}{d\ell} \qquad \text{(A10)}$$

where $dp/d\ell$ = static pressure gradient in tunnel without an airfoil. The manner in which these corrections are incorporated into the data reduction process is discussed in Appendix C.

APPENDIX B

INTEGRATION OF WAKES

Drag on a model in a wind tunnel can be determined by comparing the momentum in the air ahead of the model with the momentum behind the model. The drag force is equal to the loss of momentum suffered by the air as it passes over the airfoil or

$$D = \left(\frac{\text{mass}}{\text{sec}}\right)(\text{change in velocity}) \tag{B1}$$

or

$$D = \iint \rho V da(V_o - V) \quad , \tag{B2}$$

where D = drag, V_o = initial airspeed (ahead of airfoil), V = final airspeed (behind airfoil), da = small area of wake perpendicular to airstream, and ρ = density. Rearranging terms and nondimensionalizing (details in Pope [14]), one finds that

$$C_d = 2 \iint \left(\sqrt{\frac{q}{q_o}} - \frac{q}{q_o}\right)\frac{dy}{c} \quad , \tag{B3}$$

where $q = (1/2)\rho V^2$, $q_o = (1/2)\rho V_o^2$, y = unit area term measured perpendicular to the airfoil, and c = chord. In Equation (B3), the term in parenthesis can be rewritten as

$$\left(\sqrt{\frac{q}{q_o}} - \frac{q}{q_o}\right) = \left(\frac{V}{V_o} - \frac{V^2}{V_o^2}\right) \quad . \tag{B4}$$

The drag coefficient can now be determined by measuring a reference velocity, V_o, and a series of local velocities which are measured by traversing a probe through the airfoil wake.

The wake measurement tests were set up as shown in Figure B1. The traversing probe was a kiel probe which accurately measures dynamic pressures for relative wind angles within $\pm 35^o$ of the probe centerline. The static pressure reading taken at the reference probe location was used for both V and V_o computations. This is acceptable since both probes are located the same distance downstream of the panel leading edges. It proved to be very difficult to make local static pressure readings from the traversing probe due to streamline curvature in the airfoil wake.

The movable probe measured local velocities (dynamic pressures) as it was traversed in 0.1-in. increments vertically through the wake. This profile of velocity ratios (such as depicted in Figure 14) was then integrated using the trapezoidal rule to give the value of the double integral in Equation (B3). The computer program and the associated variables are listed in Appendix C.

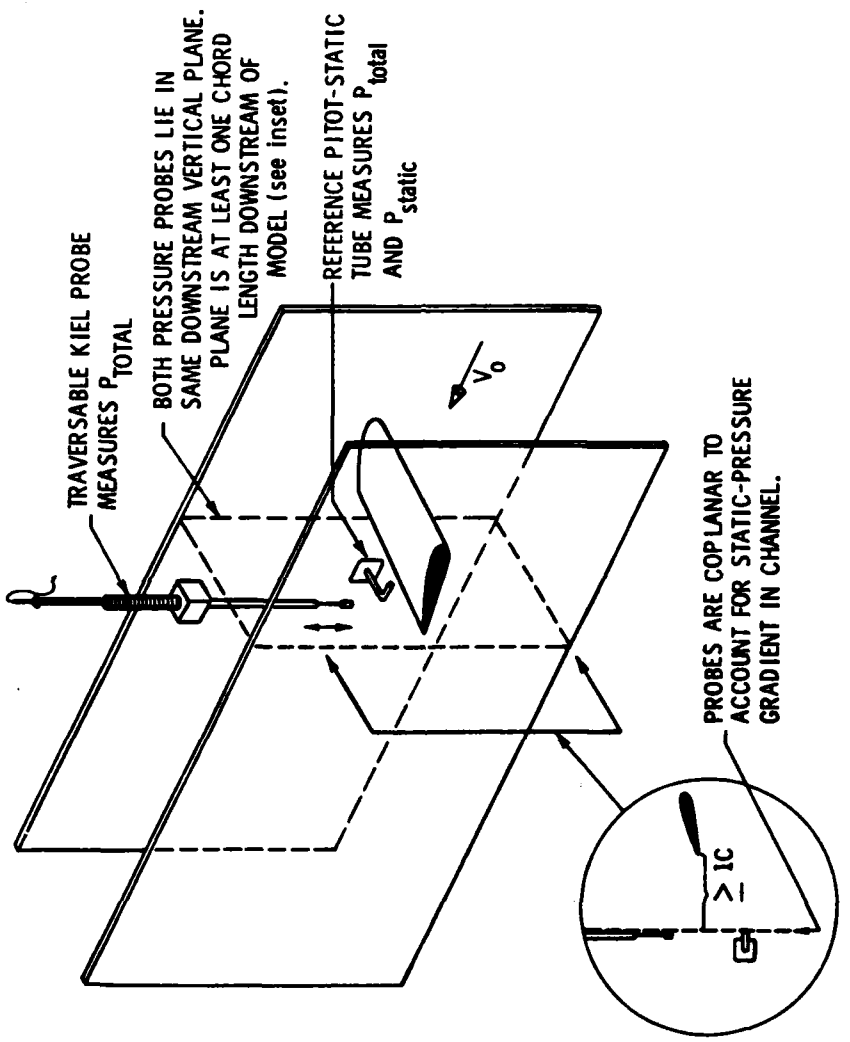

Figure B1. Wake traverse installation.

APPENDIX C

COMPUTER PROGRAMS AND DATA REDUCTION PROCEDURE

The two computer programs which were used to calculate the force coefficients and integrate the airfoil wakes are presented herein. The force coefficient program takes measured temperatures, pressures, angle of attack, and balance voltages and determines corrected C_ℓ, C_d, and Re.

The final wind tunnel balance configuration is represented in the top of Figure C1. Tension members A and B are calibrated ($K_{A,B}$ = calibration constant) such that the tensile force and direction along the ribbon's long axis can be determined, e.g.,

$$\text{Force}_{A,B}(\text{lb}) = K_{A,B}(\frac{\text{lb}}{\text{volt}})\text{Volts}_{A,B} \quad , \tag{C1}$$

where the sign of A's or B's voltage reading would indicate whether the force was directed up or down along the ribbon (indicated by double-headed arrows in Figure C1. In order to determine lift and drag, normal and axial forces must be transformed. The lower portion of Figure C1 shows the appropriate vector diagram. To produce a lift force or vector, $\vec{L}$, ribbons A and B must be stressed as vectors $\vec{L}_A$ and $\vec{L}_B$ as shown. Likewise, to produce a drag vector, $\vec{D}$, ribbons A and B must be stressed as vectors $\vec{D}_A$ and $\vec{D}_B$. Therefore, when both lift and drag exist on an airfoil, ribbon A will reflect the vector sum of $\vec{L}_A$ and $\vec{D}_A$ and ribbon B will reflect the vector sum of $\vec{L}_B$ and $\vec{D}_B$. To determine how much of each ribbon's total measured force contributes to lift or drag, two simultaneous equations must be solved. From the vector diagram of Figure C1, it can be shown that

$$D(\text{lb}) = F_A(\text{lb})\sin\alpha + F_B(\text{lb})\cos\alpha \tag{C2}$$

and

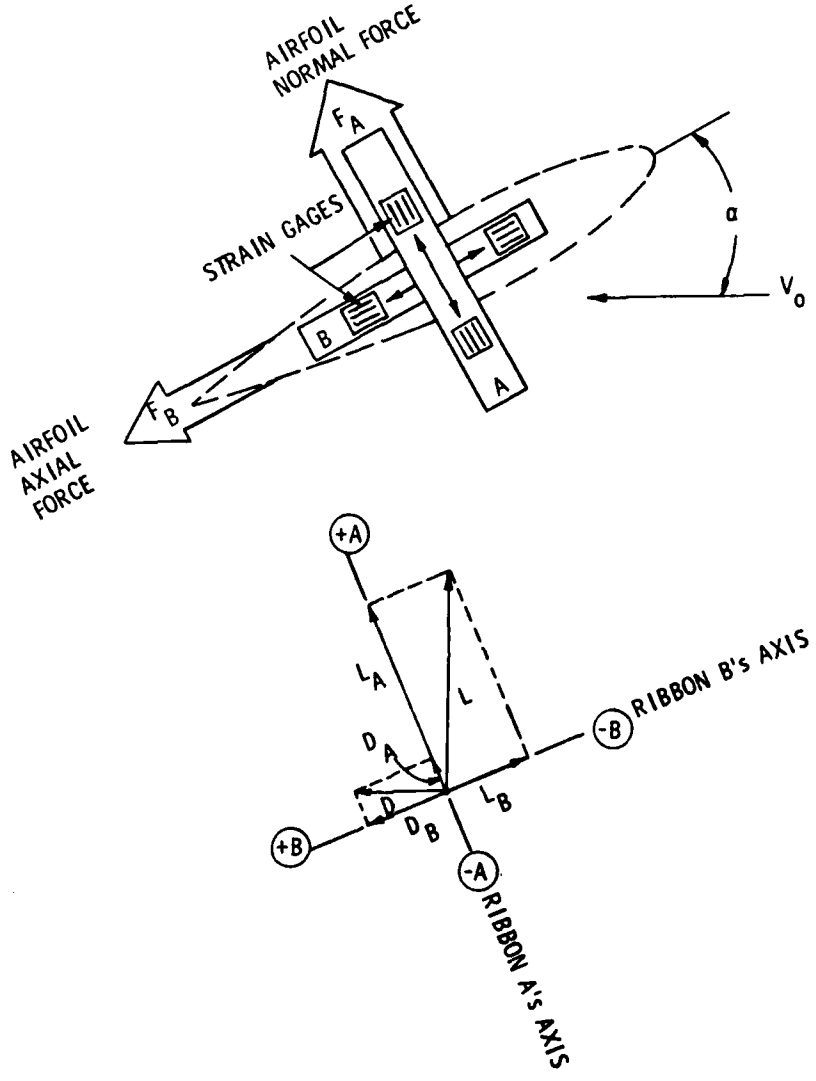

Figure C1. Schematic diagram of relationship between aerodynamic forces and cantilever balance elements. Ribbon B is aligned with the airfoil chordline and rotates with the airfoil. Ribbon A is perpendicular to ribbon B. In the lower portion of the figure, the circled values represent sign conventions for the individual ribbons.

$$L(1b) = F_A(1b)\cos\alpha - F_B(1b)\sin\alpha \quad , \tag{C3}$$

where $F_{A,B}$ represents the forces measured by the two ribbons (determined as per Equation (C1).

The force coefficient program then follows this sequence:

a. Read barometric pressure, number of events, transducer constant, airfoil chord, and static pressure gradient.

b. Calculate repeatable terms: σ, ε_{sb}, τ.

c. Establish elements of simultaneous equations subroutine. The matrix is of the form

$$\begin{pmatrix} B_1 \\ B_2 \end{pmatrix} = \begin{pmatrix} A_{1,1} A_{1,2} \\ A_{2,1} A_{2,2} \end{pmatrix} \begin{pmatrix} X_1 \\ X_2 \end{pmatrix} \quad , \tag{C4}$$

where $A_{i,j}$ = trignometric functions of α in Equations (C2) and (C3); B_i = forces A and B in pounds as determined by Equation (C1); and X_i = unknown forces, lift and drag.

d. Determine uncorrected lift and drag in pounds.

e. Determine buoyancy drag increment from Equation (A10),

$$D_B = -\frac{6h^2}{\pi} \Lambda\sigma \frac{dp}{d\ell} \quad . \tag{C5}$$

f. Nondimensionalize coefficients

$$C_{\ell_u} = \frac{L}{(1/2)\rho V^2 sc} \tag{C6}$$

and

$$C_{d_u} = \frac{D - D_B}{(1/2)\rho V^2 sc} \quad . \tag{C7}$$

g. Correct coefficients and α for solid blockage, wake blockage, and lift effect:

$$\alpha = \alpha_u + \frac{(57.3)\sigma}{2\pi}(C_{\ell_u} + 4C_{m\ 1/4_u}) \quad , \tag{C8}$$

(The moment term of Equation (C8) was neglected in this study since moment forces were not measured. It is included here in the event that moments are measured in future testing.)

$$C_\ell = C_{\ell_u}(1 - \sigma - 2\varepsilon) \quad , \tag{C9}$$

$$C_d = C_{d_u}(1 - 3\varepsilon_{sb} - 2\varepsilon_{wb}) \quad , \tag{C10}$$

and

$$Re = R_{e_u}(1 + \varepsilon_{sb} + \varepsilon_{wb}) \quad . \tag{C11}$$

The program is listed with an explanation of variables at the end of the appendix.

The wake integration program is listed here alone. The wake integration program is discussed in Appendix B.

VARIABLES IN FORCE COEFFICIENT PROGRAM

A = matrix coefficient (Equation (C4))

ALFA = airfoil angle of attack (in degrees)

ALFAC = airfoil angle of attack with classic corrections applied (in degrees)

ANGL = angle formed by top edge of balance and horizontal; equal to ALFA in final balance configuration (in degrees)

B = matrix coefficient (Equation (C4))

BAR = barometric pressure (in inches of mercury)

BETA = ALFA (in radians)

C = airfoil chord (in inches)

CD = drag coefficient

CDC = drag coefficient with classic corrections applied

CL = lift coefficient

CLC = lift coefficient with classic corrections applied

CON = transducer constant (in inches of water/volt)

D = drag (in pounds)

DB = buoyancy drag (in pounds)

DPDL = static pressure gradient $\left(\frac{lb/F^2/F}{(1/2)\rho V^2}\right)$

ESB = solid blockage

EVENT = test number

L = lift (in pounds)

N = number of angle-of-attack positions surveyed

PI = 3.14159

R = gas constant

RDELP = reference velocity measurement, total pressure-static pressure

RRE = reference Reynolds number

REC = reference Reynolds number corrected

RRHO = reference density

RVEL = reference velocity

RXNU = reference dynamic viscosity

SIGMA = σ as in Equation (A1)

TAU = τ as in Equation (A2)

TEMP = temperature (in degrees Fahrenheit)

VA = ribbon A's voltage (in volts)

VB = ribbon B's voltage (in volts)

XKA = ribbon A's calibration constant (in pounds/volt)

XKB = ribbon B's calibration constant (in pounds/volt)

FORCE COEFFICIENT PROGRAM

```
      PROGRAM FORCE2
      REAL L(50)
      INTEGER EVENT
      DIMENSION TEMP(50),ALFA(50),VA(50),VB(50),D(50),ANGL(50),
     1ALFAC(50),CL(50),CD(50),DB(50),CLC(50),CDC(50),REC(50),RRHO(50),
     2RDELP(50),RVEL(50),RXNU(50),RRE(50),BETA(50),A(50),B(50)
      READ(4,99) N,EVENT,BAR,CON,C,DPDL
   99 FORMAT(2I5,4F10.5)
      PI = 3.1415927
      SIGMA=(PI**2/48.)*(C/48.)**2
      ESB = (.24)*SIGMA
      TAU = (C/48.)/4.
      R = 1715.
      DO 100 I=1,N
      READ(4,101)ALFA(I),ANGL(I),VA(I),VB(I),RDELP(I),TEMP(I)
  101 FORMAT(6F10.5)
      TEMP(I) = (TEMP(I)*100.0)+460.0
  100 CONTINUE
      WRITE(3,598)
  598 FORMAT('0',5X,'ALFA',5X,'ALFAC',6X,'CL',8X,'CLC',7X,'CD',8X,'CDC',
     17X,'REC',5X,'L(LB)',5X,'D(LB)',3X,'RVEL(F/S)')
      XKA = -.17598
      XKB = -.14485
      VAVE = 0.0
      DO 10 I=1,N
      BETA(I) = (ANGL(I)/17.777778)*(PI/180.0)
      A(1) = SIN(BETA(I))
      A(2) = COS(BETA(I))
      A(3) = COS(BETA(I))
      A(4) = SIN(BETA(I))*(-1.0)
      B(1) = VA(I)/XKA
      B(2) = VB(I)/XKB
      CALL SIMQ(A,B,2,KS)
      IF(KS.EQ.1) WRITE(5,597)
  597 FORMAT('MATRIX ERROR')
      D(I) = B(1)
      L(I) = B(2)
      RDELP(I) = RDELP(I)*CON*5.20128
      RRHO(I) = .002378*(BAR/29.92)*(519.0/TEMP(I))
      RVEL(I) = SQRT((2.*RDELP(I))/RRHO(I))
      RXNU(I) = (.37E-6)/RRHO(I)
      RRE(I) = (RVEL(I)*(C/12.))/RXNU(I)
      DB(I) = (6.*(48./12.)**2./PI)*.24*SIGMA*(DPDL*.5*RRHO(I)*RVEL(I)**
     12.*(C/12.))
      VAVE = VAVE+RVEL(I)
   10 CONTINUE
      VAVE = VAVE/N
      DO 11 I=1,N
      CL(I) = L(I)/(.5*RRHO(I)*(VAVE**2.)*1.53646*(C/12.))
      CD(I) = (D(I)-DB(I))/(.5*RRHO(I)*VAVE**2.*1.53646*(C/12.))
      REC(I) = RRE(I)*(1.+(ESB+TAU*CD(I)))
      CLC(I) = CL(I)*(1.-SIGMA-(2.*ESB)-(2.*TAU*CD(I)))
```

```
      CDC(I) = CD(I)*(1.-(3.*ESB)-(2.*TAU*CD(I)))
      ALFA(I) = ALFA(I)/17.777778
      ALFAC(I) = ALFA(I)+((57.29*SIGMA/2./PI)*CL(I))
      WRITE(3,105) ALFA(I),ALFAC(I),CL(I),CLC(I),CD(I),CDC(I),REC(I),
     1L(I),D(I),RVEL(I)
  105 FORMAT('0',6F10.5,F10.1,3F10.5)
   11 CONTINUE
      WRITE(3,599) EVENT,VAVE
  599 FORMAT('0','RUN NO.',2X,I5,5X,'AVG VEL IS',2X,F10.5)
      STOP
      END
```

VARIABLES IN WAKE INTEGRATION PROGRAM

AREA = area under velocity profile curve being integrated

BAR = barometric pressure (in inches of mercury)

C = airfoil chord (in inches)

CD = two-dimensional drag coefficient

CON = transducer constant (in inches of water/volt)

DELP = local velocity measurement; local total pressure-reference static pressure (in volts)

DLPF = reference velocity measurement; reference total pressure-reference static pressure (in volts)

END = integration limit

EVENT = test number

IS = sign of voltage measurement (+ or -)

ISZER = amplifier offset voltage

N = number of positions in wake at which measurements were taken

P = absolute static pressure (in pounds/cubic foot)

PDT = local total pressure (in volts)

PIS = reference static pressure (in volts)

PIT = reference total pressure (in volts)

R = gas constant

RATIO = ratio of local velocity to reference velocity

RHO = density

START = integration limit

STAT = static pressure difference from atmospheric (in pounds/cubic foot)

TEMP = temperature (in degrees Fahrenheit)

VEL = local velocity

VELIF = reference velocity

VINTGL = rectangular increment of wake velocity curve which is summed to measure area under wake velocity curve

VOLT = any of the voltage measurements as recorded on paper tape. This term is used for subtracting out instrument offsets from all measured quantities.

ZERVT = pressure transducer offset voltage

WAKE INTEGRATION PROGRAM

```
      PROGRAM WAKE
      INTEGER START,EVENT
      DIMENSION PIT(150),PIS(150),PDT(150),TEMP(150)
      DIMENSION RATIO(150),STAT(150),P(150),DELP(150),RHO(150)
      DIMENSION VINTGL(150),VEL(150),VOLT(200),IS(10)
      DIMENSION DLPF(200),VELIF(200)
      READ(4,50)N,EVENT,BAR,CON,C,START,IEND
   50 FORMAT(2I5,3F10.5,2I5)
      WRITE(3,888)
  888 FORMAT(///,' ',5X,'PSN',7X,'RATIO',10X,'VEL',10X,'VREF')
      DO 100 I=1,N
      READ(4,101)ISZER,ZERVT,(IS(J),VOLT(J),J=1,5)
  101 FORMAT(8X,5(I1,F5.3,5X),I1,F5.3)
      CALL CONVRT(5,IS,VOLT,ZERVT,ISZER)
      DO 102 J=2,4
      VOLT(J)=VOLT(J)-VOLT(1)
  102 CONTINUE
      PIT(I)=VOLT(2)
      PDT(I)=VOLT(3)
      PIS(I)=VOLT(4)
      TEMP(I)=(VOLT(5)*100.0)+460.0
  100 CONTINUE
      R=1715.0
C     BAROMETRIC PR NOW CONVTD FROM IN. MERC TO LB/SQ FT
      BAR=BAR*70.7328
      DO 3 I=1,N
C     STATIC PR NOW CONVTD FROM VOLTS TO LB/SQ FT
      STAT(I)=PIS(I)*CON*5.20128
      P(I)=BAR+STAT(I)
C     ABSOLUTE STATIC PR IS NOW IN LB/SQ FT
      DELP(I)=(PDT(I)-PIS(I))*CON*5.20128
      DLPF(I)=(PIT(I)-PIS(I))*CON*5.20128
      RHO(I)=(P(I)/(R*TEMP(I)))*32.174
      VEL(I)=SQRT((2.*DELP(I)*32.174)/RHO(I))
      VELIF(I)=SQRT((2.*DLPF(I)*32.174)/RHO(I))
      RATIO(I)=VEL(I)/VELIF(I)
      WRITE(3,510)I,RATIO(I),VEL(I),VELIF(I)
  510 FORMAT(' ',5X,I3,F12.4,2X,F12.4,2X,F12.4)
    3 CONTINUE
C     CONVERT BAR PR BACK INTO INCHES FOR PRINTOUT
      BAR=BAR/70.7328
      AREA=0.0
      DO 70 I=START,IEND
      VINTGL(I)=(((RATIO(I)-RATIO(I)**2)+(RATIO(I+1)-RATIO(I+1)**2))/
     12.)*(.1/12.)
      AREA=AREA+VINTGL(I)
   70 CONTINUE
      CD=(2./(C/12.))*AREA
      WRITE (3,501)CD
  501 FORMAT('0',8X,'DRAG COEFF IS',2X,F8.4/)
      WRITE(3,108)BAR,EVENT
  108 FORMAT(' ',8X,'BAROM PRESS IS',2X,F6.3,1X,'IN. HG',5X,'SURVEY NO',
     112X,I5/)
      STOP
      END
```

APPENDIX D

DATA TABLES

The tabulated data included here consist of lift and drag data measured by the doubly supported balance, lift and drag measured by the cantilever balance with both the 9- and 11-inch chord airfoils and with and without disk, and mid-span wake traverses which produced C_d values for various α's.

TABLE D1

Lift and Drag Data - Doubly Supported Balance.*

V = 110 f/s
Re = 330,000
c = 6 in.

α (deg)	C_L (±0.0024)	C_D (±0.0002)
8.26	0.773	0.0170
6.47	0.626	0.0136
4.91	0.480	0.0114
2.70	0.215	0.0087
1.04	0.053	0.0084

*data corrected for tunnel interference effects and Equations (1) and (5)

TABLE D2

Lift and Drag Data - Cantilever Balance -
9-in.-Chord Airfoil, 11-in. Disk.*

V = 70 f/s
Re = 330,000
c = 9 in.

α (deg)	C_L (±0.0020)	C_D (±0.0006)
8.77	0.794	0.0271
6.92	0.682	0.0219
5.18	0.549	0.0174
2.90	0.338	0.0131
0.91	0.086	0.0101
-1.11	-0.086	0.0102
-3.17	-0.346	0.0122
-5.19	-0.530	0.0151
-7.16	-0.686	0.0194
-9.37	-0.805	0.0265

*data corrected except for disk tare forces and Equation (13)

TABLE D3

Lift and Drag Data - Cantilever Balance
(Disk Tare Forces).*

V = 70 f/s
Re = 330,000
disk dia = 11 in.

α (deg)	C_L (±0.0014)	C_D (±0.0004)
9.34	0.0094	0.0021
6.26	0.0078	0.0014
3.21	0.0055	0.0018
0.47	0.0039	0.0012
-3.43	0.0027	0.0009
-6.17	-0.0008	0.0014
-9.01	-0.0004	0.0020

*coefficients nondimensionalized by c = 9 in.

TABLE D4

Lift and Drag Data - Cantilever Balance -
18-in.-Chord Airfoil, No Disk.*

V = 37 f/s
Re = 330,000

α (deg)	C_L (±0.0035)	C_D (±0.0007)
-10.38	-0.838	0.0289
-8.55	-0.736	0.0207
-6.30	-0.593	0.0150
-4.12	-0.427	0.0113
-1.98	-0.177	0.0087
-0.26	-0.018	0.0076
2.08	0.195	0.0096
3.10	0.324	0.0102
3.95	0.415	0.0121
6.03	0.575	0.0158
6.17	0.595	0.0158
8.02	0.715	0.0220
9.44	0.799	0.0276
10.29	0.830	0.0329

*all corrections applied except Equation (13)

TABLE D5

Lift and Drag Data - Cantilever Balance -
9-in.-Chord Airfoil, No Disk.*

V = 70 f/s
Re = 330,000

α (deg)	C_L (±0.0038)	C_D (±0.0005)
11.41	0.909	0.0460
10.78	0.890	0.0400
10.44	0.875	0.0371
8.78	0.790	0.0273
8.12	0.757	0.0249
6.75	0.672	0.0206
6.01	0.613	0.0179
5.17	0.559	0.0163
3.95	0.463	0.0138
2.98	0.358	0.0120
-0.51	-0.026	0.0089
-3.34	-0.361	0.0109
-6.34	-0.618	0.0150
-9.09	-0.796	0.0233

*all corrections applied except Equation (13)

WAKE TRAVERSE DATA

The following computer printouts are wake traverse data for the 9-in.-chord airfoil at various angles of attack. "Position" indicates vertical location; "VEL" is local velocity. "VREF" is the reference velocity measured at the same instant as the local velocity to eliminate any temperature change effects during the test. "RATIO" is VEL/VREF and is the value (V/V_o) used in Equation (B2). Listed in Table D6 are the starting positions of each traverse (Position 1). Positions 2-51 move toward the tunnel ceiling in 0.1-in. increments. All velocities are in feet/second. Tunnel height is 48 in. Re = 330,000. The probes are located 3.1 c behind the airfoil.

TABLE D6

Traverse Geometry.

Survey No.	α (deg)	Position 1 Location	C_d
45	0.30	21.5 in. from tunnel floor	0.0075 (±0.00007)
46	1.57	21.5 in. from tunnel floor	0.0099 (±0.00007)
47	4.00	21.5 in. from tunnel floor	0.0097 (±0.00012)
48	5.92	21.5 in. from tunnel floor	0.0120 (±0.00014)
49	9.95	20.0 in. from tunnel floor	0.0253 (±0.00011)
51	10.36	20.0 in. from tunnel floor	0.0280 (±0.00010)

TABLE D6a

Survey 45, $\alpha = 0.3^{o}$.

PSN	RATIO	VEL	VREF
1	1.0023	67.8481	67.6930
2	1.0034	67.8666	67.6338
3	0.9977	67.9059	68.0606
4	1.0017	68.0405	67.9244
5	1.0006	68.0018	67.9631
6	0.9994	68.0533	68.0920
7	1.0000	67.9495	67.9495
8	0.9994	68.0721	68.1108
9	1.0011	68.1620	68.0847
10	1.0017	68.2780	68.1622
11	1.0023	68.3297	68.1753
12	1.0006	68.0585	68.0198
13	1.0017	68.1361	68.0200
14	1.0000	68.0586	68.0586*
15	0.9966	67.5655	67.7992
16	0.9954	67.4544	67.7664
17	0.9931	67.2318	67.7008
18	0.9868	67.1934	68.0901
19	0.9814	66.4883	67.7459
20	0.9767	66.1243	67.7008
21	0.9715	65.9032	67.8367
22	0.9661	65.4953	67.7914
23	0.9639	65.5018	67.9535
24	0.9587	65.7164	68.5476
25	0.9662	65.5564	67.8517
26	0.9697	65.8034	67.8577
27	0.9744	66.0833	67.8185
28	0.9779	66.3286	67.8246
29	0.9884	66.9173	67.7018
30	0.9919	67.2778	67.8251
31	0.9936	67.2836	67.7140
32	0.9983	67.6299	67.7469
33	0.9988	67.5124	67.5905
34	1.0012	67.6028	67.5246*
35	1.0012	67.6878	67.6097
36	1.0035	67.7657	67.5313
37	1.0012	67.6093	67.5311
38	1.0000	67.7266	67.7266
39	1.0012	67.6939	67.6158
40	1.0023	67.7388	67.5826
41	1.0023	67.8623	67.7062
42	1.0006	67.4712	67.4320
43	1.0012	67.6279	67.5497
44	1.0041	67.7061	67.4323
45	1.0029	67.7517	67.5563
46	0.9971	67.4838	67.6794
47	1.0000	67.5227	67.5227
48	1.0023	67.6733	67.5168
49	1.0006	67.7191	67.6800
50	1.0000	67.5621	67.5621
51	0.9994	67.7313	67.7703

DRAG COEFF IS 0.0075

BAROM PRESS IS 28.960 IN. HG SURVEY NO 45

TABLE D6b

Survey 46, $\alpha = 1.57^{o}$.

PSN	RATIO	VEL	VREF	
1	1.0196	67.3955	66.0989	
2	1.0023	67.5704	67.4150	
3	1.0035	67.7057	67.4727	
4	1.0011	67.8350	67.7575	
5	1.0023	67.9573	67.8026	
6	0.9960	67.6601	67.9315	
7	1.0011	67.7886	67.7112	*
8	0.9983	67.8010	67.9173	
9	0.9983	67.8077	67.9240	
10	0.9994	67.8654	67.9042	
11	0.9960	67.5091	67.7814	
12	0.9948	67.5219	67.8719	
13	0.9926	67.4108	67.9167	
14	0.9851	66.9590	67.9742	
15	0.9838	66.5975	67.6958	
16	0.9754	66.5706	68.2513	
17	0.9693	65.9470	68.0323	
18	0.9669	65.7121	67.9603	
19	0.9623	65.4774	68.0446	
20	0.9571	65.2289	68.1540	
21	0.9545	64.9101	68.0047	
22	0.9583	65.3626	68.2058	
23	0.9571	65.2883	68.2125	
24	0.9647	65.6903	68.0956	
25	0.9741	66.3419	68.1083	
26	0.9787	66.5404	67.9918	
27	0.9880	67.2631	68.0822	
28	0.9925	67.2233	67.7318	
29	0.9943	67.8488	68.2367	
30	1.0000	68.1332	68.1332	*
31	0.9994	67.7437	67.7827	
32	1.0006	67.7825	67.7436	
33	1.0023	67.9901	67.8345	
34	0.9994	67.8738	67.9127	
35	1.0017	68.0228	67.9063	
36	1.0035	67.8739	67.6400	
37	1.0017	67.8470	67.7300	
38	1.0023	68.0808	67.9254	
39	1.0034	67.9702	67.7365	
40	1.0029	68.0804	67.8860	
41	1.0040	68.2417	67.9701	
42	1.0006	67.9381	67.8992	
43	1.0023	68.0928	67.9373	
44	1.0011	68.0607	67.9830	
45	1.0006	67.8660	67.8270	
46	1.0017	68.1833	68.0669	
47	0.9994	67.9885	69.0274	
48	0.9989	68.1441	68.2217	
49	1.0046	68.1441	67.8329	
50	1.0000	67.7998	67.7998	
51	1.0017	68.4291	68.3130	

DRAG COEFF IS 0.0099

BAROM PRESS IS 28.960 IN. HG SURVEY NO 46

TABLE D6c

Survey 47, $\alpha = 4.00^{\circ}$.

PSN	RATIO	VEL	VREF
1	1.0234	67.2530	65.7140
2	1.0029	67.6356	67.4411
3	1.0006	67.5309	67.4920
4	1.0006	67.6993	67.6605
5	1.0000	67.7573	67.7573
6	1.0023	67.8017	67.6464
7	1.0011	67.8984	67.8208 *
8	0.9954	67.5550	67.8660
9	0.9971	67.4892	67.6840
10	0.9819	66.2346	67.4558
11	0.9753	65.6419	67.3060
12	0.9640	65.0028	67.4295
13	0.9508	64.1640	67.4874
14	0.9441	63.4199	67.1738
15	0.9425	63.4317	67.3040
16	0.9424	63.3904	67.2651
17	0.9454	63.8936	67.5843
18	0.9604	64.8418	67.5123
19	0.9729	65.5761	67.4014
20	0.9808	66.3027	67.6032
21	0.9918	66.7778	67.3287
22	0.9977	67.1382	67.2953
23	1.0006	67.4649	67.4258 *
24	1.0006	67.6994	67.6604
25	1.0035	67.6992	67.4648
26	1.0017	67.7510	67.6340
27	1.0029	67.6728	67.4773
28	1.0029	67.7964	67.6013
29	1.0012	67.6072	67.5290
30	1.0041	67.7758	67.5022
31	0.9983	67.4899	67.6072
32	1.0029	67.7698	67.5745
33	1.0017	67.6851	67.5680
34	1.0012	67.6204	67.5421
35	0.9983	67.5092	67.6266
36	0.9994	67.3581	67.3974
37	1.0029	67.6263	67.4305
38	1.0000	67.6387	67.6387
39	1.0052	67.8729	67.5213
40	1.0035	67.7557	67.5211
41	1.0035	67.7620	67.5274
42	1.0017	67.7164	67.5992
43	1.0012	67.4876	67.4092
44	1.0000	67.7623	67.7623
45	1.0023	67.7417	67.5852
46	1.0000	67.6575	67.6575
47	1.0023	67.8136	67.6574
48	1.0052	67.9242	67.5728
49	1.0023	67.6695	67.5128
50	1.0017	67.7086	67.5912
51	1.0000	26.6953	26.6953

DRAG COEFF IS 0.0097

BAROM PRESS IS 28.940 IN. HG SURVEY NO 47

TABLE D6d

Survey 48, $\alpha = 5.92^{\circ}$.

PSN	RATIO	VEL	VREF
1	1.0114	66.8497	66.0957
2	0.9988	67.2359	67.3144
3	1.0029	67.4379	67.2418
4	1.0000	67.3263	67.3263*
5	0.9988	67.2996	67.3781
6	0.9925	67.1098	67.6198
7	0.9878	66.7213	67.5483
8	0.9749	65.9762	67.6778
9	0.9677	65.4994	67.6840
10	0.9551	64.6051	67.6451
11	0.9378	63.3761	67.5787
12	0.9287	62.8306	67.6566
13	0.9322	63.0049	67.5848
14	0.9353	63.1727	67.5456
15	0.9423	63.8157	67.7210
16	0.9551	64.6694	67.7086
17	0.9621	65.4486	68.0271
18	0.9745	66.2990	68.0336
19	0.9872	66.8219	67.6882
20	0.9954	67.4469	67.7603
21	1.0000	67.8053	67.8053*
22	1.0029	68.1300	67.9352
23	0.9988	67.7784	67.8565
24	1.0029	68.0970	67.9022
25	1.0006	67.9740	67.9350
26	0.9966	67.7852	68.0193
27	1.0023	68.0256	67.8696
28	1.0023	67.7912	67.6347
29	1.0006	67.7518	67.7127
30	1.0029	67.7975	67.6017
31	1.0017	68.0379	67.9209
32	0.9977	67.4108	67.5679
33	1.0040	67.9142	67.6404
34	1.0029	67.7309	67.5349
35	1.0017	67.6919	67.5743
36	1.0012	67.6197	67.5412
37	1.0006	67.7828	67.7436
38	1.0058	67.7825	67.3900
39	1.0035	67.9779	67.7433
40	1.0000	67.7825	67.7825
41	1.0029	67.9778	67.7824
42	1.0029	67.9391	67.7436
43	1.0006	67.7500	67.7108
44	1.0000	67.8343	67.8343
45	0.9977	67.6113	67.7681
46	1.0006	67.7498	67.7106
47	1.0017	67.9584	67.8412
48	1.0017	67.6776	67.5598
49	1.0000	67.6837	67.6837
50	0.9965	67.4870	67.7226
51	1.0029	67.8013	67.6053

DRAG COEFF IS 0.0120

BAROM PRESS IS 28.940 IN. HG SURVEY NO 48

TABLE D6e

Survey 49, $\alpha = 9.95^{\circ}$.

PSN	RATIO	VEL	VREF
1	1.0018	66.9651	66.8470
2	1.0000	67.0167	67.0167
3	1.0029	67.1530	66.9564
4	1.0018	66.9081	66.8498
5	1.0000	67.2502	67.2502
6	1.0035	67.3802	67.1447
7	1.0012	67.2689	67.1903
8	1.0041	67.3138	67.0386
9	1.0012	67.3202	67.2417
10	0.9988	67.1359	67.2145
11	1.0000	67.3780	67.3780 *
12	0.9988	67.4241	67.5024
13	0.9912	66.8000	67.3910
14	0.9866	66.5677	67.4751
15	0.9813	66.2616	67.5269
16	0.9763	65.8615	67.4487
17	0.9657	65.1812	67.4941
18	0.9565	64.4172	67.3495
19	0.9441	63.8807	67.6629
20	0.9315	62.9208	67.5456
21	0.9275	62.5466	67.4339
22	0.9183	61.7857	67.2827
23	0.9168	61.6139	67.2038
24	0.9134	61.5339	67.3677
25	0.9100	61.4481	67.5251
26	0.9124	61.5941	67.5044
27	0.9166	61.9746	67.6161
28	0.9263	62.4850	67.4588
29	0.9339	63.0337	67.4981
30	0.9430	63.5895	67.4322
31	0.9516	64.1703	67.4322
32	0.9590	64.7050	67.4715
33	0.9703	65.3221	67.3202
34	0.9799	65.8934	67.2473
35	0.9888	66.5402	67.2929
36	0.9907	66.9381	67.5689
37	0.9930	67.0170	67.4901
38	0.9988	67.4902	67.5687
39	1.0000	67.5682	67.5682 *
40	1.0023	67.7648	67.6081
41	1.0000	67.5414	67.5414
42	0.9988	67.5418	67.6203
43	0.9983	67.5021	67.6198
44	1.0012	67.9393	67.8612
45	1.0023	67.6257	67.4686
46	1.0029	67.8346	67.6387
47	1.0006	67.7502	67.7110
48	1.0012	67.7503	67.6720
49	0.9983	67.4813	67.5992
50	1.0041	67.8408	67.5663
51	1.0017	67.5395	67.4215

DRAG COEFF IS 0.0253

BAROM PRESS IS 28.940 IN. HG SURVEY NO 49

TABLE D6f

Survey 51, $\alpha = 10.36^{\circ}$.

PSN	RATIO	VEL	VREF
1	0.9983	67.7351	67.8489
2	1.0000	67.7478	67.7478
3	1.0000	67.7160	67.7160
4	1.0006	67.5315	67.4934
5	1.0017	67.5060	67.3914
6	1.0011	67.6334	67.5572
7	0.9994	67.5635	67.6016
8	1.0023	67.6342	67.5317
9	0.9994	67.4997	67.5379
10	1.0006	67.6653	67.6272 *
11	0.9955	67.2890	67.5948
12	0.9915	67.1035	67.6776
13	0.9881	66.8790	67.6841
14	0.9846	62.1710	63.1439
15	0.9788	66.0304	67.4606
16	0.9704	65.8869	67.8933
17	0.9594	65.1049	67.8617
18	0.9514	64.3127	67.6009
19	0.9427	63.9162	67.7982
20	0.9322	63.0675	67.6514
21	0.9195	62.2489	67.6960
22	0.9131	61.7069	67.5812
23	0.9111	61.5449	67.5492
24	0.9085	61.3346	67.5110
25	0.9071	61.3886	67.6769
26	0.9058	61.3043	67.6769
27	0.9116	61.7721	67.7595
28	0.9191	62.3138	67.7977
29	0.9303	62.9446	67.6575
30	0.9365	63.4416	67.7402
31	0.9460	64.0161	67.6704
32	0.9543	64.5854	67.6766
33	0.9643	65.2292	67.6445
34	0.9738	66.0122	67.7914
35	0.9789	66.2592	67.6892
36	0.9857	66.6547	67.6188
37	0.9926	67.0544	67.5547
38	0.9977	67.4780	67.6314
39	0.9977	67.4459	67.5994
40	1.0000	67.5165	67.5165 *
41	1.0011	67.7465	67.6700
42	1.0000	27.8397	27.8397
43	1.0017	67.8048	67.6901
44	1.0011	67.6947	67.6190
45	1.0011	67.8418	67.7654
46	1.0017	67.8479	67.7332
47	1.0011	67.7841	67.7076
48	1.0000	67.7138	67.7138
49	1.0017	67.7458	67.6308
50	1.0011	67.6433	67.5665
51	1.0034	67.7643	67.5343

DRAG COEFF IS 0.0280

BAROM PRESS IS 29.140 IN. HG SURVEY NO 51

APPENDIX E

ERROR ANALYSIS

Two types of data were measured during the course of the investigation: (1) data measured by either of the two force balances and (2) data measured by the wake traverse procedure. In the force balance phase of the study, there were several intermediate measurements and calculations involved. The air density was determined from

$$\rho = 0.002378\left(\frac{\text{barometer reading}}{29.92}\right)\left(\frac{519}{\text{temperature reading}}\right) \quad . \quad \text{(E1)}$$

Barometric pressure was measured to ±0.01 in. Hg (±0.71 lb/ft^2). Temperature was measured electronically and accurate to ±0.01° F. Velocity was determined from

$$V = \sqrt{\frac{2\Delta P}{\rho}} \quad , \quad \text{(E2)}$$

where ΔP = pressure difference across the transducer and ρ = density. ΔP was measured as a voltage and converted to lb/ft^2. Individual voltage measurements were obtained by integrating voltage outputs of the voltmeter over a 10-sec interval. Voltage measurements of ΔP were accurate to ±0.003 volt. Forces as sensed by the strain gages were derived from

$$F_{A,B}(lb) = K_{A,B}\left(\frac{lb}{volt}\right)Volts_{A,B} \quad \text{(E3)}$$

where $K_{A,B}$ = calibration constants for ribbons A and B. Calibration constants were verified by using the balance system to measure known weights. The balance system was able to measure known standard calibration weights to within ±0.6% of their value. The strain gages were calibrated numerous times with a resulting variation of

±0.000135 lb/volt. The airfoil dimensions, span and chord, were accurate to ±0.001 in. Equations (E1), (E2), and (E3) were combined to generate lift and drag force coefficients in the form

$$C_{force} = \frac{Force}{(1/2)\rho V^2 (span)(chord)} \quad . \tag{E4}$$

The airfoil angle of attack was measured with an artillery gunner's quadrant in mils (1^{o} = 17.78 mils). Angles were measured with an accuracy of ±0.01 mil or $\pm 0.0056^{o}$.

The individual accuracies of the elements making up Equation (E4) can be used to examine a worst-case condition for a typical C_L or C_D calculation. A relative error for each of the terms in Equation (E4) can be obtained by using logarithmic differentiation. For example, Equation (E1) can be expressed as

$$\rho = K(\frac{B}{T}) \quad , \tag{E1}$$

where B = barometer reading, T = temperature reading, and K = constant. Equation (E1) can also be expressed as

$$\ell n\rho = \ell nK + \ell nB - \ell nT \quad . \tag{E1}$$

Differentiating both sides of this form of Equation (E1) relates the relative errors among the various terms in Equation (E1),

$$\frac{\Delta\rho}{\rho} = \frac{\Delta B}{B} - \frac{\Delta T}{T} \quad . \tag{E1a}$$

The sign of the $\Delta T/T$ term can be + or -. Therefore, for a maximum error term, Equation (E1a) becomes

$$\frac{\Delta\rho}{\rho} = \frac{\Delta B}{B} + \frac{\Delta T}{T} \quad . \tag{E1b}$$

Performing the same operation on Equations (E2) and (E3), one gets

$$\frac{\Delta V}{V} = \frac{\Delta\rho}{2\rho} + \frac{\Delta(\Delta P)}{2\Delta P} \tag{E2a}$$

and

$$\frac{\Delta F_{A,B}}{F_{A,B}} = \frac{\Delta K_{A,B}}{K_{A,B}} + \frac{\Delta Volt_{A,B}}{Volt_{A,B}} \quad . \tag{E3a}$$

Performing a similar operation on Equation (E4) and substituting (E1b), (E2a), and (E3a), one gets an expression for the overall relative error for C_L or C_D,

$$\frac{\Delta C_F}{C_F} = \frac{\Delta K_{A,B}}{K_{A,B}} + \frac{\Delta Volt_{A,B}}{Volt_{A,B}} + 2\left(\frac{\Delta B}{B}\right) + \frac{2\Delta T}{T} + \frac{\Delta b}{b} + \frac{\Delta c}{c} + \frac{\Delta(\Delta P)}{\Delta P} \quad , \tag{E4a}$$

where b = span and c = chord.

Inserting the specified or experimentally determined accuracy data for the individual components of Equation (E4a) on a term-by-term basis, one finds the following worst-case relative error:

$$\frac{\Delta C_f}{C_f} = \frac{0.0005 \text{ lb/volt}}{0.176 \text{ lb/volt}} + \frac{0.0003 \text{ volt}}{0.9 \text{ volt}} + 2\left(\frac{0.02 \text{ in. Hg}}{30.0 \text{ in. Hg}}\right) + 2\left(\frac{0.3^\circ F}{530.0^\circ F}\right)$$

$$+ \frac{0.002 \text{ in.}}{18.375 \text{ in.}} + \frac{0.002 \text{ in.}}{18.00 \text{ in.}} + \frac{0.01 \text{ psi}}{1.00 \text{ psi}}$$

$$\frac{\Delta C_f}{C_f} = 0.0158 \quad .$$

The corresponding absolute error, ΔC_f, can now be determined from

$$\Delta C_f = \left(\frac{\Delta C_f}{C_f}\right) C_f \quad . \tag{E5}$$

For a typical $C_D = 0.0250$ corresponding to a voltage of 0.900 volts, the cumulative system error would result in a final coefficient error of

$$\Delta C_D = (0.0158)(0.025) = 0.0004 \quad ,$$

which is four counts of drag.

As an independent assessment, the Student-t distribution was considered to appraise statistically the possible size of C_{force} errors. The t-distribution is expressed as

$$t = \frac{\bar{X} - \mu}{s} \sqrt{n} \quad , \tag{E6}$$

where $\bar{X}$ and s are the mean and standard deviation of a random sample of xize n from a population which has a mean μ, a standard deviation σ, and which can be approximated closely by a normal curve. For each angle of attack, three measurements of C_L and C_D were made. Rearranging Equation (E6), one obtains

$$\frac{ts}{\sqrt{n}} = \bar{X} - \mu \tag{E7}$$

If a value for t is selected from a t-distribution table corresponding to a probability of 90%, Equation (E7) will give a corresponding error. Then, for a sample of n measurements, one can assert with a 90%

probability that the mean of that sample has an error of less than that computed by Equation (E7).

For example, consider data measured during a test using the 18-in.-chord airfoil without disk for an angle of attack of 6.17°, three measurements of C_D were made; namely, 0.01582, 0.01553, and 0.01577. The sample size (n) is 3. The sample mean ($\bar{X}$) is 0.01571. The standard deviation (s) is given by

$$s = \sum_{i=1}^{n} \sqrt{\frac{(X_i - \bar{X})^2}{n - 1}} \quad . \tag{E8}$$

For this example,

$$s = \sqrt{\frac{1.28(10^{-8}) + 3.13(10^{-8}) + 3.969(10^{-9})}{2}} = 0.00016 \quad .$$

For n = 3 and a probability of 90%, a t-distribution table (20) yields t = 2.920. Substituting these values in Equation (E7), one gets

$$\frac{ts}{\sqrt{n}} = \frac{2.920}{\sqrt{3}}(0.00016) = 0.00027 \quad .$$

For measurements of C_D made at $\alpha = 6.17^{\circ}$, there is a 90% chance that the mean of the measurements is within ±0.00027 of the correct value. As would be expected, the 0.00027 error is within the bounds of the worst-case analysis. This type of analysis was performed on each of the various force balance experiments. For a given experiment, the largest error calculated in this manner was selected and listed at the head of each column of C_L and C_D data. See the tables in Appendix D.

Drag coefficients obtained from the wake integration process are subject to the previously discussed errors associated with velocity measurement. Since the airfoil wake is measured as a series of velocity ratios, errors in velocity tend to cancel out. There is an error associated with use of the trapezoidal rule of integration. For a function of $y = F(x)$, integrated from a to b and divided into trapezoidal subintervals of width h, an expression for the so-called global error is given by Reference (21) as

$$|E| \leq -\left(\frac{b-a}{12}\right)h^2 f''(\xi) \quad . \tag{E8}$$

If ξ is chosen in the interval (a,b) such that it is a maximum value, then Equation (E8) gives the upper bound of the error.

Pope (13) *suggests* that the curve of an airfoil wake profile may be approximated by a $(\text{cosine})^2$ function. Consider Survey No. 45 (Appendix D), where $(b - a) = 2.0$ in. (0.1667 ft) and $h = 0.1$ in. (0.0083 ft). The wake profile can be expressed as

$$\left(\frac{\sqrt{q}}{q_o} - \frac{q}{q_o}\right)_x = \left(\frac{\sqrt{q}}{q_o} - \frac{q}{q_o}\right)_{max} \cos^2\left(\left(\frac{\pi/2}{L/2}\right)x\right) \quad -\frac{L}{2} \leq x \leq \frac{L}{2} \quad , \tag{E9}$$

where $L = (b - a)$ = width of the wake (integration limits).

The quantity in the first set of brackets represents the maximum amplitude of the wake profile curve. Equation (E9) models a curve similar to that shown on Figure 14. Substituting (E9) into (E8) gives

$$|E| \leq \left(\frac{b-a}{12}\right)(-2)\left(\sqrt{\frac{q}{q_o}} - \frac{q}{q_o}\right)_{max}\left(\frac{\pi}{L}\right)^2 \cos\left(\left(\frac{\pi}{L}\right)x\right) . \qquad \text{(E10)}$$

The maximum value that the cosine term can take is 1.0; therefore, the error upper bound can be determined. Substituting values from Survey No. 45, one finds

$$|E| \leq \frac{0.1667}{12}(0.0083)^2 2(0.0413)\left(\frac{\pi}{0.1167}\right)^2 = 0.00003 \quad .$$

This value represents the integral in Equation (B3),

$$C_d = 2\iint \left(\sqrt{\frac{q}{q_o}} - \frac{q}{q_o}\right)\frac{dy}{c} \quad . \qquad \text{(B3)}$$

The corresponding error in terms of C_d is therefore

$$E_{C_d} = \frac{2(0.00003)}{0.75} = 0.00008 \quad .$$

The same operation was carried out for each survey and the resulting errors are listed on Table D6.

DISTRIBUTION LIST FOR UNCLASSIFIED TM 80-44 by Paul P. Jacobs, Jr., dated March 31, 1980

Commander
Naval Sea Systems Command
Department of the Navy
Washington, DC 20362
Attn: Library
Code NSEA-09G32
(Copy Nos. 1 and 2)

Naval Sea Systems Command
Attn: T. E. Peirce
Code NSEA-63R3
(Copy No. 3)

Commanding Officer
Naval Underwater Systems Center
Newport, RI 02840
Attn: Library
Code 54
(Copy No. 4)

Naval Underwater Systems Center
Attn: R. H. Nadolink
Code 3634
(Copy No. 5)

Commanding Officer
Naval Ocean Systems Center
San Diego, CA 92152
Attn: D. Nelson
Code 6342
(Copy No. 6)

Naval Ocean Systems Center
Attn: M. M. Reischman
Code 2542
(Copy No. 7)

Commander
David W. Taylor Naval Ship R&D Center
Department of the Navy
Bethesda, MD 20084
Attn: W. B. Morgan
Code 154
(Copy No. 8)

David W. Taylor Naval Ship R&D Center
Attn: Y. T. Shen
Code 1524
(Copy No. 9)

David W. Taylor Naval Ship R&D Center
Attn: R. W. Brown
Code 1942
(Copy No. 10)

David W. Taylor Naval Ship R&D Center
Attn: Library - Code 522
(Copy No. 11)

Officer-In-Charge
David W. Taylor Naval Ship R&D Center
Department of the Navy
Annapolis Laboratory
Annapolis, MD 21402
Attn: E. R. Quandt
Code 272
(Copy No. 12)

David W. Taylor Naval Ship R&D Center
Annapolis Laboratory
Attn: J. G. Stricker
Code 2721
(Copy No. 13)

Commander
Naval Surface Weapons Center
Silver Spring, MD 20910
Attn: J. L. Baldwin
Code WA-42
(Copy No. 14)

Office of Naval Research
Department of the Navy
800 N. Quincy Street
Arlington, VA 22217
Attn: R. D. Cooper
Code 438
(Copy No. 15)

Defense Technical Information Center
5010 Duke Street
Cameron Station
Alexandria, VA 22314
(Copy Nos. 16 through 27)

National Bureau of Standards
Aerodynamics Section
Washington, DC 20234
Attn: P. S. Klebanoff
(Copy No. 28)

Naval Research Laboratory
Washington, DC 20390
Attn: R. J. Hansen
(Copy No. 29)

NASA Lewis Research Center
21000 Brookpark Road
Cleveland, Ohio 44135
Attn: M. J. Hartmann
MS 5-9
(Copy No. 30)

DISTRIBUTION LIST FOR UNCLASSIFIED TM 80-44 by Paul P. Jacobs, Jr., dated March 31, 1980

NASA Lewis Research Center
Attn: W. M. McNally
MS 5-9
(Copy No. 31)

NASA Lewis Research Center
Attn: N. C. Sanger
MS 5-9
(Copy No. 32)

California Institute of Technology
Jet Propulsion Laboratory
48000 Oak Grove Drive
Pasadena, CA 91109
Attn: Dr. L. Mack
(Copy No. 33)

Rand Corporation
1700 Main Street
Santa Monica, CA 90406
Attn: C. Gazley
(Copy No. 34)

Dr. Peter van Oossanen
Netherlands Ship Model Basin
Haagsteeg 2
P. O. Box 28
67 AA Wageningen
The Netherlands
(Copy No. 35)

Carl-Anders Johnsson
Statens Skeppsprovningsanstalt
Box 24001
S-400 22 Goteborg
Sweden
(Copy No. 36)

Dr. Ir. A. De Bruijn
Technisch Physische Dienst TNO-TH
Stieltjesweg 1
Postbus 155
Delft
The Netherlands
(Copy No. 37)

Dr. Allen Moore
Admiralty Research Laboratory
Teddington, Middlesex
England
(Copy No. 38)

J. Lewis
University of Newcastle
Newcastle
England
(Copy No. 39)

Dr. John H. Horlock
Vice Chancellor
University of Salford
Salford, M5 4WT
England
(Copy No. 40)

Von Karman Institute for Fluid Dynamics
Turbomachinery Laboratory
Rhode-Saint-Genese
Belgium
Attn: Library
(Copy No. 41)

Dr. D. S. Thompson
Turbine Research Department
Rolls Royce Ltd.
P. O. Box 31
Derby
England
(Copy No. 42)

Whittle Turbomachinery Laboratory
Madingley Road
Cambridge, England
Attn: Sir William Hawthorne
(Copy No. 43)

Whittle Turbomachinery Laboratory
Attn: Dr. D. S. Whitehead
(Copy No. 44)

Professor R. E. Peacock
School of Mechanical Engineering
Cranfield Institute of Technology
Cranfield, Bedford MK430AL
England
(Copy No. 45)

Professor J. P. Gostelow
School of Mechanical Engineering
NSW Institute of Technology
Broadway, Sidney
Australia
(Copy No. 46)

DISTRIBUTION LIST FOR UNCLASSIFIED TM 80-44 by Paul P. Jacobs, Jr., dated March 31, 1980

Dr. V. H. Arakeri
Department of Mechanical Engineering
Indian Institute of Science
Bangalore 560 012
India
(Copy No. 47)

Institute of High Speed Mechanics
Tohoku University
Sendai
Japan
(Copy No. 48)

Dr. Allan J. Acosta
California Institute of Technology
Division of Engineering for
Applied Sciences
Pasadena, CA 91109
(Copy No. 49)

Professor Patrick Leehey
Department of Ocean Engineering
Room 5-222
Massachusetts Institute of Technology
77 Massachusetts Avenue
Cambridge, MA 02139
(Copy No. 50)

Dr. John L. Lumley
Sibley School of Mechanical and
Aeronautical Engineering
Upson Hall
Cornell University
Ithaca, NY 14850
(Copy No. 51)

Calspan Corporation
4455 Genessee Street
Buffalo, NY 14221
Attn: Head Librarian
(Copy No. 52)

Dr. G. K. Serovy
Mechanical Engineering Department
Iowa State University
Ames, Iowa 50010
(Copy No. 53)

Superintendent (Code 1424)
Naval Postgraduate School
Monterey, CA 93940
(Copy No. 54)

Iowa Institute of Hydraulic Research
The University of Iowa
Iowa City, Iowa 52240
(Copy No. 55)

Dr. Roger E. A. Arndt
St. Anthony Falls Hydraulic Laboratory
University of Minnesota
Mississippi River at 3rd Ave., S.E.
Minneapolis, MN 55414
(Copy No. 56)

Defense Advanced Research Projects Agency
1400 Wilson Boulevard
Arlington, VA 22209
Attn: P. Selwyn, TTO
(Copy No. 57)

Hydronautics, Inc.
Pindell School Road
Laurel, MD 20810
(Copy No. 58)

The Pennsylvania State University
Applied Research Laboratory
P. O. Box 30
State College, PA
Attn: G. B. Gurney
(Copy No. 59)

Applied Research Laboratory
Attn: A. L. Treaster
(Copy No. 60)

Applied Research Laboratory
Attn: B. R. Parkin
(Copy No. 61)

Applied Research Laboratory
Attn: Garfield Thomas Water Tunnel Files
(Copy No. 62)

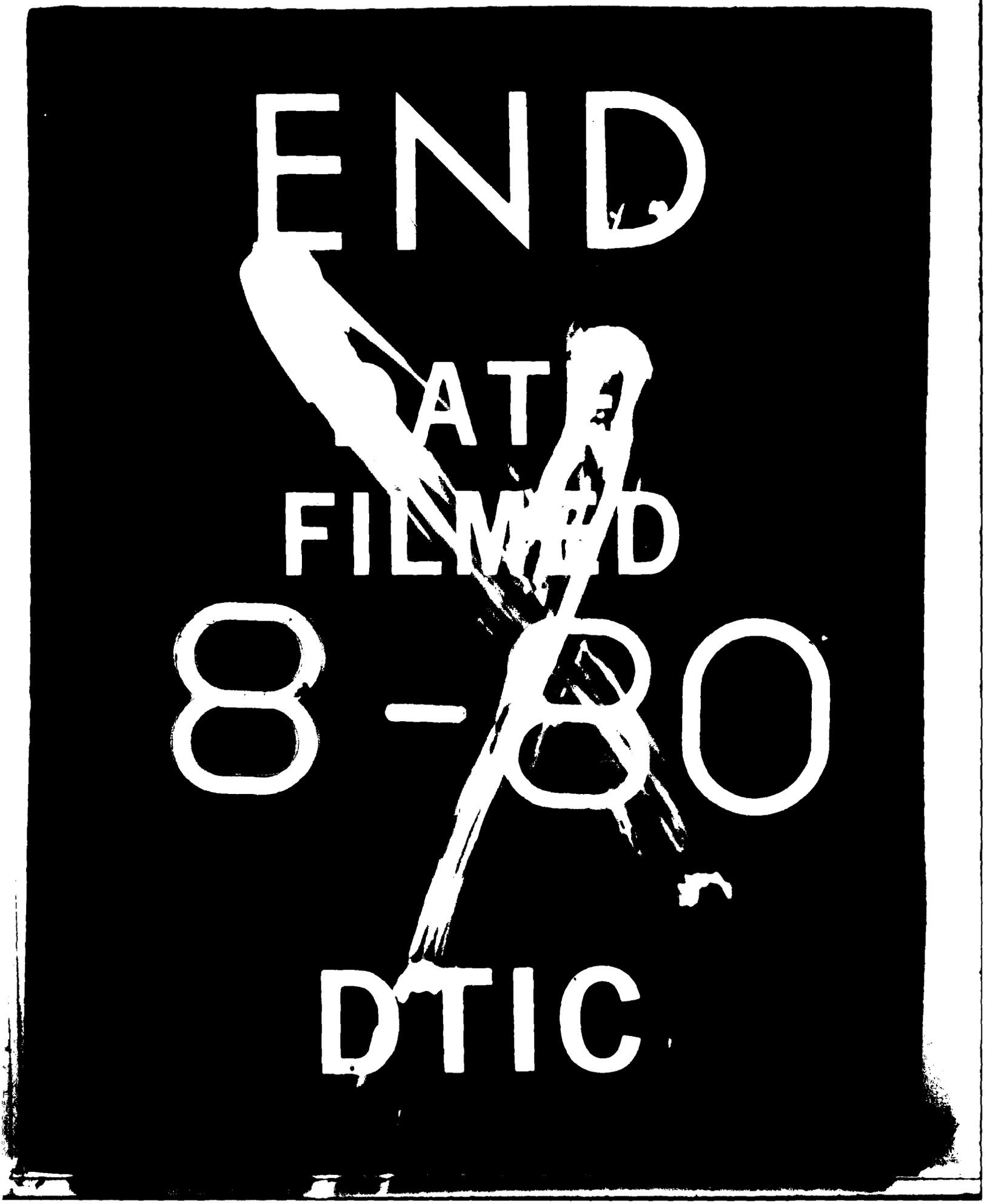
END
AT
FILMED
8-80
DTIC

AD-A086 079 PENNSYLVANIA STATE UNIV UNIVERSITY PARK APPLIED RESE--ETC F/G 20/4
A METHOD OF CORRECTING FOR THE EFFECTS OF THE SIDEWALL BOUNDARY--ETC(U)
MAR 80 P P JACOBS N00024-79-C-6043
UNCLASSIFIED ARL/PSU/TM-80-44 NL

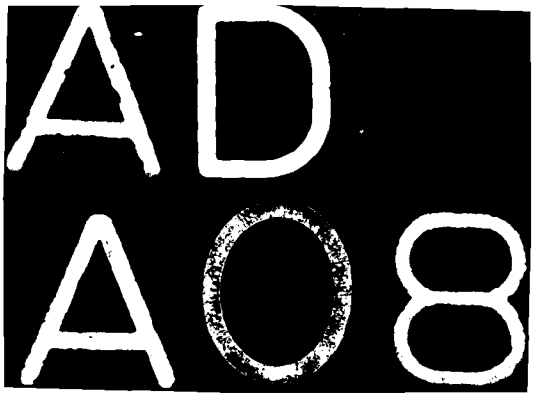
AD
A08

SUPPLEMENTARY

INFORMATION

THE PENNSYLVANIA STATE UNIVERSITY
INTERCOLLEGE RESEARCH PROGRAMS AND FACILITIES
APPLIED RESEARCH LABORATORY

ADDRESS REPLY TO:
APPLIED RESEARCH LABORATORY
P. O. BOX 30
STATE COLLEGE, PENNSYLVANIA 16801

25 August 1981

To: Distribution List

Subject: Forwarding of Errata for ARL TM 80-44

Please replace Page 82 of ARL TM 80-44, "A Method of Correcting for the Effects of the Sidewall Boundary Layer in Two-Dimensional Airfoil Testing," by Paul P. Jacobs, Jr., dated March 31, 1980.

An error in definition was found in Paragraph 1 and also a typographical error was made in Equation (13).

Defense Technical Information Center
5010 Duke Street
Cameron Station
Alexandria, VA 22314
(Copy Nos. 16 through 27)

where $C_{\ell_\alpha} = dC_\ell/d\alpha$ and $C_{\ell_{\alpha_o}} = (dC_\ell/d\alpha)_o$. As the experimental data show, the drag correction must be zero at $C_\ell = 0$. Thus, the C_ℓ contribution should be directly proportional to the ΔC_d term. The assumed C_d correction can be the term which "individualizes" the correction to specific airfoils if it is set equal to C_{d_o} (the drag coefficient at zero lift) of the tested airfoil. The correction now takes the form

$$\Delta C_d = K \frac{C_{d_o} C_\ell (C_{\ell_\alpha}/C_{\ell_{\alpha_o}})^{1/2}}{\left((\delta/c)/0.1\right)(t/c)^4} f(AR) \quad . \tag{12}$$

At this point, Equation (12) can be applied to the data of Figures 40-42. On a trial-and-error basis, setting $K = 0.00015$ and $f(AR) = 1/\sqrt{AR}$, one finds for the final correction that

$$\Delta C_d = \frac{0.00015\left(C_{d_o} C_\ell (C_{\ell_\alpha}/C_{\ell_{\alpha_o}})^{1/2}\right)}{\left((\delta/c)/0.1\right)(t/c)^4\sqrt{AR}} \quad . \tag{13}$$

Shown in Figures 43-45 are the results of the three experiments with Equation (13) applied to the data. The correction works extremely well for the ARL/PSU data. There is also exceptionally good agreement when it is applied to Kermeen's data. With Kermeen's data, there is a slight deviation at the higher C_ℓ values. It must be noted that in the range $C_\ell = 1.1$ Kermeen's curve exceeds the published NACA data by approximately 90%. Another consideration is the advances made in instrumentation between Kermeen's tests and the present study. Also noteworthy is the fact that the Reynolds numbers of the two curves